Universidade de Aveiro Departamento de Electrónica, Telecomunicações e Informática,
2016

Tiago Manuel Coelho Morgado

Circuitos Óticos Integrados para uso em Redes NG-PON2

Photonic Integrated Circuits for use in NG-PON2 Networks

Universidade de Aveiro
Departamento de Electrónica, Telecomunicações e Informática,
2016

Tiago Manuel Coelho Morgado

Circuitos Óticos Integrados para uso em Redes NG-PON2

Photonic Integrated Circuits for use in NG-PON2 Networks

Dissertação apresentada à Universidade de Aveiro para cumprimento dos requisitos necessários à obtenção do grau de Mestre em Engenharia Electrónica e Telecomunicações, realizada sob a orientação científica do Doutor António Luís Jesus Teixeira e do Doutor Mário José Neves de Lima, Professores do Departamento de Electrónica, Telecomunicações e Informática da Universidade de Aveiro

O júri / The jury

Presidente / President

Prof. Dr. Paulo Miguel Nepomuceno Pereira Monteiro

Professor Associado da Universidade de Aveiro

Vogais / Examiners committee

Prof. Dr. Henrique Manuel de Castro Faria Salgado

Professor Associado da Faculdade de Engenharia da Universidade do Porto

Prof. Dr. Mário José Neves de Lima

Professor Auxiliar da Universidade de Aveiro

Agradecimentos

Em primeiro lugar, gostaria de agradecer aos Professores António Teixeira e Mário Lima por me orientarem ao longo deste último ano, por todos os conhecimentos científicos que me transmitiram e também por toda a confiança e autonomia que depositaram em mim. Gostava também de agradecer ao Francisco Ruivo pelas dúvidas que me foi esclarecendo ao longo deste percurso e pelas sugestões que me deu para resolver os problemas que foram surgindo.

Ao Instituto de Telecomunicações por ter disponibilizado todos os recursos necessários para a realização desta dissertação.

De seguida, gostaria de agradecer aos meus pais, avós e irmão pelo apoio e pela educação que me deram o que me tornou na pessoa que sou hoje. Sem eles não teria sido possível estar aqui.

Em seguida, quero agradecer ao André Barros por ter sido o meu companheiro de batalha ao longo destes últimos meses, nos quais trabalhamos de dia e de noite sem tempo para respirar. Um agradecimento também a todos os meus amigos por todos os bons momentos que passámos ao longo deste curso, em especial ao Rúben e ao André Cajus que me ajudaram nos momentos em que mais precisei.

Por fim, gostaria de agradecer á minha namorada, a Vanessa, por ter sido o meu pilar ao longo destes anos, pela sua compreensão quando eu quase não tinha tempo para ela, por todo o amor e a força que sempre me deu.

Palavras-chave

Comunicações Óticas, VPItoolkit PDK HHI, NG-PON 2, Transcetor, DFB laser, Fotodíodo, MMI, MZM, PICs.

Resumo

Nos dias que correm com a adoção generalizada de smartphones, conteúdos de vídeo, computação em nuvem e redes sociais, o volume de tráfego não para de aumentar. Assim, existe uma procura constante para melhorar a largura de banda das redes existentes. Neste contexto surgiu a *Next Generation Passive Optical Network Phase (*NG-PON) 2 a qual é um novo *standard* que vai permitir um aumento da largura de banda que pode chegar aos 80Gbps. O conhecimento dos requisitos do *standard* NG-PON 2 é importante, para que se possam produzir equipamentos que possam vir a ser utilizados nestas redes.

Atualmente existe uma grande evolução nas comunicações óticas. Esta evolução tecnológica levou ao aparecimento de Photonic Integrated Circuits(PICs). Os PICs permitem a integração no mesmo chip de diversos componentes óticos permitindo assim construir circuitos com maior desempenho e fiabilidade. Cada vez mais, existe um grande investimento nesta área, estão inclusivamente a aparecer *softwares* cujo propósito é permitir aos utilizadores criar e simular PICs, para que estes possam ser posteriormente construídos. É então importante o conhecimento das caraterísticas mais importantes dos blocos que estes softwares permitem simular. Neste trabalho serão testados alguns blocos do "VPItoolkit PDK HHI" que é um toolkit que quando adicionado no software VPItransmissionMaker™, permite simular os componentes produzidos pelo Heinrich Hertz Institute (HHI). Com estes componentes, serão ainda feitas simulações visando a sua utilização em uma rede NG-PON2. Foi também dada grande atenção ao estudo dos *Multimode Interference Devices* (MMI) dos quais foi feito um modelo em MATLAB. E ao mach *Zehnder Modulator* (MZM) do qual foi realizada uma animação a demostrar dinamicamente a propagação da Luz dentro dele. Foram ainda sugeridas duas arquiteturas possíveis para um *tranceiver* a ser utilizado no Optical Network Unit (ONU) em redes NG-PON 2.

keywords

Optical Communications, VPItoolkit PDK HHI, NG-PON 2, DFB laser, Photodiode, MMI, MZM, Transceiver, PICs.

abstract

Nowadays with the widespread adoption of smartphones, video content, cloud computing and social networks, the volume of traffic is constantly increasing. Therefore, it exists a constant demand to improve the bandwidth of the existing networks. In this context emerged the Next Generation Passive Optical Network Phase (NG-PON 2), which is a new standard that will allow an increase in the bandwidth up to 80 Gbps. The knowledge of the requirements of the standard NG-PON 2 is important, to allow the production of equipment that can be used in these networks.

Currently there is a major evolution in optical communications. This technological evolution has led to the emergence of Photonic Integrated Circuits (PICs). By using PICs various optical components can be integrated on the same chip, allowing to build circuits with higher performance and reliability. Currently there is a large investment in this area, software whose purpose is to allow users to create and simulate PICs are starting to appear, to subsequently allow a correct manufacturing of the PICs. It is important to know the most important features of these software blocks and what do they allow to simulate. During this work some blocks from "VPItoolkit PDK HHI" will be tested. "VPItoolkit PDK HHI" is a toolkit that when added in VPItransmissionMaker ™ software allows the simulation of the components produced by the Heinrich Hertz Institute (HHI). With these components, simulations were made to test their use in a NG-PON2 network. It was also given attention to the study of the *Multimode Interference Devices* (MMI) from which was created a model in MATLAB. And to the Mach Zehnder Modulator (MZM) from which was made an animation to dynamically demonstrate the propagation of light inside him. It was also suggested two possible architectures for a transceiver to be used on the Optical Network Unit (ONU) in NG-PON 2 networks.

Contents

List of Figures

List of Tables

List of Acronyms

APD	Avalanche Photodiode
AWG	Arrayed Waveguide Grating
BER	Bit Error Rate
BPM	Beam Propagation Method
BPON	Broadband PON
BPM	Beam propagation method
CAPEX	Capital Expenditure
CB	Conduction band
CWDM	Coarse WDM
CP	Channel Pair
CG	Channel Group
CTs	Channel terminations
CW	Continuous Wave
DBR	Distributed Bragg Reflector
DCF	Dispersion Compensation Fiber
DEMUX	Demultiplexer
DFB	Distributed feedback laser
DS	downstream
DBR	distributed Bragg reflector
DML	Directly modulated laser
EPON	Ethernet-PON
EMLs	External Modulated Lasers
ER	Extinction Ratio
FPR	Free Propagation Region
FP-SOA	Fabry-Perot SOA
FSR	Free Spectral range
GPON	Gigabit-Capable PON
HHI	Heinrich Hertz Institute
IEEE	Institute of Electrical and Electronics

	Engineers
ITU	International Telecommunication Union
MMI	Multimode interference devices
MUX	Multiplexer
MZM	Mach-Zehnder modulator
NG-PON 2	*Next Generation Passive Optical Network Phase 2*
ODN	Optical Distribution Network
OLT	Optical Line Terminal
OOK	On-Off Keying
ONU	Optical Network Unit
OPEX	Operational Expenditure
PDK	Process Design Kit
PIC	Photonic Integrated Circuits
PIN	p-i-n Photodiode
PM	Phase Modulator
PON	Passive Optical Networks
PtP WDM	Point to point wavelength division multiplexing
RES	Reach Extender
SMSR	Side Mode Suppression Rate
SOA	Semiconductor optical amplifier
SSMF	Standard Single Mode Fiber
TFF	Thin-Film Filter
TWDM	Time and wavelength division multiplexing
TWDM-PON	Time and wavelength division multiplexed passive optical network
TW-SOA	Travelling – wave SOA
TE	Transverse Electric
TECs	Thermoelectric Coolers
TM	Transverse magnetic
US	Upstream
VB	Valence band

WDM	Wavelength Division Multiplexing
WM	Wavelength Multiplexer
XG-PON	10 Gigabit-Capable Passive Optical Network
λ	Wavelength

1. Introduction

1.1 Context and Motivation

Nowadays, with the widespread adoption of smartphones, video content, cloud computing, and social networks, the volume of Internet traffic continues to increase. By 2020 it is expected that there will be 50 billion connected devices, using fixed and mobile broadband networks. According to Cisco's Visual Networking Index, from 2012 to 2017 the total amount of data exchanged between mobile users will be increased to around 66 percent annually.[1]

The competition within the telecommunications market is large, so operators always seek to improve their services. Therefore the search for new technologies is a constant center of attention to overcome the competition. So, ensure the highest bandwidth at the lowest possible cost it's the main requirement. In this perspective the standard NG-PON 2 was developed with the aim to improve transmission rates, but also to be compatible with some of the technologies already implemented. Therefore it is important to understand the requirements of the standard in order to build transceivers that can be used in the Optical Line Terminal (OLT) and in the Optical Network Unit (ONU).

The PICs will have an important role during this technology evolution. Because they can be used in the OLT and ONU transceivers, but also because they can be used to construct other optical hardware, for example the one used in the central offices. By using PICs, it will be possible to reduce the volume, weight and power consumption of these devices.

Reduce the volume and power consumption in central offices is very important because, with the growth of the deployment of optical networks, the amount and complexity of equipment used on it is also increased leading to problems of space and huge energy consumption. Much of optical hardware used nowadays is based on discrete components. The circuits that are created with discrete components are large and have a big energy consumption. Replacing this equipment by PICs will make it possible to overcome these problems.

It is expected that the market for PICs grows 25.2% during the forecast period 2015 to 2022 [2], which makes the market for PICs an attractive target for the investors. With increased investment in this sector, there are emerging new simulation software in order to allow the PIC developers to simulate the behavior of optical components.

Recently VPIphotonics launched the "VPI toolkit PDK HHI", which is a toolkit to be used in VPItransmissionMaker. This software allows the user to simulate and optimize the behavior of photonic circuits. Then its layout can be exported to software PhoeniX OptoDesigner, fit it to the package, add proper electrical wire routing, perform a design-rule-check (DRC) verification, and

export the final mask for optical chip fabrication. Within the scope of this work it will be possible to test some of the toolkit´s components. Furthermore it will be then analyzed the possibility for them to be used in a transceiver for the ONU or OLT in the NG-PON2.

1.2 Objectives

- Study of NG-PON2 for deriving main optical interfaces requirements
- Study of the main component's used in optical communications
- Understand PICs and their limitations
- Analyze several integrated optical components of the VPItoolkit PDK HHI
- Propose an architecture for a transceiver for NG-PON2

1.3 Structure

This work is divided into 5 chapters:

- 1. Introduction
- 2. NG-PON 2 Description
- 3. PICs Components
- 4. Toolkit components characterization
- 5. Transceiver for the ONU
- 6. Conclusion and Future work

The first chapter presents the context and the motivation of the dissertation, the objectives, the contributions and how it is structured.

In the second chapter the context of the NG-PON 2 standard and the main requirements are explained.

In the third chapter it will be explained the operation and main characteristics of some of the components which are used in PICs. Furthermore it also be presented a script developed in MATLAB, which allows the modelling of a MMI and it will as well be presented a developed animation that demonstrates the behavior of a MZM.

The fourth chapter contains the tests of several components of the VPItoolkit PDK HHI in different scenarios. The accuracy of the models is analyzed in comparison with the expected behavior of the components and it is also studied their viability within the NG-PON 2 networks.

In the fifth chapter is tested both the transmission and the reception, using the components of the toolkit which will integrate the ONUs of a NG-PON2 network. Due the characteristic of these components, it is suggested two possible transceiver architectures to be used in an ONU.

The sixth is the last chapter which contains the conclusions and the future work. Thus it is given an overview of the dissertation with the main conclusions of the work done and is also suggested the future work that can be made in this research.

1.4 Contributions

The main contributions of this work are:

- Summarization of the main characteristics of NG-PON2 standard;
- Listing and simulation of several PIC components;
- Development of a script in the software MATLAB to model MMI;
- Simulation of a MZM in software OptoDesigner, and development of an animation with obtained results;
- Test in VPItransmissionMaker™ of some "VPItoolkit PDK HHI" components:
    - Distributed feedback laser (DFB);
    - Current-injection phase-modulator;
    - PIN Photodiode;
    - High Speed PIN Photodiode;
- Simulation of transmission and reception with toolkit components in a NG-PON 2 scenario;
- Suggestion of two possible transceiver architectures that can be used in an ONU.

2. NG-PON2 Description

2.1 Overview

The number of services that use communications systems and the bandwidth that they need, have exponentially grown in the last decade. So in order to guarantee the quantity and the quality of services expected by the consumers the NG-PON2 was developed. On December of 2014 the G.989.2[3] recommendation was approved by ITU-T.

In the Passive Optical Networks (PONs) all the elements should be passive, which means no power supply is needed to make them operate. Around 90% of the power consumption and 50% of the cost of an overall network are due to the access network[4]. So in order to reduce the Capital Expenditures (CAPEX) and Operational Expenditure OPEX it is very important for the operators to efficiently use the optical access infrastructure. PONs are access networks with flexibility and adaptability. The key elements in PONs are the optical line terminal (OLT), the Optical Distribution Network (ODN) and the Optical Network Unit (ONU). The OLT is usually located in a central office, while the ONU is located in subscriber's buildings. The ODN is located on the outside, and contains the fiber and the splitters, typically in poles and ducts and the communication between the OLT and the ONU are done through it.

An NG-PON2 network has at least a capacity of 40 Gbps downstream and 10 Gbps upstream, however it can support up to 80 Gbps in each direction. NG-PON2 uses Time and Wavelength Division Multiplexing (TWDM) because telecommunication operators consider it to be less risky, less disruptive and less expensive than others technologies due to the fact it reuses components and technologies that already exist.

When operators started planning the NG-PON2 it was consider the possibility that the NG-PON2 could be a disruptive technology, since it could use a new ODN with wavelength splitters rather than power splitters. However, this would implicate a big investment by the operators in λ-splitters. So NG-PON2 networks must be compatible with ODNs already deployed, but this does not mean that λ-splitter based ODNs are not within the scope, only that the optical transmission technology must not require a λ-splitter to work [5].

2.2 PON Evolution

In the last few years, the evolution of PON has been constant. In 2001 the Broadband PON (BPON) was the first PON standard that was completed by ITU-T. The BPON provides 622 Mbps downstream bitrate and 155 Mbps upstream bitrate. BPON has a reach of 20 km, and can serve up to 64 users.[6] An alternative standard was introduced by the Institute of Electrical and Electronics Engineers (IEEE) in 2004, the Ethernet-PON (EPON)[7]. Using Ethernet as the transport protocol, EPON provides symmetric 1.25 Gbps. EPON quickly became the most common standard in Asia and, in 2009 evolved into 10G-EPON providing 10 Gbps downstream and 1 Gbps upstream bitrate[8]. As response to EPON, in 2004 the ITU-T introduces the Gigabit-Capable PON (GPON)[9]. This standard has encountered great success in Europe and America. It supports various bitrate options but it typically provides 2488 Mbps downstream bitrate and 1244 Mb/s upstream bitrate, with 30 km available reach and up to 128 end-users. In 2010, the 10 Gigabit-Capable Passive Optical Network (XG-PON) was standardized by ITU-T[10], as an evolution of GPON, providing for 10 Gbps downstream bitrate and 2.5–10 Gbps upstream bitrate. The XG-PON has a capacity to 64-128 end users with 20–60 km available reach, but there exists a dependency between the maximum number of users and the maximum reach. [11]

The next step of PON evolution is the NG-PON 2, in December of 2014 the G.989.2 recommendation was approved by ITU-T. The NG-PON 2 has at least a capacity of 40 Gbps downstream and 10 Gbps upstream, however it can support 80 Gbps in each direction. This bit rate is achieved using TWDM-PON. The maximum passive fiber reach will be 40 km, or up to 60 km by using Reach Extender (REs) and it will support more than 64 users. As it happened with the XG-PON, the maximum number of users and the maximum reach distance are dependents from each other. The NG-PON2 was planned to co-exist with GPON, XG-PON and RF video.[3]

2.3 TWDM - The chosen transmission technique

TWDM uses a combination of time and wavelength division multiple access. The wavelength-division multiplexing in the downstream direction is achieved by combining light from several fixed wavelength OLT lasers with a wavelength MUX. The light is then filtered at each ONU with a tunable filter that only allows to go through the desired wavelength to the specific receiver. In the upstream direction, the tunable lasers at each ONU are dynamically assigned to a wavelength. A time slot is assigned to each user to transmit and receive data on a shared optical carrier. To avoid packet collision, complex algorithms of ranging and dynamic bandwidth assignment are generally used. One of the main advantages of the TWDM solutions it is the fact that they can count on mature technology and cheap components. Consequently, they are the

simplest and fastest way to deploy PONs, according to a short-term technical and economic analysis.[12] In the Figure 1 is shown the use of TWDM in an NG-PON 2 system.

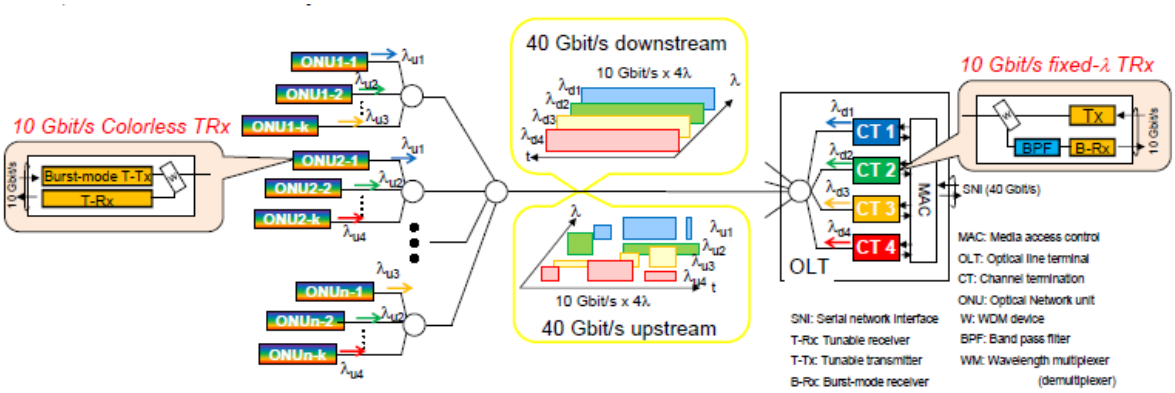

Figure 1- Example of configuration of 40 Gbit/s symmetric NGPON2 system [38].

2.4 PtP WDM PON

The point-to-point wavelength division multiplexing (PtP WDM) PON, is a multiple wavelength PON system that allows a point-to-point connectivity using a dedicated wavelength channel per ONU for the upstream direction and a dedicated wavelength channel per ONU for the downstream direction.[3]

2.5 The Reference Architecture

The NG-PON 2 reference logical architecture is shown in the Figure 2. Each ONU is equipped with a tunable transmitter and receiver. The tunable transmitter is tunable to any of the four upstream wavelengths. The receiver is tunable to any of the four downstream wavelengths. The wavelength in which each ONU operates is previously selected by the OLT.

The OLT is usually composed by multiple OLT channel terminations (CTs) connected by a wavelength multiplexer (WM). This allows simultaneously data transmission in several channels that makes possible to attend quickly each one of the ONUs.

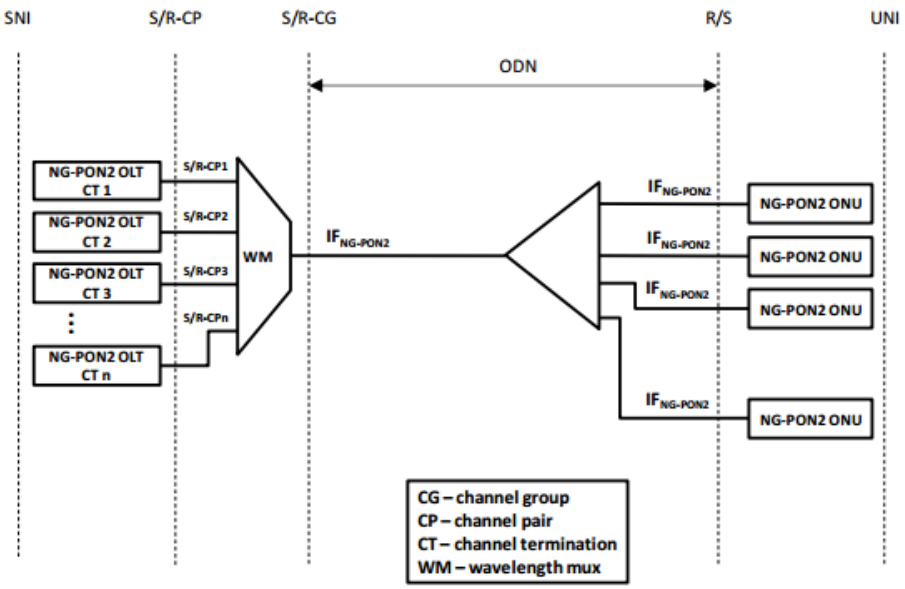

Figure 2- NG-PON2 reference logical architecture

There are two directions for optical transmission in the ODN. The downstream that is the direction of the signal that travel from the OLT to the ONU and the upstream which is the direction of the signal that travels in opposite direction. The transmission in the ODN in both directions go thought the same fiber and components.

2.6 Requirements for NG-PON2

The general requirements of NG-PON2 will be explained in more detail during the following sections. The main topics that will be explained are the general requirements for the ONU and OLT with different bitrates, the wavelength plans and the ODN optical classes. First an explanation will be given about the types of bit rates available and the fiber reach.

2.6.1 Bit Rate

NG-PON2 systems must have multiple wavelength channels in a TWDM architecture (4-8 TWDM channel pairs). In the beginning it is expected the use of only 4 channel pairs, in this case there are three types of bit rates available per wavelength, 2.5 Gbps for upstream (US) and 10 Gbps downstream (DS), 10 Gbps symmetry, 2.5 Gbps symmetry. So, the transmission capacities for each line rate are, 10 Gbps US and 40 Gbps (DS), 40 Gbps symmetry, and 10 Gbps symmetry. In one hand is expected that 10/40 Gbps asymmetric capacity will be used by domestic users, on the

other hand, it is expected that 40 Gbps symmetric is used by business users. In the case that all the 8 wavelengths are used, it will be possible to have 80 Gbps downstream and upstream.[3]

2.6.2 Fiber Reach

NG-PON2 systems must have at least 40 km of fiber reach without any REs, however if is necessary it is possible to reach more 20 km using REs, so the max fiber reach will be 60 km.[3]

2.6.3 Wavelength plans for NG-PON2

The wavelength bands for NGPON-2 are show in Table 1. The plan is defined to enable the coexistence through wavelength overlay with the already implemented PON systems. Using a shared spectrum allows full co-existence with GPON, XG-PON1, RF video overlap and TWDM.[3]

Table 1 – NG-PON2 wavelength plan [3]

TWDM PON		PtP WDM PON
Downstream	Upstream	US/DS
1596-1603 nm	Wide Band option 1524-1544 nm Reduced Band option 1528-1540 nm Narrow Band option 1532-1540 nm	Expanded Spectrum 1524-1625 nm (Note 1) Shared Spectrum 1603-1625 nm (Note 2)

The wavelength bands available in NGPON-2 for PtP WDM depend on the coexistence requirements. If the expanded spectrum window (1524-1625) is used the coexistence with the legacy PON systems (GPON, RF Video, XG-PON1) and also with NG-PON2 TWDM is lost.

In the case of TWDM PON three bands are available. The narrow band is the one who has the less spectrum available, and so the channel spacing has to be reduced. The use of the narrow band will require lasers with a narrow linewidth, however the laser tuning range can be shorter due to the fact that the channels are closer. In Figure 3 it can be seen the available spectrum for NG-PON 2.

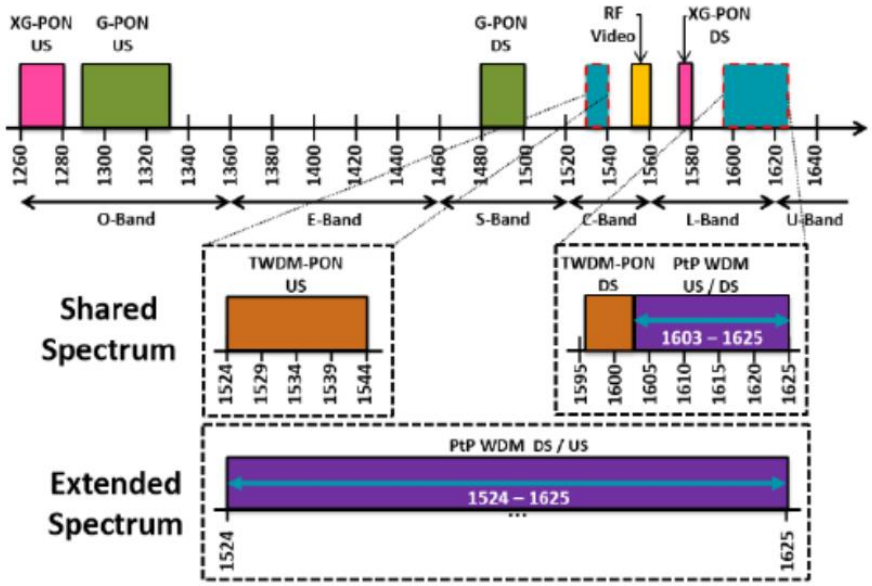

Figure 3 Optical spectrum available for NG-PON2. [13]

The central frequencies used for the downstream are fixed, so the respective band used is respected and the channels space of 100GHz is guaranteed. However for the upstream, the central frequencies vary with the chosen band. In Table 2, it's possible to observe the central frequency and consequently the wavelength of the several channels, for both downstream and upstream (with narrow band).

Table 2 – NG-PON2 Downstream and Upstream (narrow band) channels with central frequency and respective wavelength[3]

	Downstream		**Upstream**	
Channel	**Central Frequency (THz)**	**Wavelength (nm)**	**Central Frequency (THz)**	**Wavelength (nm)**
1	187.8	1596.34	195.6	1532.68
2	187.7	1597.19	195.5	1533.47
3	187.6	1598.04	195.4	1534.25
4	187.5	1598.89	195.3	1535.04.
5	187.4	1599.75	195.2	1535.82
6	187.3	1600.60	195.1	1536.61
7	187.2	1601.46	195.0	1537.40
8	187.1	1602.31	194.9	1538.19

2.6.4 ODN Optical Path Loss Classes

The OND optical classes takes into account a 15dB differential optical path loss and optical path penalties. They specify the maximum and the minimum losses that ODN should have. This values are specified in Table 3.

Table 3 - ODN Optical Path Loss Classes (ODN Classes)[3]

	Class N1	**Class N2**	**Class E1**	**Class E2**
Maximum differential optical path loss	15 dB			
Minimum optical path loss	14 dB	16 dB	18 dB	20 dB
Maximum optical path loss	29 dB	31 dB	33 dB	35 dB

ODNs may have less optical path losses than the stated minimum loss values above. However ODN must contain measures to guarantee the minimum optical path loss for the relative class, in order to prevent the Bit Error Rate (BER) degradation and potential losses in the receivers.[3]

2.6.5 ONU Requirements

Each ONU is equipped with a tunable transmitter and receiver, which are important to implement colorless ONUs [5]. If the ONU is capable of tuning, it becomes possible to change the channel which is being propagated, but also to select the channel that is going to retrieve the signal. Based on the tuning, the ONUs can be divided onto 3 classes. Class 1 is the most demanding, since it requires a lower limit of tuning time, bellow 10 μs, while for class 2 the limit is between 10 μs – 25 ms. However for class 3, the tuning time is the longer, permitting a tuning time between 25ms – 1s.[3]

The requirements for the ONU vary according the bitrate but also the ODN class and link type. In Table 4 and Table 5, the requirements are summarized for bitrates on the order of 2.5Gbits/s and 10Gbits/s, respectively.

Table 4 – Optical Interface Parameters of the ONU at 2.5 Gbps

Transmitter	Nominal line rate	2.48832 Gbit/s
	Minimum Operating channel spacing	50 GHz
	Maximum Operating channel spacing	200 GHz
	Line Code	Scrambled NRZ

	Minimum side mode suppression ration	30 dBm			
	ODN Class	N1	N2	E1	E2
	Mean Channel Launch power minimum				
	Type A link	+4 dBm	+4 dBm	+4 dBm	+4 dBm
	Type B link	0 dBm	0 dBm	0 dBm	0 dBm
	Mean Channel Launch power maximum				
	Type A link	+9 dBm	+9 dBm	+9 dBm	+9 dBm
	Type B link	+5 dBm	+5 dBm	+5 dBm	+5 dBm
	Minimum Extinction Ratio	8.2 dBm			
Receiver	BER reference level	10^{-4}			
	ODN Class	N1	N2	E1	E2
	Sensitivity	-30 dBm	-30 dBm	-30 dBm	-30 dBm
	Overload	-10 dBm	-10 dBm	-10 dBm	-10 dBm

Table 5 - Optical Interface Parameters of the ONU at 10 Gbps

Transmitter	Nominal line rate	9.95328 Gbit/s			
	Minimum Operating channel spacing	50 GHz			
	Maximum Operating channel spacing	200 GHz			
	Line Code	Scrambled NRZ			
	Minimum side mode suppression ration	30 dBm			
	ODN Class	N1	N2	E1	E2
	Mean Channel Launch power minimum				
	Type A link	+4.0 dBm	+4.0 dBm	+4.0 dBm	NA
	Type B link	+2.0 dBm	+2.0 dBm	+2.0 dBm	+4.0 dBm
	Mean Channel Launch power maximum				
	Type A link	+9.0 dBm	+9.0 dBm	+9.0 dBm	NA
	Type B link	+7.0 dBm	+7.0 dBm	+7.0 dBm	+9.0 dBm
	Minimum Extinction Ratio	6 dBm			
Receiver	BER reference level	10^{-3}			
	ODN Class	N1	N2	E1	E2
	Sensitivity	-28.0 dBm	-28.0 dBm	-28.0 dBm	-28.0 dBm
	Overload	-7.0 dBm	-7.0 dBm	-7.0 dBm	-9.0 dBm

2.6.6 OLT Requirements

The main requirements for the OLT, are described on Table 6 and Table 7, respectively for 2.5Gbits/s and 10Gbits/s.[3]

Table 6 - Optical Interface Parameters of the OLT at 2.5 Gbps

Transmitter	Nominal line rate	2.48832 Gbit/s
	Operating wavelength band	1596-1603 nm
	Operating channel spacing	100 GHz

	Line Code	Scrambled NRZ			
	Minimum side mode suppression ration	30 dBm			
	ODN Class	N1	N2	E1	E2
	Mean Channel Launch power minimum	+ 0 dBm	+2.0 dBm	+4.0 dBm	+6.0 dBm
	Mean Channel Launch power maximum	+4.0 dBm	+6.0 dBm	+8.0 dBm	+10 dBm
	Minimum Extinction Ratio	8.2 dBm			
Receiver	BER reference level	10^{-4}			
	ODN Class	N1	N2	E1	E2
	Sensitivity				
	Type A link	-26 dBm	-28 dBm	-30.5 dBm	-32.5 dBm
	Type B link	-30 dBm	-32 dBm	-34.5 dBm	-36.5 dBm
	Overload				
	Type A link	-5 dBm	-7 dBm	-9 dBm	-11 dBm
	Type B link	-9 dBm	-11 dBm	-13 dBm	-15 dBm

Table 7 - Optical Interface Parameters of the OLT at 10 Gbps

Transmitter	Nominal line rate	9.95328 Gbit/s			
	Operating wavelength band	1596-1603 nm			
	Operating channel spacing	100 GHz			
	Line Code	Scrambled NRZ			
	Minimum side mode suppression ration	30 dBm			
	ODN Class	N1	N2	E1	E2
	Mean Channel Launch power minimum	+ 3.0 dBm	+5.0 dBm	+7.0 dBm	+9.0 dBm
	Mean Channel Launch power maximum	+7.0 dBm	+9.0 dBm	+11.0 dBm	+11.0 dBm
	Minimum Extinction Ratio	8.2 dBm			
Receiver	BER reference level	10^{-3}			
	ODN Class	N1	N2	E1	E2
	Sensitivity				
	Type A link	-26.5 dBm	-28.5 dBm	-31.0 dBm	NA
	Type B link	-28.5 dBm	-30.5 dBm	-33.0 dBm	-33.0 dBm
	Overload				
	Type A link	-5.0 dBm	-7.0 dBm	-9.0 dBm	NA
	Type B link	-7.0 dBm	-9.0 dBm	-11.0 dBm	-11.0 dBm

2.6.7 Considerations relatives to ONU and OLT parameters

- Type A link values assume an unamplified OLT receiver. However, an amplified OLT receiver is not prohibited.
- Type B link values assume an amplified OLT receiver with the amplifier at the S/R-CG reference point. However, other amplifier approaches, including an unamplified OLT receiver are not prohibited.
- It is possible to use a lower extinction ratio, however it must be compensated by a larger transmitter launch power within the limits of the “Mean launch power maximum” value. [3]

3. PICs Components

PICs are the equivalent of electronic integrated circuits in the optical domain. In electronics integrated circuits an extensive range of functionalities is realized from a relatively small set of basic building blocks, like transistors, resistors, diodes capacitors and interconnection tracks. By connecting these building blocks in different numbers and topologies we can observe a huge variety of circuits and systems, with complexities ranging from a few hundred up to over a billion transistors. In photonics we can do something comparable. Observing the functionality of the optical circuits we see that most of them consist of a rather small set of components. Some of them actives like: lasers, modulators, optical amplifiers and photodetectors. Others passives like couplers, filters and de/multiplexers. These components can be reduced to an even smaller set of basic building, the passive waveguides and the active waveguides where its functionalities are dependent on the type of the guide, length, width, and in case of the actives also the electrical current.

In this chapter it will be explained the operation and main characteristics of some of the optical components used in PICs. In the section about MMIs, a script developed in MATLAB which allows modeling a MMI also will be presented. In the section about MZM will be presented an animation that demonstrates the behavior of a MZM. This animation was developed with the results of the simulation of an MZM using the OptoDesigner software.

3.1 Distributed-feedback laser (DFB)

One of the most used lasers in the construction of the PICS it's the DFB laser, and its main alternative the Distributed Bragg Reflector (DBR) laser. Single-mode lasers such as distributed feedback lasers are suitable candidates to ONU transmitters. That is due to their high-speed direct modulation property, tunable capacity and excellent single-mode behavior with a very small spectral width (in order of a few MHz).[14] To understand how DFB laser works, is important to understand the radiation mechanisms in a semiconductor. There are three radiative mechanisms possible: spontaneous emission, stimulated emission and stimulated absorption (see Figure 4).

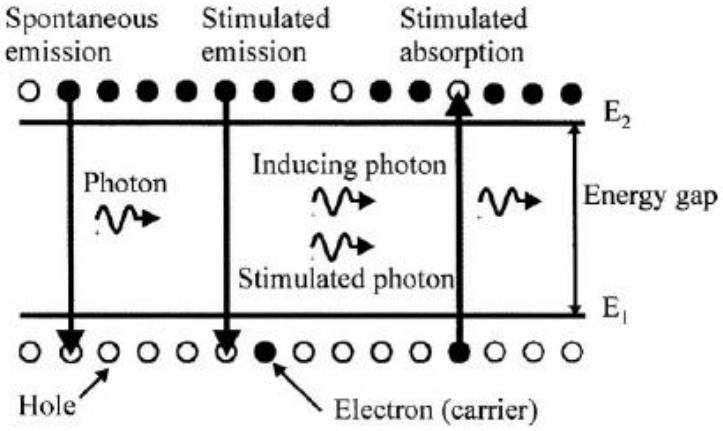

Figure 4 - Spontaneous and stimulated processes [15]

In the spontaneous emission process, a carrier from the conduction band (CB) spontaneously recombine with a valence band (VB) hole and emit a photon with random phase, direction and can have a wide range of frequencies. The stimulated emission occurs due the incidence of a photon with proper energy on the semiconductor that causes a stimulated recombination of a conduction band CB carrier with a VB hole. The carrier loses its energy in the form of a photon of light identical to the incident photon. The incident photon and the stimulated photon, can continue to induce more stimulated transitions. In stimulated absorption an incident photon with enough energy, stimulates a carrier from the VB to the CB. In this process the incident photon is extinguished.[15]

All lasers, emit light due the process of stimulated emission. To have gain, stimulated emission must be dominant, so it is necessary population inversion. The light emitted by the lasers is called coherent light because the photons emitted have the same characteristic of frequency, direction and phase.

The DFB laser is constructed placing a grating close to the active region. A periodic variation of the waveguide refractive index is given by the grating. The optical feedback is provided in the whole cavity in a DFB laser. The waves that propagate in forward and backward directions are coupled with each other. However with the grating the coupling only occurs for wavelength λ_B, which related with refractive index n_{eff} and Λ the grating period.

$$\lambda_B = 2n_{eff}\Lambda \quad (1)$$

Basically the grating acts as the wavelength selective element. The Figure 5, shows the DFB structure.

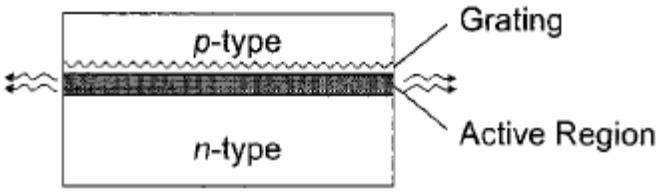

Figure 5- Structure of a DFB laser [16]

The output power of a DFB laser follows the injected current. An on-off keying (OOK) signal can be generated by turning on and off the laser, injecting or not a current. [16]

The emission wavelength of a DFB laser largely depends on temperature, this can lead to have problems if temperature is not controlled. However the dependence of the emission wavelength with temperature can also be used to make tunable DFB lasers, where the temperature can be changed by injecting current in a resistor join to the laser. The increasing of current in the resistor will lead to more power dissipation in the form of heat, due to this fact the laser cavity volume and their refractive index will change resulting in a wavelength variation. [17]

With the increasing of the laser drive current, and consequent output power, the temperature of the laser also changes, this leads to wavelength variations. The laser temperature is also controlled using thermoelectric coolers (TECs) that allow reduce the laser temperature

When energy is pumped into the laser, the fast transition from a spontaneous emission mode to stimulated emission mode occur, it is called the threshold. The current that needs to be injected in the laser to achieve the threshold is called the threshold current. [18]

The threshold current increase exponentially with the temperature and can be obtained by:

$$I_{th}(T) = I_0 e^{\left(\frac{T}{T_0}\right)} \quad (2)$$

Where, I_0 and T_0 are constants experimentally determined and T is the temperature. The emission proprieties of a semiconductor laser are characterized by the P-I curve. It indicates the threshold level and also the current that needs to be applied to reach a certain output power. An example of P-I curves for an InGaAsP laser at different temperatures is show in Figure 6.[19]

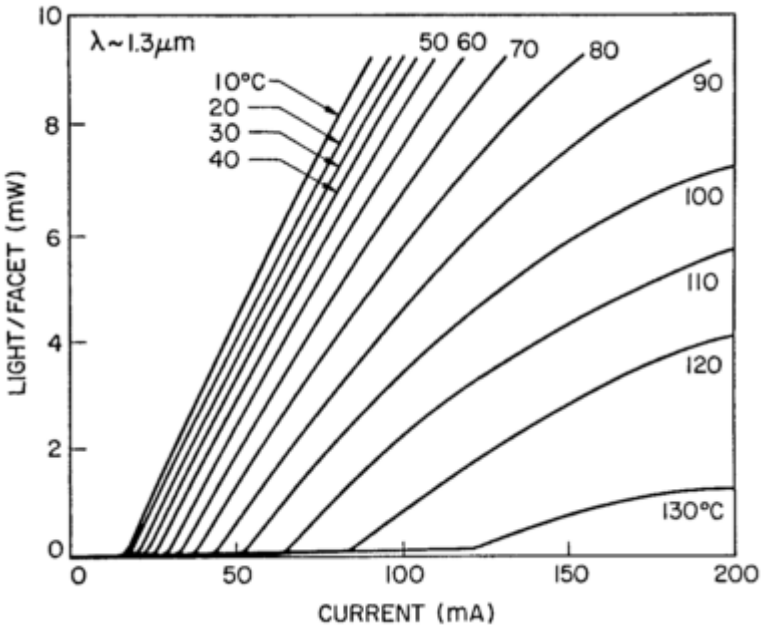

Figure 6 -Example of a semiconductor laser P-I curve for different temperatures[19]

The laser can be directly or externally modulated. In direct modulation, the radiant power of the light source is modulated by the laser drive current. The main advantage of this type of modulation is their simple design. Light sources in direct modulation transmitters are represented by light emitting diodes or direct modulation lasers. A schematic of direct modulation is presented in Figure 7.

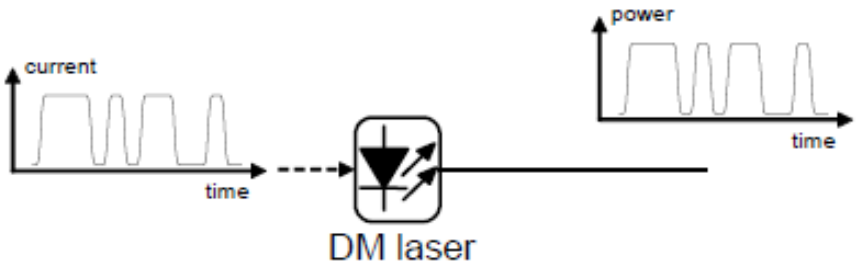

Figure 7 - Directed modulation System [20].

In terms of costs, the use of direct modulation is cheaper. However it has problems like distortion, lower extinction rate, chirp and bandwidth limitations. This limitations will condition the most complex transmission systems.

To overcome the distortion, chirp, and bandwidth limitations of direct modulation, it is desirable to apply the external modulation to the laser cavity, using a separate modulator component. A schematic of external modulation is presented in Figure 8.

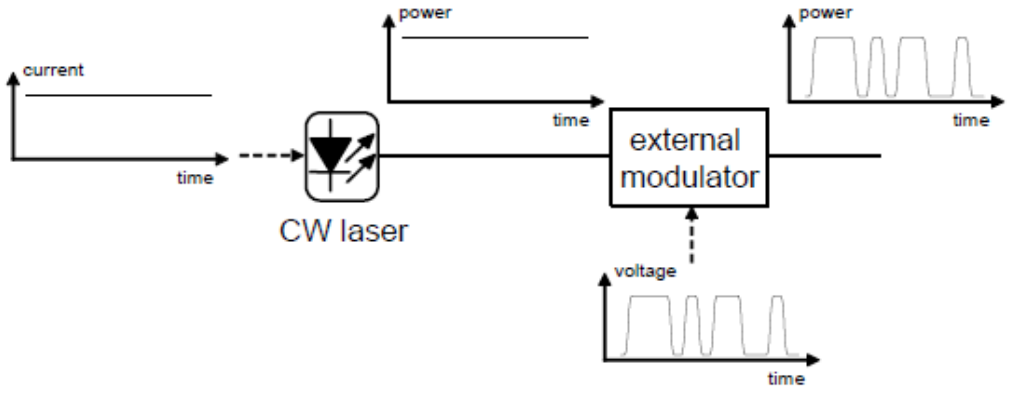

Figure 8 - External modulation System [20].

Due that the laser operates with a continuous wave (CW) regime, the output power can be optimized for a highest value without regards for its modulation bandwidth. The use of external modulators also allows increase the extinction ratio.

3.2 Modulators

3.2.1 Electroabsorption Modulators

The electroabsorption modulators uses the principle that the effective bandgap of a semiconductor material decreases when a voltage is applied. If the frequency v of the received light wave is chosen so that its energy E = hv is smaller than the bandgap, the material will be transparent when no voltage is applied. In case that an external voltage is applied, the effective bandgap will be reduced, leading that the light wave will be absorbed by the material when E > Eg. Selecting the signal wavelength that experiences a significant change in absorption when the voltage is applied, it thus becomes possible to achieve optical modulation controlled by an electrical signal[20].

3.2.2 Phase modulator

In an optical phase modulator (PM) a voltage signal changes the material refractive index, and consequently the phase of the output the electrical field. It can be fabricated as an integrated optical device by embedding an optical waveguide in an electro-optical substrate. A schematic of a phase modulator can be seen in Figure 9.

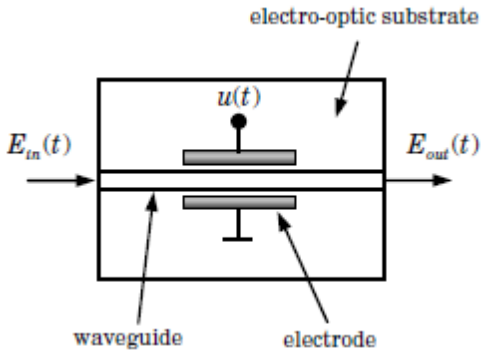

Figure 9 - Phase modulator.[21]

The necessary driving voltage for achieving a phase shift of π, represented as V_π, is typically given. The relation of the input optical carrier $E_{in}(t)$ and the output phase modulated optical field $E_{out}(t)$, when neglecting the constant optical phase shift of the modulator, can be expressed as [21].

$$E_{out}(t) = E_{in}(t)e^{j\frac{u(t)}{V_\pi}\pi} \tag{3}$$

3.2.3 Mach-Zehnder Interferometer Modulators

The Mach-Zehnder interferometer-based modulator structure, uses the same principle of interference as phase modulator. The MZM exploits the phase difference between the two branches to modulate the signal. The light inputs and through a Y-junction is split into two beams. Each of the beams go through the phase modulator of each arm, the fields are then recombined at the Y-junction on the output. Depending on the phase delay between them the interference can be constructive or destructive.

The MZMs can be single-drive or dual-drive depending if they have the phase modulators in one or in both arms. In dual-drive MZMs, the phase modulators in both arms can be driven independently. A MZM dual-drive can be seen in Figure 10.

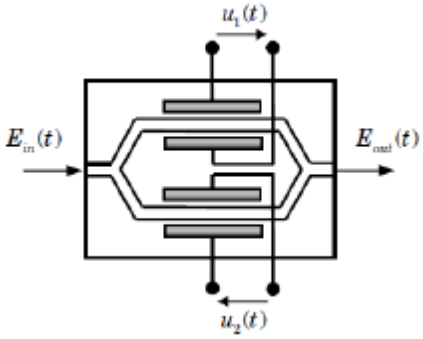

Figure 10 - Optical Mach-Zehnder modulator [21].

The phase in the modulator branch can be controlled through a bias voltage or current that change the refractive index of the material. Without considering the insertion loss, MZM have the following transfer function

$$\frac{E_{out}(t)}{E_{in}(t)} = \frac{1}{2} \cdot (e^{j\varphi 1(t)} + e^{j\varphi 2(t)}) \tag{4}$$

Where $\varphi_{1(t)}$ and $\varphi_{2(t)}$ represents phase shifts in the upper and lower arms of the MZM. The phase shifts are related to the driving signals with

$$\varphi 1(t) = \frac{u_1(t)}{V_{\pi_1}}\pi, \ \varphi 2(t) = \frac{u_2(t)}{V_{\pi_2}}\pi \tag{5}$$

Where $u_1(t)$ and $u_2(t)$ are the driving voltages defined in Figure 10, $V_{\pi 1}$ and $V_{\pi 2}$ are the drive voltages required to obtain a phase shift of π in the upper and lower arms respectively.

When the MZM operates "push-push" mode, which means that an identical phase shift exist between both arms, the MZM operates like a simple PM. If there is a negative phase difference from one arm to another, the MZM operates in "push-pull" mode and is obtained an amplitude modulation without chirp.[21].

3.2.3.1 MZM Simulation in OptoDesigner

In this section a MZM was simulated using the software OptoDesigner®. OptoDesigner® is a software from Phoenix Software® which allows to simulate the propagation of light over integrated optic devices. In OptoDesigner®, the simulations are done through component description using the programming language C++.In the process of designing a PIC, this software is used for placing the components together, simulate the behavior of some of them and generate the mask for the foundry.

MZM Construction

The construction of the MZM is made by steps. First is created a straight waveguide where the signal will enter. After the straight waveguide is connected to a splitter. In each arm of the splitter is connected other straight wave guide. Next is used an inverted splitter with an arm connected to the top waveguide and other to the bottom waveguide. Finally a straight waveguide is connected to the splitter, which will be the output of the MZM.

For the background of the refractive index was used 1.45. For the other parts the refractive index is 1.475. However the refractive index of the upper arm (at green in Figure 11) was defined in a separate variable, to allow its incrementation during the simulation without changing the refractive index of the rest of the elements. The waveguide width was 2μm, with this width it is a single mode waveguide. The wavelength used was 1550 nm.

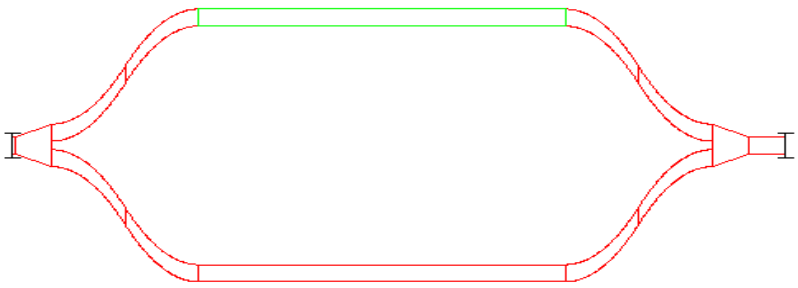

Figure 11 – Layout of the MZM

Simulation with the beam propagation method (BPM)

To simulate the light propagation in the MZM the BPM was used. With this method during each propagation step the refractive index profile is constant. This means that if waveguide runs at an angle with respect to the propagation direction, it is subdivided into straight, horizontal sections. The BPM is unidirectional, so a "forward only" propagation is simulated. The reflection effects are neglected. The simulation was done for transverse electric (TE) propagation, but is also possible to choose transverse magnetic (TM) propagation. In order to launch power in one of the inputs the software provides a ModeLauncher. The user defines the position to put it as well as the beam characteristics (power and phase). For the outputs, the software provides a ModeOverlap. The user can choose where to place them. In this case ModeLauncher and ModeOverlap were placed on the left and right extremity of the MZM respectively. In this simulation the BPM was applied to the entire structure. However it is possible to a run BPM simulation for a specific zone. This is useful, especially in simulations that includes several components, and that their simulation takes a long time to finish.

For running 22 iterations of the BMP simulation a "for" cycle was used. At each time the refractive index of the MZM upper arm was increased 0.0002. So the refractive index will vary from 1.4750 to 1.4794. In the practice the refractive index variation can be done by applying an external voltage or increasing the material temperature. The obtained transfer function obtained is shown in Figure 12.

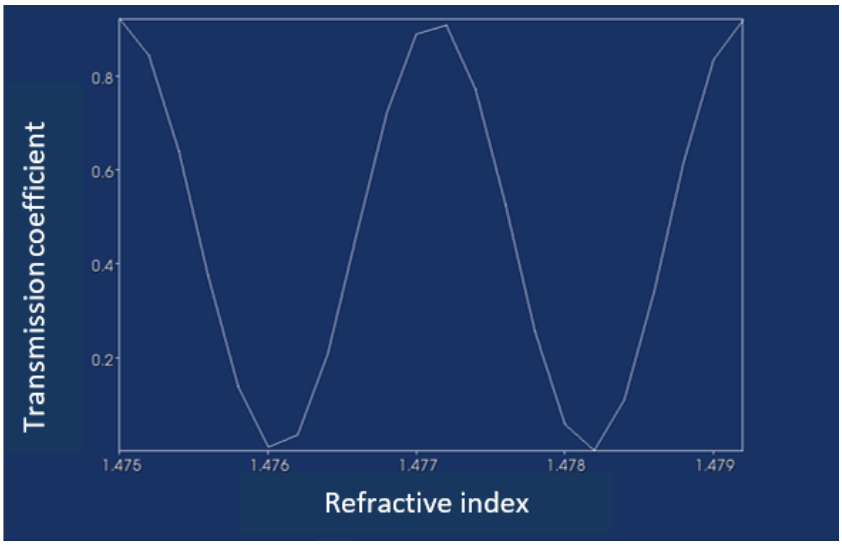

Figure 12 – MZM transfer function

At each iteration, the plots of the electrical field strength and the phase were saved. Figure 13 shown the BPM results in phase and opposition of phase. In the left is shown the electric field strength and in right the respective phase. In Figure 13-a) is possible to observe that all the energy is divided equally by the two arms of the MZM, and when both waves join they interfere constructively. This happens due the fact that they are in phase. Figure 13 -c) is shown that the energy also is equally divided by both arms, however in this case when the waves are join the all energy spreads. This happens because the waves are in phase opposition leading to destructive interference.

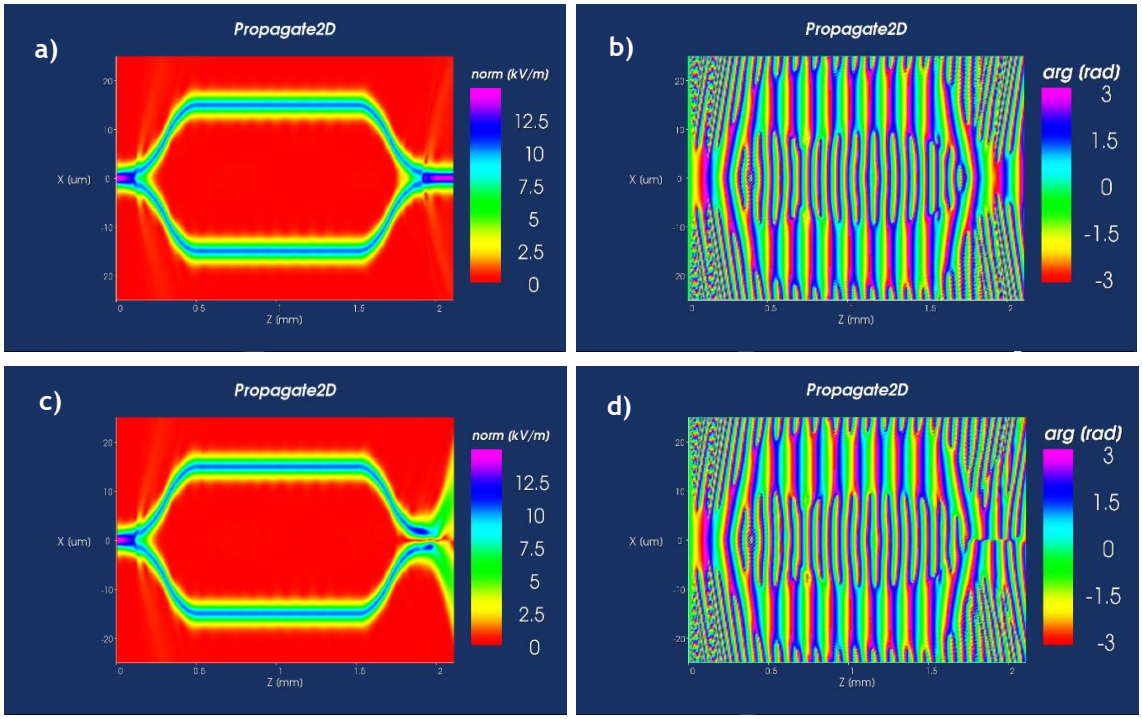

Figure 13 –BPM results: a) electric field strength, b) phase, in the case that both harms are in phase. c) Electric field strength, d) phaser, in the case that both harms are in opposition of phase.

With all results obtained, an animation was developed, a picture of the animation is shown in Figure 14. The animation shows the electric field strength, and the respective phase changing with the variation of the refractive index. In the upper left corner it is possible to see the transfer

function. The red dot, points the value of the reflective index and the respective transmission coefficient in each iteration of the animation.

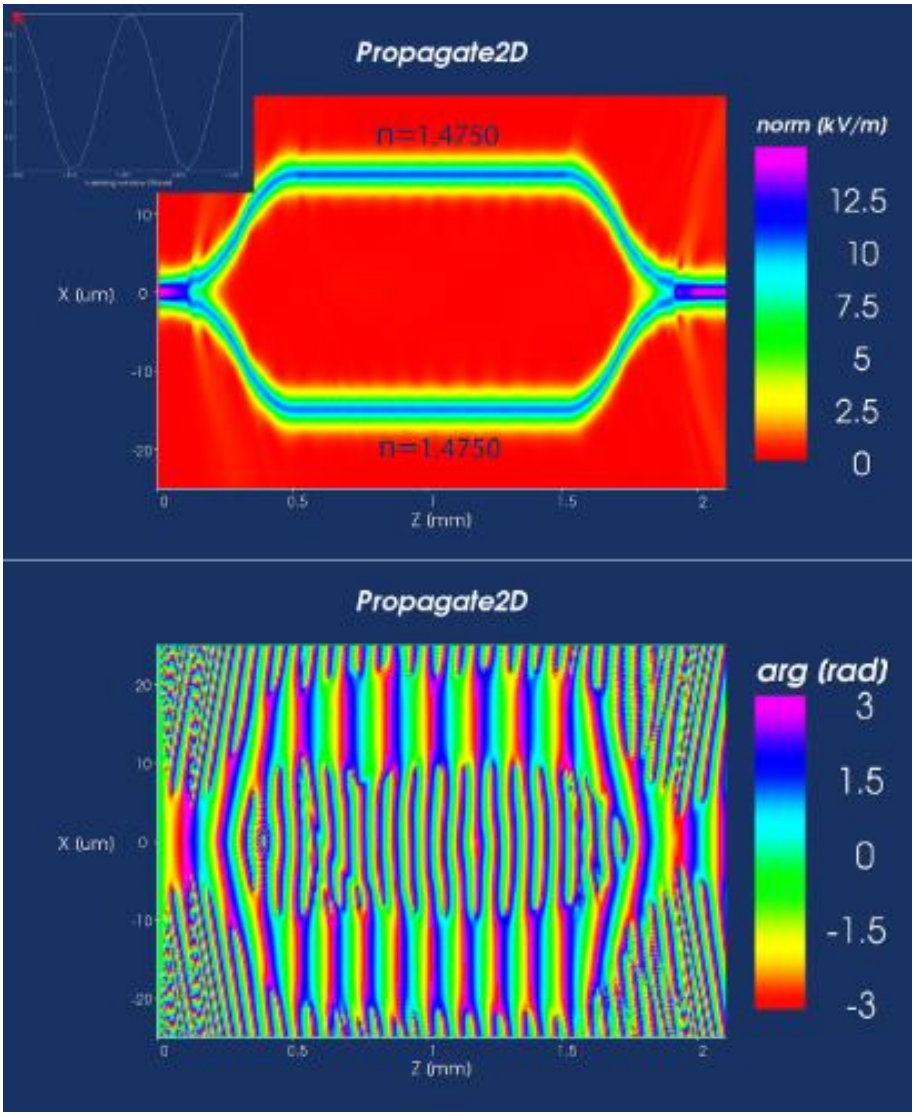

Figure 14 – Picture of the developed animation

Looking into the animation it can be observed that the light waves are spreading between the two arms. The electric field strength is equal in both arms. However when the waves are coupled, the electric field strength, depends on the lag between the waves propagated in the upper and bottom arms. When the propagated waves are in phase almost all power is transmitted. However, the transmission power reduces with the increase of the phase lag. In the case of the opposition of phase, the guided modes will disperse what leads to a null strength of the electric field.

3.3 Arrayed Waveguide Grating (AWG)

In modern optical communication systems, the Arrayed waveguide grating passive optical waveguide devices are the most widely deployed de/multiplexing devices. AWGs can be used, on chip-scale, to realize optical multiplexer, demultiplexer, cross-connect and router functions, as well different digitally tunable diode laser cavities. The AWG function is similar to an optical prism, which imaging the input optical field in different spatial output locations based on the wavelength of the input light. The layout of an AWG is presented in Figure 15 [22].

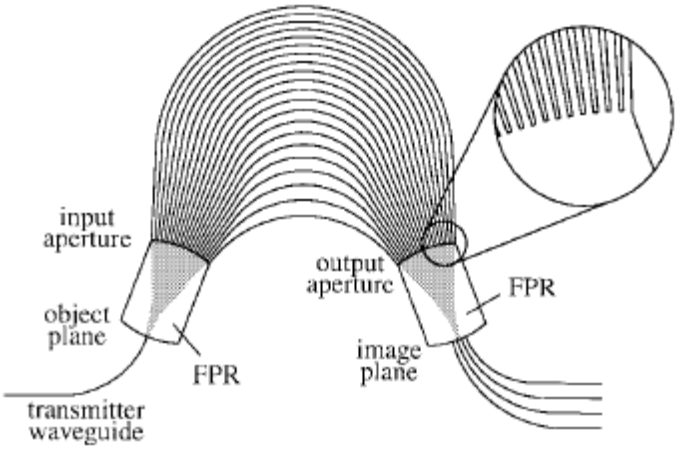

Figure 15 - Layout of an AWG demultiplexer [22]

AWGs has three main elements: a set of two star couplers, which are a free propagation region (FPR), and a set of interconnecting arrayed waveguides. The star couplers are generally based on the Rowland circle construction, where the radius of curvature of the input and output waveguide planes is half of the radius of internal waveguide array planes.

In terms of device operation, the light from the input waveguide radiates into the first star coupler slab waveguide and excites the modes of the arrayed waveguides at the star coupler output. After traveling through the arrayed waveguides, the light from the waveguides is diffracted into the output star slab waveguide, where it constructively converges in one focal point at the output of the star coupler. Due the path length difference between the arrayed waveguides results in a relative phase delay in each waveguide, which changes with wavelength. This will lead to different wavelengths being coupled to different output waveguides.[22]

3.4 SOA

The Semiconductor optical amplifier (SOA) is an optical amplifier which use a semiconductor to provide the gain. In Figure 16 is illustrated a schematic of the SOA. An optical signal launched into the input of an SOA will get gain through stimulated emission. But in addition it also will be affected by optical noise, caused by the spontaneous emission, and the noise also will be amplified through stimulated amplification while propagating through the SOA.

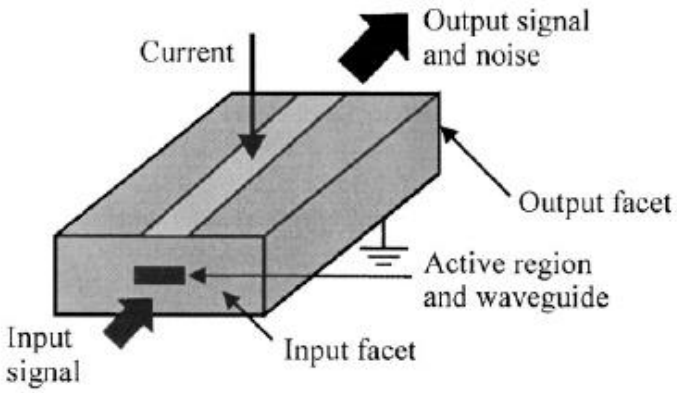

Figure 16 - Schematic of an SOA [15].

Spontaneously emitted photons are essentially noise and also reduce the carrier population available for optical gain.

For the SOA to exhibit optical gain, the stimulated emission needs to be greater than stimulated absorption, for that the injected current need be sufficiently high to create a population inversion.[15].

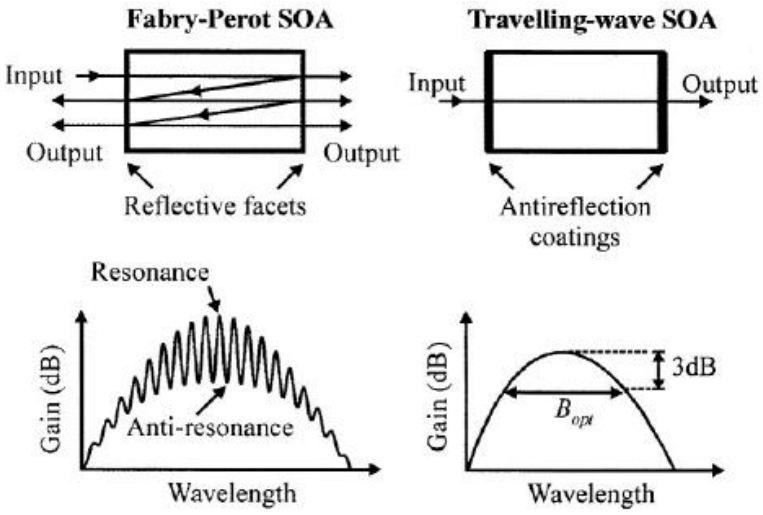

Figure 17 - Types of SOA and respective gain spectrums.

There are two main types of SOAs, both illustrated in FIGURE 17 with respective gain spectrums, the Fabry-Perot SOA (FP-SOA) where the light gets amplified as it reflects back and forth between the mirrors until emitted at a higher intensity. And the travelling-wave SOA (TW-SOA) where the end surfaces are either antireflection coated or cleaved at an angle so that internal reflection does not take place and the input signal gets amplified only once during a single pass through the device [15].

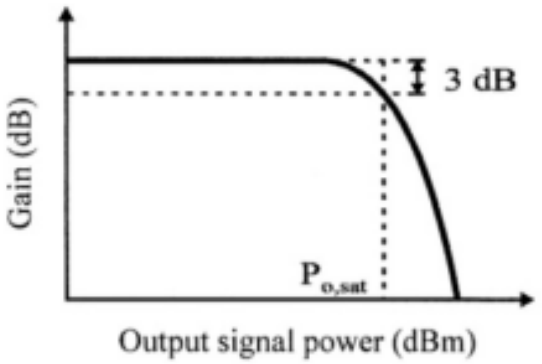

Figure 18 – Typical curve of SOA gain vs output signal power [15]

In Figure 18, is shown a typical curve of SOA gain vs output power. With increasing input power, the carriers in the active region become depleted leading to a decrease in the amplifier gain. This effect can lead to signal distortion. When are used multiple wavelength channels the SOA gain also is limited for this effect, because is necessary exist free carriers for each channel.

3.5 MMI

3.5.1 Principles

The devices based on multimode interference (MMI), have been used in several applications such as optical couplers, splitters, Mach Zehnder modulators, switches, waveguide division de/multiplexers, optical gates and ring lasers. Many of this devices are used in PIC [23].

The MMI devices are based on the self-imaging principle that say:

"Self-imaging is a property of multimode waveguides by which an input field profile is reproduced in single or multiple images at periodic intervals along the propagation direction of the guide."

This principle was described more than 170 years ago, and the possibility of perform self-imaging in uniform index slab waveguides was first suggested by Bryngdahl and explained in more detail by Ulrich [24]. This is a property of the multimode waveguides by which an input field profile is periodically reproduced as a single or multiple images while propagating through the multimode waveguide, as shown in Figure 19.

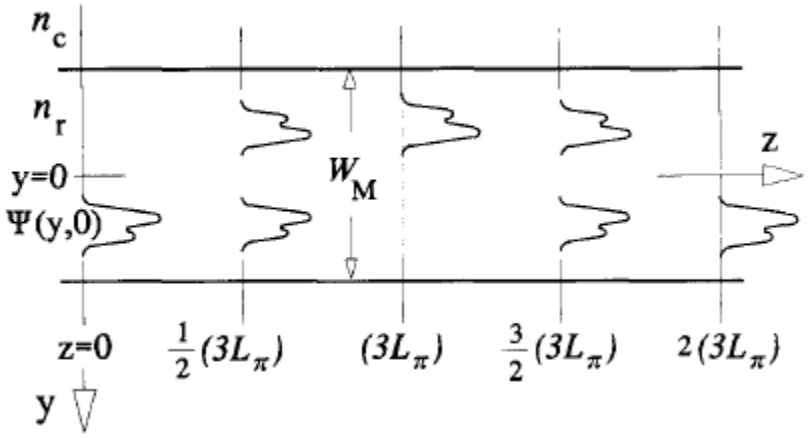

Figure 19 - Multimode waveguide showing the input field using general interference, a mirrored single image at (3Lπ), a direct single image at 2(3Lπ), and two-fold images at ½ (3Lπ) and 3/2(3L) [24].

In [24] Lucas B. Soldano demonstrated three main interference mechanisms, general paired and symmetric.

The summary characteristics of each one are resumed in following table.

Table 8 - Summary characteristics of general, paired and symmetric interference. [24]

Interference mechanism	**General**	**Paired**	**Symmetric**
Inputs x Outputs	M x N	2 x N	1 x N
First single image distance	$(3\ L_\pi)$	(L_π)	$(3\ L_\pi)/4$
First N-fold image distance	$(3\ L_\pi)/N$	$(L_\pi)/N$	$(3\ L_\pi)/4\ N$
Excitation requirements	None	$c_v=0$ for v =2,5,8…	$c_v=0$ for v =1,3,5…
Input(s) location (s)	any	$y= \pm W_e/6$	y=0

W_e is the effective width of corresponding the fundamental mode. For high-contrast waveguides, the penetration depth is very small so the value of W_e can be approximated to W_M. However taking into account the polarization dependence of the lateral penetration depth of each mode field, W_e is given by,

$$W_e = W_M + \left(\frac{\lambda 0}{\pi}\right)\left(\frac{n_c}{n_r}\right)^{2\sigma}(n_r^2 - n_c^2)^{-(1/2)} \quad (6)$$

Where W_M is the waveguide width, λ_0 the used wavelength, n_r the effective refractive index of the ridge, n_c effective refractive index of the cladding, σ=0 for TE and σ=1 for TM.

In the excitation requirements, C_v is the field excitation coefficients and v the mode numbers.

The L_π is the beat length of two lowest-order modes and is given by:

$$L_\pi = \frac{\pi}{\beta_0 - \beta_1} \approx \frac{4n_r W_e^2}{3\lambda_0} \quad (7)$$

As show in previous equation, L_π is proportional to the square of the effective width of the waveguide, so to obtain a small MMI the width must be small. However to obtain low-loss well-balanced 1-to-N splitting of a Gaussian field, the multimode waveguide is required to support at least one more mode than the number of outputs.[24]

With the general interference mechanism, an MMI can be built with M inputs and N outputs, there is no excitation requirements and no requirements in the position of the input. The first single image will appear in a symmetric position, according to the propagating axis of the input location.

The paired interference mechanism requires 2 input for N outputs. It allows to construct shorter devices comparing to the ones created using the general interference mechanism, because the first single image and first N-fold image will appear at a shorter distance. However the excitation requirements described in previous table need to be respected, and the location of the inputs must be at $\pm W_e/6$.

The symmetric mechanism requires that the input location must be in the y=0. And it also has excitation requirements. Exciting only the even symmetric modes, 1-to-N beam splitters can be realized with multimode waveguides four times shorter. This interference mechanism is the one who obtains the first single and N-fold images at shorter distance. It is followed by the paired mechanism, so if it is possible, the excitation requirements and the input location must be respected in order to design devices as small as possible.

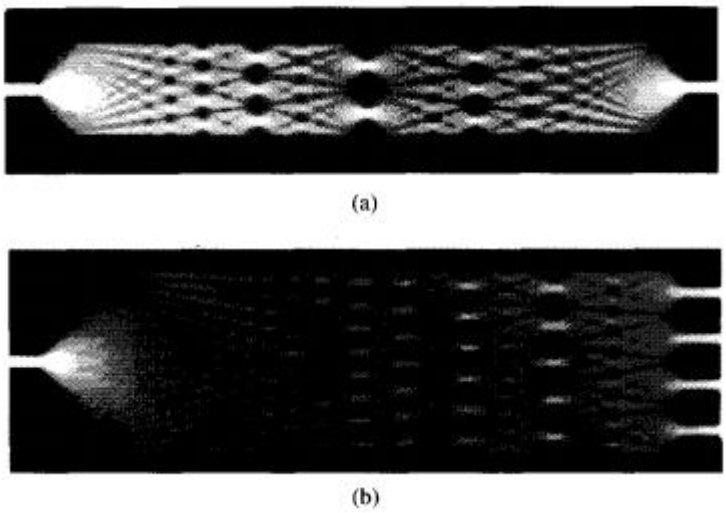

Figure 20 - Theoretical light intensity patterns corresponding to (single-input) symmetric interference mechanisms in a 20μm-wide multimode waveguide, showing "1x1" imaging (a); and in a 40μm-wide multimode waveguide, showing 1-to-4 way splitting (b) [24]

The Figure 20 shows the intensity patterns, using the symmetrical mechanism, inside the multimode waveguide with a single-input. In the mid-way of the self-imaging length, it is possible to observe the formation of two fold images. If the MMI had half of the length it could be used as 1x2 splitter.

Using the L_π dependence with the wavelength, it is possible to use an MMI as a demultiplexer of two wavelengths. For example, using the paired interference, the single image is formed at every even multiple of L_π, and at every odd multiple of L_π the mirror image will be formed at an anti-symmetric position. Finding the MMI length where at same time, the signal transmitted at wavelength "x" is focused in the single image and the signal transmitted in wavelength "y" is focused in the mirror image, is possible to separate them.

The structure effective length L_d necessary to separate the two wavelengths needs to satisfy the following equation:

$$L_d = pL_{\pi\lambda 1} = (p+q)L_{\pi\lambda 2} \tag{8}$$

Where p is an even integer, q is an odd integer, $L_{\pi\lambda_1}$ and $L_{\pi\lambda_2}$, are the beat lengths for the wavelengths λ_1 and λ_2. In [25] was done a polarization insensitive demultiplexer to separate

1310/1550 nm bands, in the Figure 21 is shown the field distribution for 1310 nm and 1550 nm for each polarization.

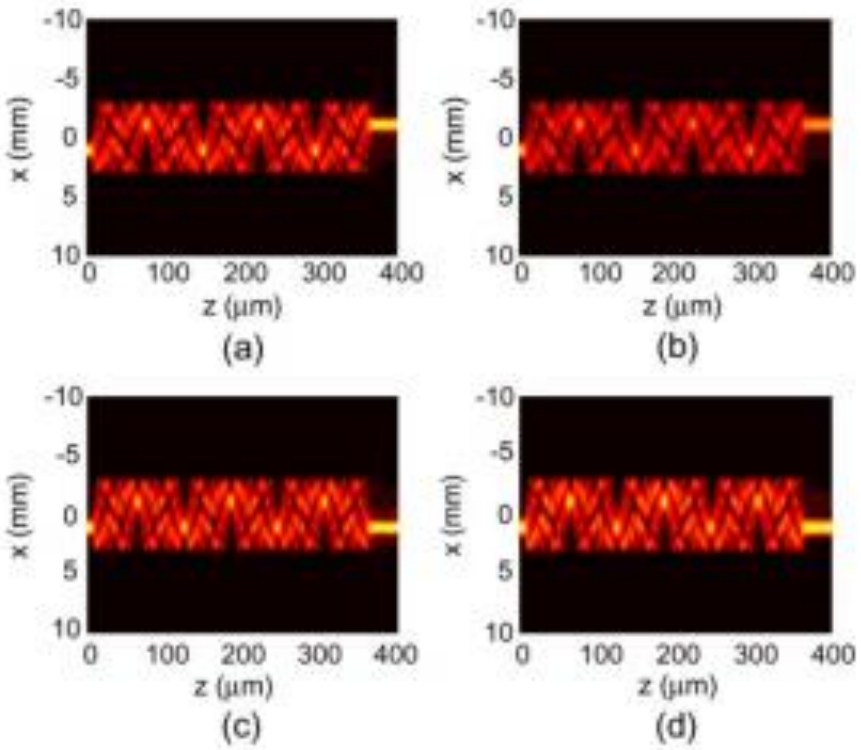

Figure 21 - Field distribution of MMI demultiplexer (a) quasi-TE mode at 1310 nm; (b) quasi-TM mode at 1310 nm; (c) quasi-TE mode at 1550 nm; (d) quasi-TM mode at 1550 nm. [25]

The polarization sensitivity of an MMI is an important factor in his construction, because the beat length depends on the polarization. This dependence can lead to different losses depending on the polarization used and to the wrong behavior of the device.

In this experiment the size of the MMI develop was relatively short, only 10μm x 360μm, this is achieved due to the specific refractive index of the materials used. However the MMI based wavelength splitters have an issue related to their extensive length when is used InP/InGaAsP, due to the low refractive index difference in the material system. In the conventional wavelength splitter structures, is verified that the optimum length to split the 1310nm and 1550 regions exceeds 5000 μm.[26]

In [26], a multi-section MMI 1.55/1.31 μm wavelength splitter with a length of 963.5μm has been demonstrated and simulated. The method is based on the use of a few multimode waveguides in sequence each one smaller than the previous one. The structure and the field simulations for 1.55μm and 1.31μm are shown in Figure 22.

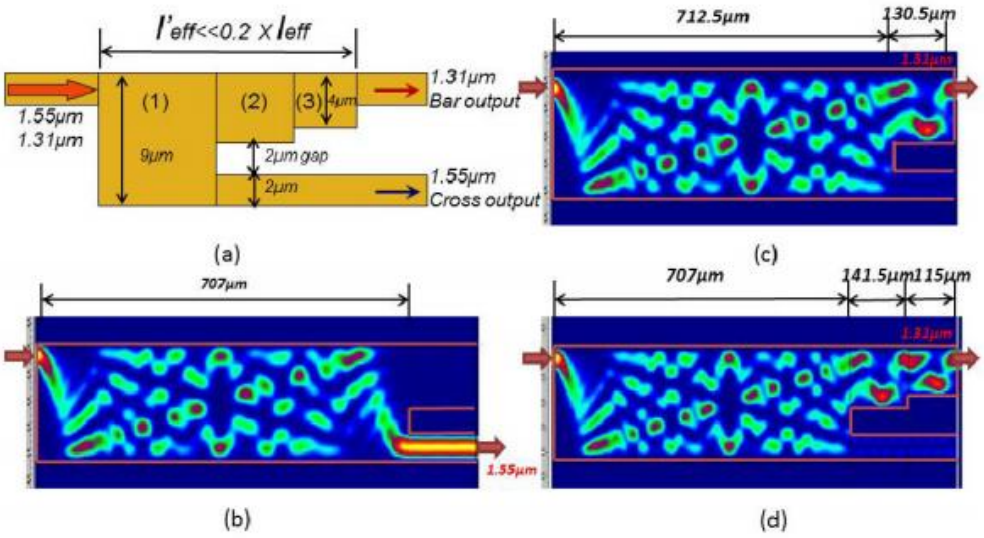

Figure 22 - (a) Multi-section MMI wavelength demultiplexer; simulation results of field distribution: (b) at 1.55 μm, (c) at 1.31 μm without sub-collection MMI (3), (d) at 1.31 μm with sub-collection MMI. [26]

The 1.55/1.31 μm wavelengths are separated at the first MMI. At this length the 1.55 μm wavelength have a single mirror image and it can be collected for the single mode waveguide without many losses. However the 1.31 μm field still is dispersed, so to be collected is used a collector (2) followed by a sub-collector (3), which his function is to guide the field until a single image is formed and guided by the output waveguides. With this device was obtained an insertion loss of −0.62dB and −1.46dB at 1.55 μm and 1.31μm, respectively[26].

Based on the MMI principles used to create these devices, it is possible to create a coupler for NG-PON 2 downstream and upstream bands.

3.5.1 MATLAB script to Modeling a MMI

A MATLAB script based on MMI principles was developed. It allows the user to know some important parameters to design a MMI splitter/coupler.

As program inputs, the user needs to insert the wavelength, the number of inputs and outputs of the MMI, the ridge and cladding effective refractive index and choose TE or TM propagation. It is advised that user should choose the width of the MMI according to the previous studies of fabrication limits, power limits in inputs/outputs and the number of modes needed.

After receive the inputs, the algorithm chooses the interference mechanism for which is possible to obtain a shorter MMI. It then calculates the beat length (L_π) and total length of the MMI waveguide necessary to perform the splitting of M inputs to N outputs. The script also gives to the

user the information about the interference mechanism, input location and excitation requirements needed. The Figure 23, shows the program inputs/outputs.

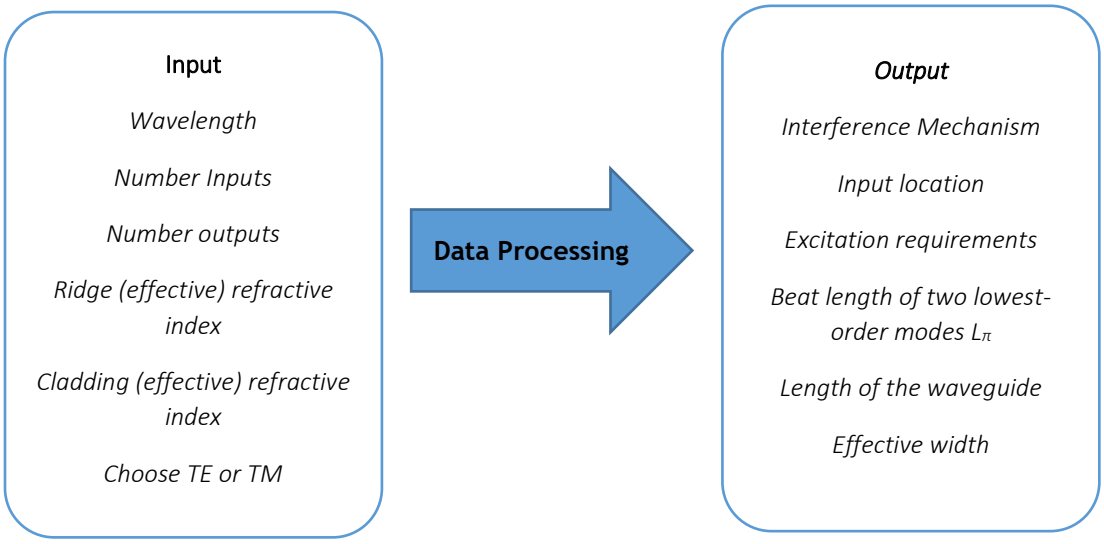

Figure 23 - Program inputs and outputs.

In Table 9 are shown some combinations of materials used in PICs construction and the respective refractive index. Due to the fact that the length of the MMI is proportional to the n_r, chose a material with low n_r allows the creation of shorter devices.

Table 9 - Some materials used in waveguides and respective refractive index.

Material	Refractive index
n_c SiO2	1.4501
n_r Si3N4	1.9792
n_c InP	3.17
n_r InGaAsP	3.364
n_c InP	3.17
n_r GaAs	3.29

In Table 10 are presented the program some of the program outputs (effective width, interference mechanism, beat length and the MMI length) for different cases. In this simulation it will always be considered a TE propagation and a wavelength of 1550 nm.

Table 10 – Simulations using the MMI MATLAB scrip for different cases

MMI Inputs	MMI Outputs	nr	nc	Width (μm)	We(μm)	Interf. Mec	L_π(μm)	Length(μm)
1	2	1.9792	1.4501	16	16.36	Symmetric	456	171
1	2	3.29	3.17	16	16.56	Symmetric	776	291
1	4	1.9792	1.4501	24	24.36	Symmetric	1010	190
1	4	3.29	3.17	24	24.56	Symmetric	1707	320
2	4	1.9792	1.4501	24	24.36	Paired	1010	253
2	4	3.29	3.17	24	24.56	Paired	1707	427
3	3	1.9792	1.4501	20	20.36	General	706	706
3	3	3.29	3.17	20	20.56	General	1196	1196

As it was expected due the lower refractive index, when SiO2/ Si3N4 is used it is possible to create shorter devices than when InP/GaAs is used. The results are according to the expectations, for example when it is used the paired interference the first 4-folded image will appear at a distance of $L_\pi/4$. In the case that is used general interference the 3 fold images will appear at L_π. Observing the results for 1x2 and 1x4 MMI it can be seen the impact of increasing the width, which leads to the length increase. And we must not forget that the 4-folded images will happen at half the distance of the 2 folded images.

3.6 Photodetectors

The function of a photodetector is to turn a signal of optical domain into a signal of electrical domain. In a photodetector the photons are absorbed and a proportional optical current is generated. When a photon has energy greater than the bandgap of a semiconductor material, the photon energy will be absorbed and an electron–hole pair will be generated in the semiconductor. With a voltage applied in semiconductor, it is created flow of electrical current.[19]. A semiconductor slab used as photodetector is shown in Figure 24.

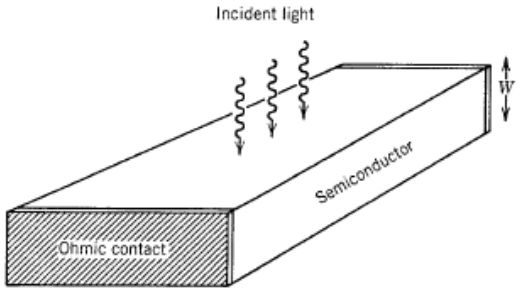

Figure 24 - A semiconductor slab used as a photodetector [19].

The electric current of photodetector I_p is directly proportional to the incident optical power P_{in},

$$Ip = R \cdot P_{in} \tag{9}$$

where R is the responsivity of the photodetector. The responsivity represents the photocurrent generated per unit of incident optical power and can be expressed as,

$$R = \frac{q\,\eta}{\mathrm{hf}} \approx \frac{\eta\lambda}{1.24} \tag{10}$$

with q the electron charge, h the Planck's constant, f and λ the photon frequency and wavelength, η the quantum efficiency. The responsivity will increase with the wavelength because more photons are present for the same optical power.

The quantum efficiency η, represent the ratio between the number of electrons generated per number of incident photons,

$$\eta = \frac{\text{electron generation rate}}{\text{photon incidence rate}} \tag{11}$$

Since each absorbed photon creates an electron–hole pair, the quantum efficiency can be written as

$$\eta = 1 - e^{-\alpha W} \tag{12}$$

Where α is the absorption coefficient and W the slab width. The absorption coefficient is dependent on the semiconductor material and the photon wavelength.

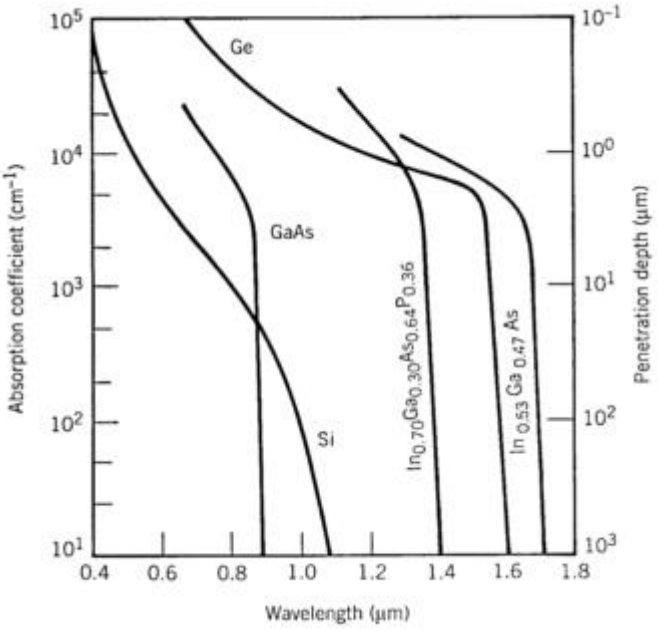

Figure 25 - Absorption coefficient as a function of wavelength for some important semiconductor materials used in photodetectors[19]

Figure 25, shows the relation between the absorption coefficient and the wavelength. To obtain an high responsivity, the absorbing material should have a bandgap very near, but above the high wavelength limit of the optical signal. The wavelength at which the absorption coefficient becomes zero is called the cutoff wavelength. Due to the change of the photodiode's responsivity with the wavelength, it will exhibit different sensitivities for different wavelengths.

The main requirements of a photodetector are [27]:

- Sensitivity at the required wavelength
- Efficient conversion of photons to electrons
- Small area for low capacitance and a fast response
- Low noise
- Sufficient area for efficient coupling to optical fiber
- Low cost

In optical systems there are used two main types of photodetectors, the p-i-n photodiode (PIN) and the avalanche photodiode (APD).The PIN photodiode will be explained in the following section.

3.6.1 PIN Photodiode

A PIN photodiode is basically a p-n photodiode with an intrinsic semiconductor layer, undoped or lightly doped, inserted in the center of the p-n junction.

The intrinsic layer increases the depletion-region width, which leads to a smaller junction capacity and consequently a greater bandwidth. The number of absorbed photons also increase, consequently the number of electron–hole pairs created rise and a better quantum efficiency is obtained. Figure 26 shows the device structure with the electric-field distribution under reverse-bias operation [19].

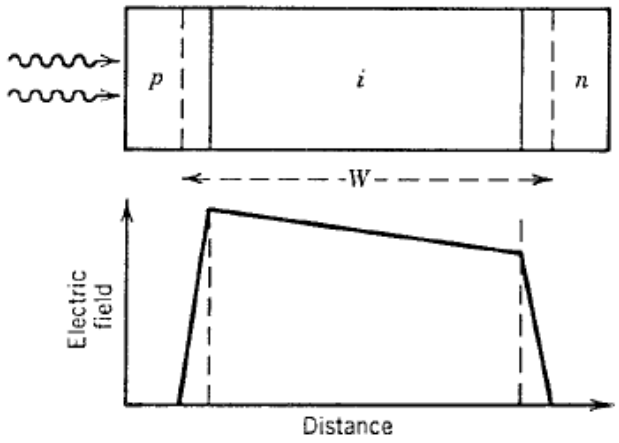

Figure 26 - A pin photodiode with the electric-field distribution under reverse bias [19].

Increasing the width of the intrinsic layer will improves the responsivity. However the speed of photodiode response is limited by the carrier transit time across the p-n junction, which is proportional to the width of the intrinsic region. The bandwidth of a photodiode is given approximately by

$$BW = \frac{1}{2\pi(\tau_{tr}+\tau_{RC})} \tag{13}$$

where τ_{tr} is the transition time and τ_{RC} is the RC time constant. A trade-off exists between the photodiode bandwidth and responsivity. To increase the bandwidth of a photodiode, is important have a thin depletion layer. On the other and, use of thinner absorption layer reduces the responsivity of the photodiode. Therefore, exists a trade-off between the photodiode bandwidth and responsivity. A Fabry–Perot cavity can be designed around the p-i-n junction, resulting in superior photon absorption with reduced intrinsic layer width, this will improve photodiode

performance. Therefore, photodiode bandwidth and responsivity can be optimized separately with little compromise. [28]

An important parameter to measure the receiver's performance, is the signal noise ratio (SNR). The SNR is the relation of the signal average power and the noise average power.

$$SNR = \frac{average\ signal\ power}{noise\ power} \tag{14}$$

The total noise of a receiver is given by the sum of the shot noise and the thermal noise. In the PIN photodetectors the contribution due the thermal noise is much higher than the contribution due the shot noise. Neglecting the shot noise, the SNR of the PIN photodiode is defined as:

$$SNR = \frac{R_L R^2 P_{in}^2}{4 k_B T F_n \Delta f} \tag{15}$$

Where R_L is the load resistor, R the responsivity, P_{in} the input power, k_b the Boltzmann constant, T the absolute temperature, F_n the factor by which the thermal noise is boosted by various resistors used in pre and main amplifiers, Δf is the e effective noise bandwidth.

The thermal noise is due to the fact that the electrons randomly move in any conductor. Even without apply any electrical current, random thermal motion of electrons in a resistor manifests as a fluctuating current. The load resistor in front of the optical receiver adds fluctuations to the current generated by the photodiode. The use of a high impedance will contribute to reduce the thermal noise and consequently increase the SNR. However, the use high impedance also will reduce the photodiode bandwidth.[19]

4. Toolkit components characterization

4.1 DFB Laser Characterization

In this section the HHI DFB Laser will be characterized by simulation in VPItransmissionMaker. The parameters that this model allows to change, are the "emission wavelength" for what the laser is constructed and the "heater current" used. The "heater current" is the current that is used to increase the laser temperature. This laser has two optical outputs and one electrical input. The electrical input is used to apply an electrical current to bias the laser. Figure 27, shown the DFB laser schematic.

Figure 27 – DFB laser schematic

4.1.1 Laser Single-sided output power

By using the setup of the Figure 28, the drive current of the laser, which is injected by the dc source, was increased from 10mA to 200mA, and the output power of the laser was measured by the power meter. The power meter measures the average power during each time window of each iteration, the time window was defined as 25.6 ns. This value was chosen to minimize the impact of the transient time of the laser. If the time window of the simulation is too small, the initial overshoot of the laser will increase the average power measure. So, in order to obtain a correct measurement the time window must be big enough to reduce the impact of the overshoot in average power measured. An example of the laser transient time and respective overshoot is shown Figure 30.

The simulation was done for three different wavelengths, 1550nm which is the wavelength for what the toolkit was optimized, 1520nm and 1570nm that are respectively the lowest and the higher wavelength supported by the model of the DFB laser.

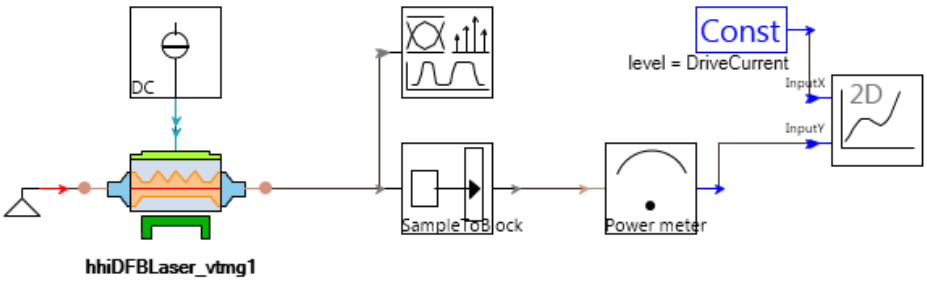

Figure 28 - Setup used to measure the output power of the laser for different drive currents

The results of simulation can be observed in the Figure 29. As expected with the increase of the drive current, after the laser threshold current, the laser linearly emits more optical power. And the optical power emitted by the laser also change for different wavelengths. In these results, it can be observed that for the same drive current, more optical power is produced for the lowest wavelength. For example with 200 mA of drive current are produced 4.5 mW for 1520 nm, while 4.35 mW are produced for 1570 nm. However, it also can be observed, that the differences of optical power emitted between wavelengths are very small when the drive current is smaller.

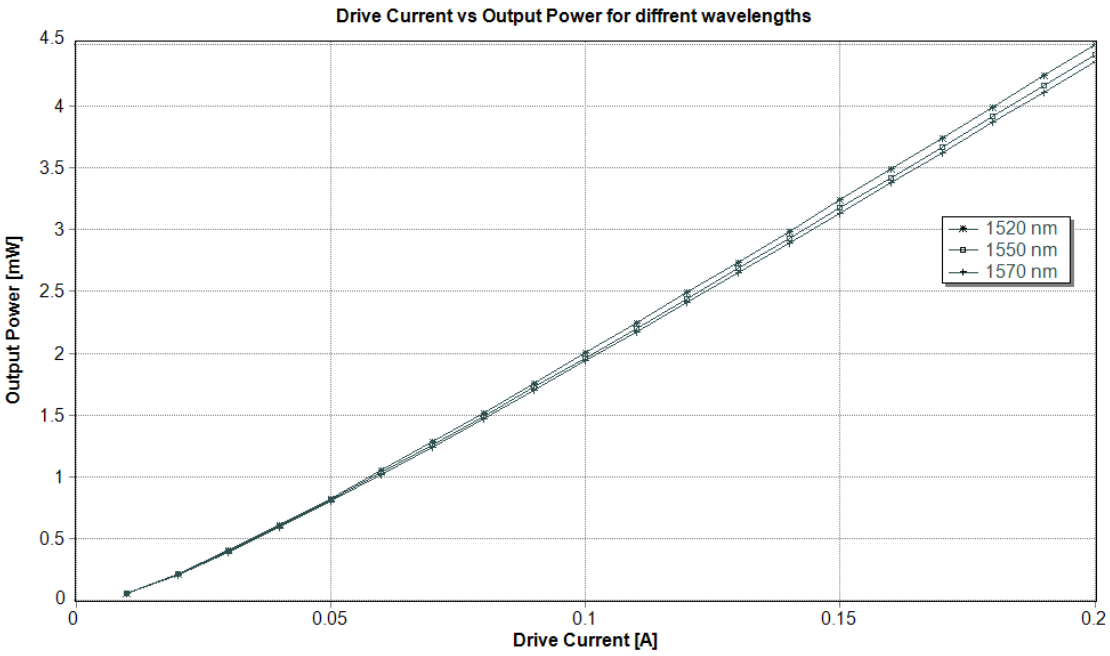

Figure 29 - Output power vs drive current for different wavelengths

In Figure 30 it can be observed the laser transient time in four different conditions. For a drive current of 15 mA and 150 mA, the transient time is represented for a heater current of 50 mA and 100 mA.

In the case that a drive current is 15 mA, the simulation results are exactly the same considering a heater current of 50 mA or 100 mA. The overshoot reaches a value of approximately 35 mW, however the high values of output power are only maintained for a short period of time, and the steady state is reached in less than 0.2 ns.

When a drive current of 150 mA is injected in the laser, it can be observed two different values of overshoot. For a heater current of 50 mA the overshoot will be around 45 mW and for a heater current of 100 mA the overshoot will be 47 mW. The time to reach the steady state will be around 0.03 ns longer than in previous case, however it is still achieved at around 0.2 ns.

The influence of the transient time in the power measure by the power meter will be very small, since the time window of the simulation is big enough. In this simulation was used a time window of 25.6 ns, this value is 128 times greater than the transient time in any case.

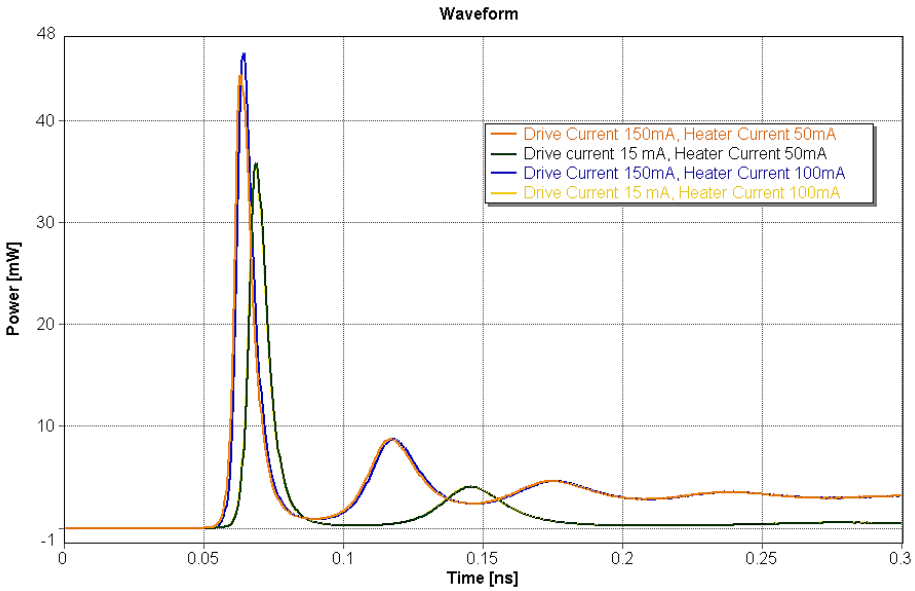

Figure 30 - Laser transient response

4.1.2 Threshold current

Adopting the same setup used in the previous section, the threshold current of the laser was measured. To find the threshold current value, the drive current was increased from 0 mA to 15mA with small steps. The simulation was also done for three different heater currents in order to observe if the threshold current changes with the temperature as expected. The results can be observed in Figure 31.

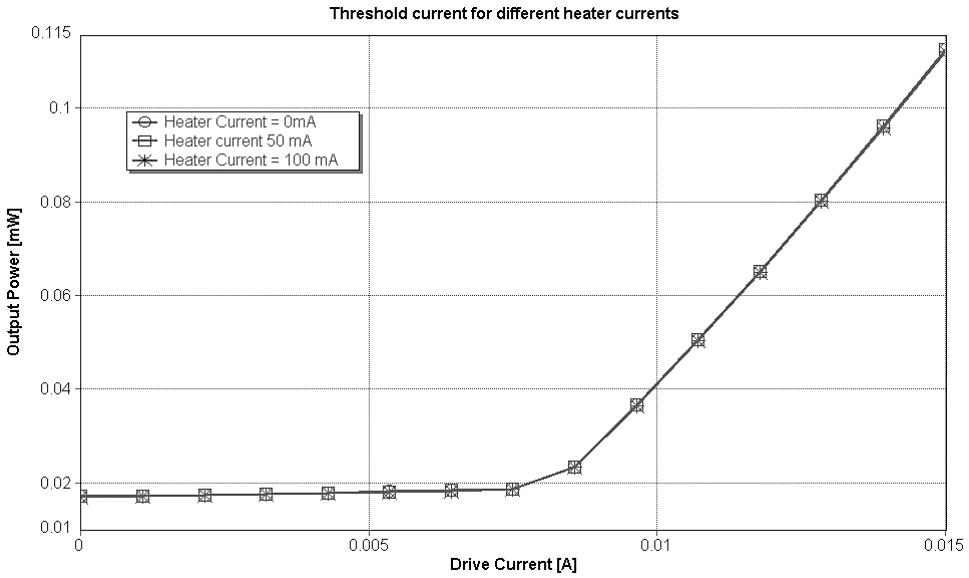

Figure 31 – Laser threshold current for different heater currents

Looking at the previous figure, it can be observed that the laser output power for a certain drive current is the same, independently of the value of the heater current. This leads to the conclusion that the value of the threshold current in the model is not sensitive to temperature changes. The threshold current value obtained is approximately 8mA, after that value the output power of the laser linearly grows with the increasing of the drive current.

4.1.3 Wavelength tuning range

The wavelength of DFB laser can be tuned by changing the temperature of the laser cavity. When temperature increases, the laser cavity expands and the refractive index changes, leading to an emission of a bigger wavelength. The way used to increase the temperature, is applying a current in a resistor closer to the laser, that current is called “heater current”. With the increase of the heater current the power is dissipated in the heater resistance increases, leading to the increase of the laser temperature.

The laser “emission wavelength” was chosen for 1.55 μm. This is the value of emission wavelength for what the laser is constructed if none heater current is applied.

Using the setup of the Figure 33, a drive current was fixed at 150mA, the heater current was swept from 0mA to 100mA, which is the range of the heater current that is allowed. The output spectrum of the laser is observed using the tool analyzer.

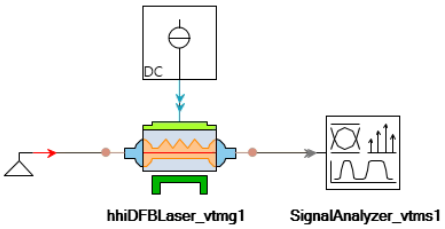

Figure 32 -Setup used to test the tuning range

In Figure 34 are shown the simulation results, there can be observed the optical spectrums for different heater currents.

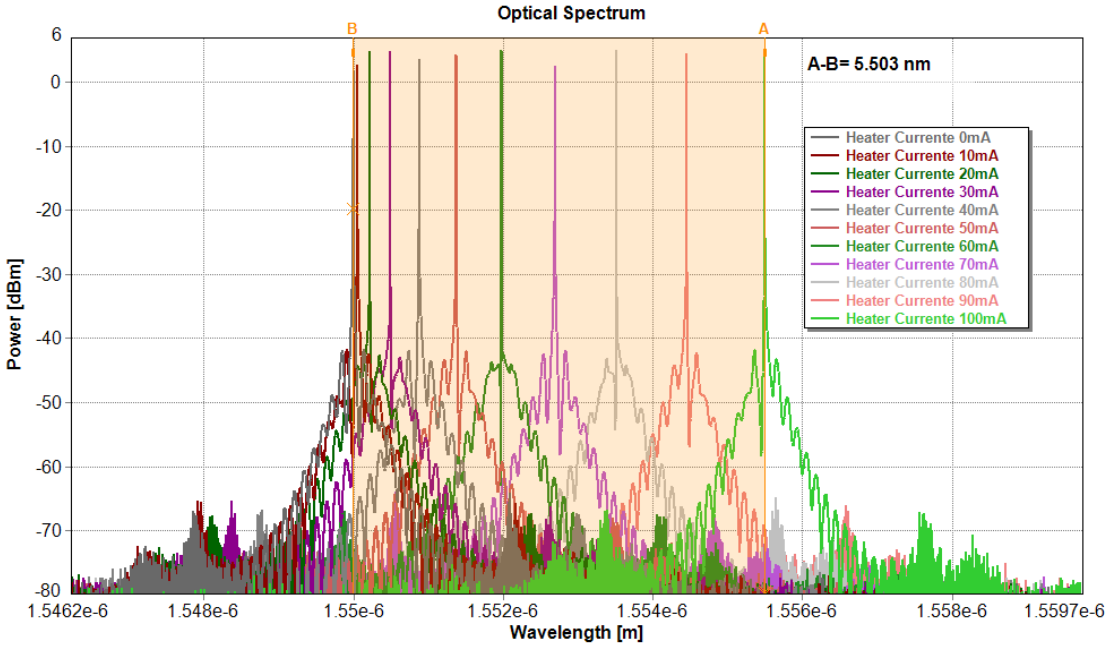

Figure 33 – Laser output spectrum for different heater currents with laser dimensioned for 1.55 μm and drive current 150mA

As expected the laser emission wavelength changes when the heater current is increased. The wavelength increases with the rise of the heater current. For example, using a heater current of 0 mA, 60 mA and 100 mA, the laser emits with a wavelength of 1550 nm, 1552 nm and 1555.5 nm respectively. With the allowed heater current variation of 100 mA, the wavelength tuning range obtained is approximately 5.5 nm.

The same simulation, to test the tuning range, was also done for different drive currents in the range of [20, 200] mA. The same results of tuning range were obtained, showing that for this model this phenomenon is independent of the value of the drive current. It was also tested

the tuning range for laser dimensioning for different wavelengths between [1520, 1570] nm, the wavelengths allowed for the model. The same results were also obtained independently of the chosen wavelength.

Observing the spectrums of the Figure 33, it can be noted that the wavelength does not have the same increase with the increment of the 10mA. The bigger the heater current is, the more will the wavelength shift, considering the same heater current increment. The graphic in Figure 34 shows how much the wavelength shifts if the heater current increases more 10 mA. For example with 50 mA of heater current, and increasing the current 10 mA, it changes from 50 mA to 60 mA, a shift of 0.6 nm is observed. Considering other case, when the heater current change from 70 mA to 80 mA, the wavelength shifts 0.8 nm.

It can be concluded that the wavelength change, grows linearly incrementing the heater current. Increase the heater current when it is already high, will result in a much bigger wavelength shift, than when it has a low value.

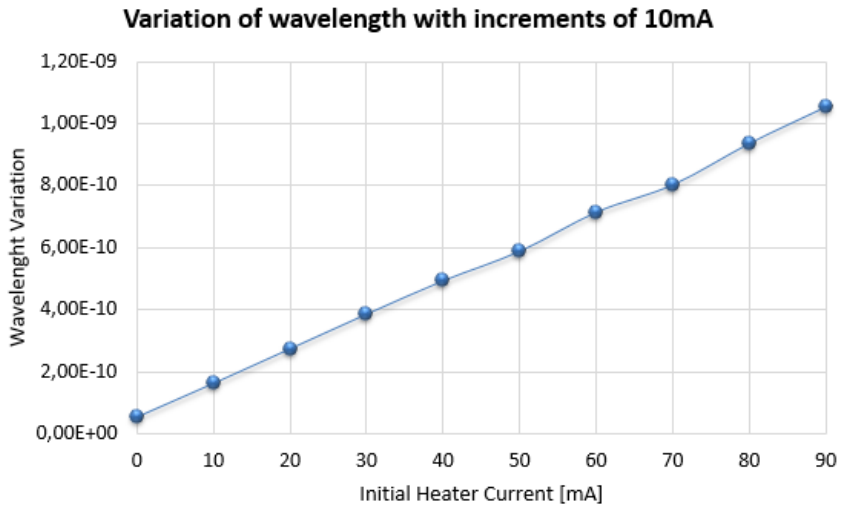

Figure 34 – Wavelength variation with increments of 10mA for different wavelengths

The following graphic shows the value of the wavelength for different heater currents. If no heater current is applied in the laser, the emission wavelength is 1550 nm. The wavelength value grows with the increase of the heater current. Reaching the value of 1555.5 nm for the max heater current allowed, the 100 mA.

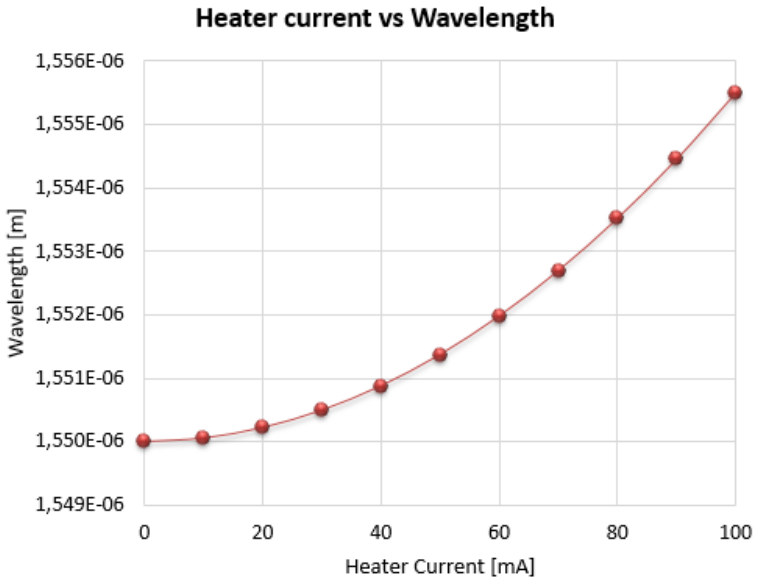

Figure 35 – Wavelengths for different heater currents with the laser dimensioning for 1550nm

In [29], a DFB laser was tested in PIC, the results experimentally obtained are shown in the Figure 36. Observing the wavelength change curves of the laser that was experimentally tested, it is possible see that, with the same heater current variation, his emission wavelength changes more than the model tested in the simulation. There is observed a wavelength variation of approximately 4.5 nm with a variation from 0 mA to 80 mA of the heater current if the. In the simulation, considering the same heater current variation, was obtained a variation of approximately 3.5nm.

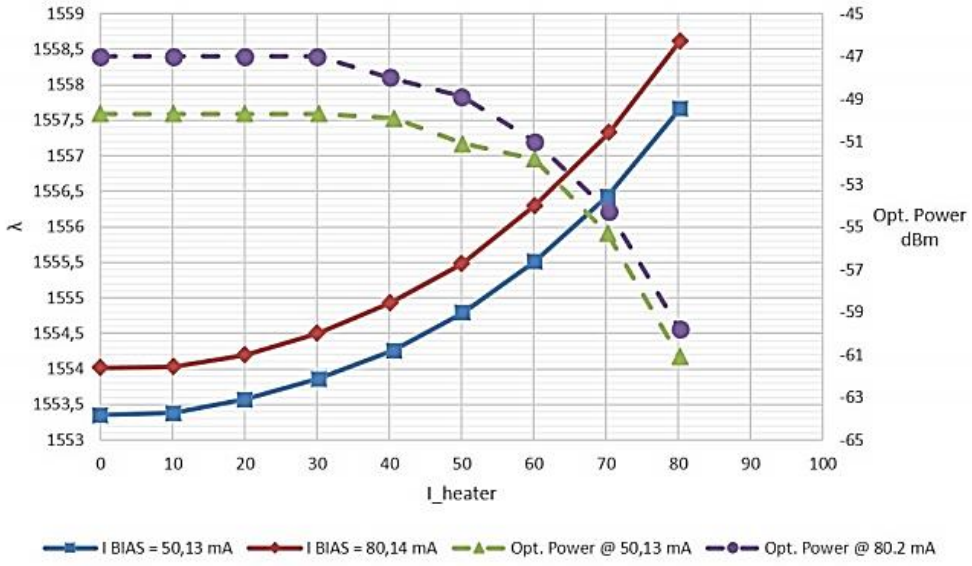

Figure 36 – Wavelength dependence with heater current (at blue and green) of a DFB laser experimentally obtained [29].

4.1.4 Dimensioning a transmitter

With the wavelength allowed by the laser model it is possible to dimension the laser to be used in the context of NG-PON 2 standard in TWDM upstream. In TWDM downstream direction it is not possible to use it, because of the range of the emission wavelength that is allowed by the laser model. So this laser can't be used for an OLT, it is just possible to use it for ONU.

This laser has a very narrow linewidth, only a few MHz, so it may be used to transmit in upstream, by using the NG-PON 2 narrow band option. The spectrum available is between [1532 - 1540] nm. The laser was dimensioned to allow the tuning in 4 different channels presented in the next table. It is important that laser is always heated to reduce the impact of the changes in the environment temperature. So the laser was dimensioned to emit at a wavelength of 1532 nm if is not applied a heater current. The first channel is at a frequency of 195.5 THz (1532.68 nm), so for laser emitting in the first channel is necessary to apply a heater current on it. As can be seen in the next table the value of heater current necessary is 35 mA.

Table 11 – Channels of the transmitter with the respective frequency, wavelength and heater current necessary

Channel	Frequency (THz)	Wavelength (nm)	Heater current (mA)
1	195.6	1532.68	35
2	195.5	1533.47	51.5
3	195.4	1534.25	64
4	195.3	1535.04	74.5

To tune the laser in the channel 2, 3 and 4, it needs to be applied a heater current of 51.5 mA, 64 mA and 74.5 mA respectively. The spectrum of the laser tuning for the different channels, with the respective heater current, can be observed in the following figure.

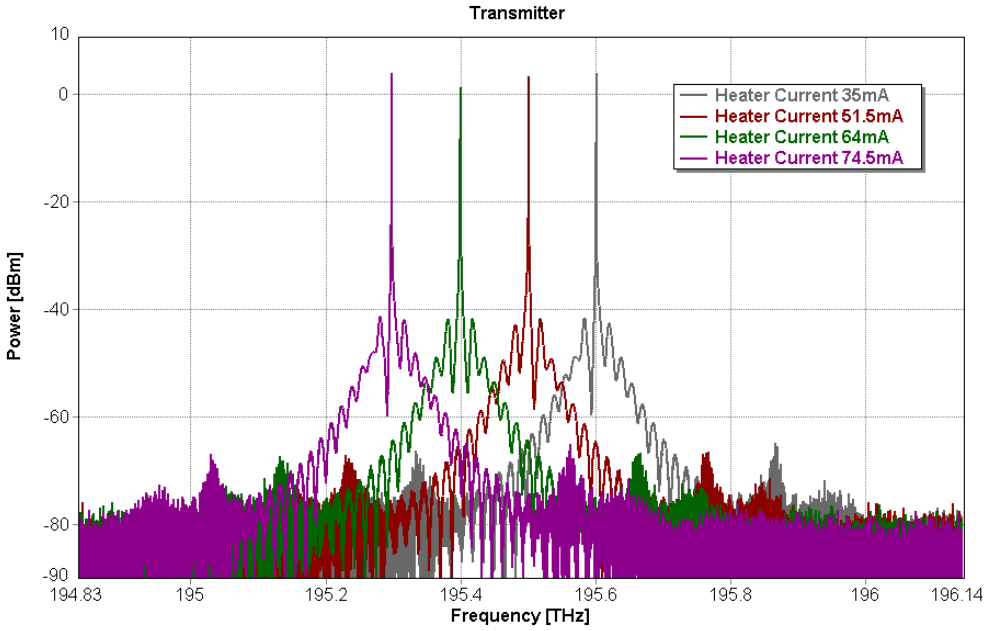

Figure 37 - The transmitter output spectrum

4.1.5 Wavelength test for different drive currents

In this experiment the heater current was maintained constant, while the drive current was increased. This test was done in order to observe if the laser emission wavelength changes with the increase of the drive current. The heater current chosen was 50 mA, and the drive current was changed between [20, 200] mA. The Figure 38 show the output spectrum of the laser for the different drive currents.

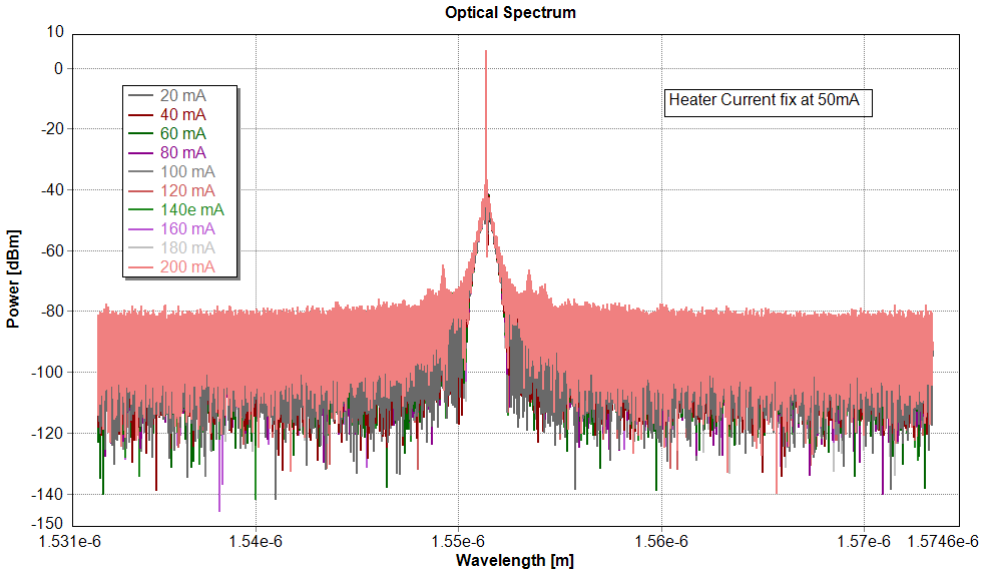

Figure 38 - Laser output spectrum for different drive currents injected

It can be observed that independently of the drive current injected, the laser emission wavelength is exactly the same. In [29] it was studied the variation of the wavelength with the bias current (drive current) of a PIC DFB laser and the results are shown in Figure 39. There is possible to see the dependence of the laser emission wavengths with the drive current. The DFB model should also be sensitive with the drive current injected, which does not happen.

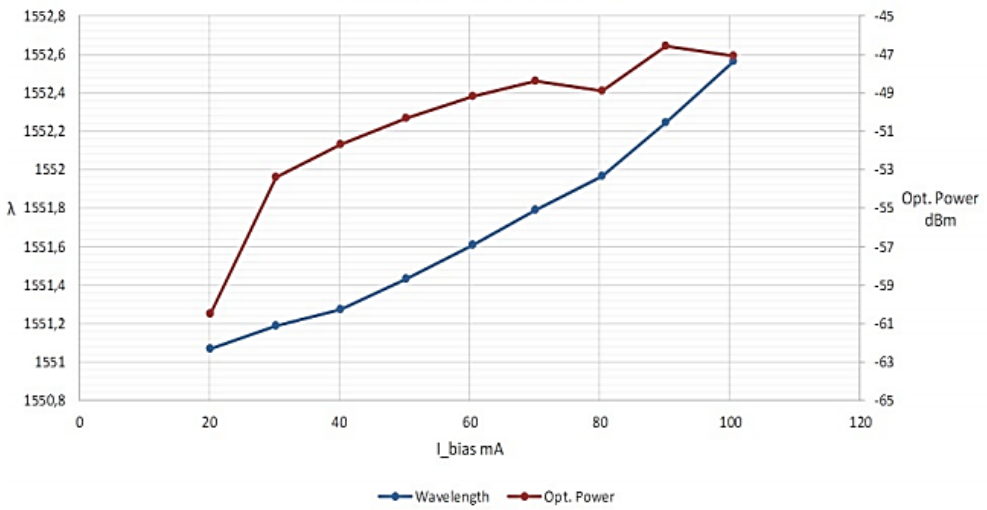

Figure 39 – Wavelength dependence with the bias current (at blue) of a DFB laser experimentally obtained [29]

4.1.6 Side mode suppression ratio and noise floor

The relation of power between center peak longitudinal mode with the nearest higher order mode, is called the side mode suppression ratio (SMSR). The side mode suppression rate was tested for different drive currents in the range of [20, 200] mA, for 0mA, 50mA and 100mA of heater current. In the Figure 41 it can be observed the measurement of SMSR in a case where the drive current is 100 mA and a heater current of 50 mA was injected.

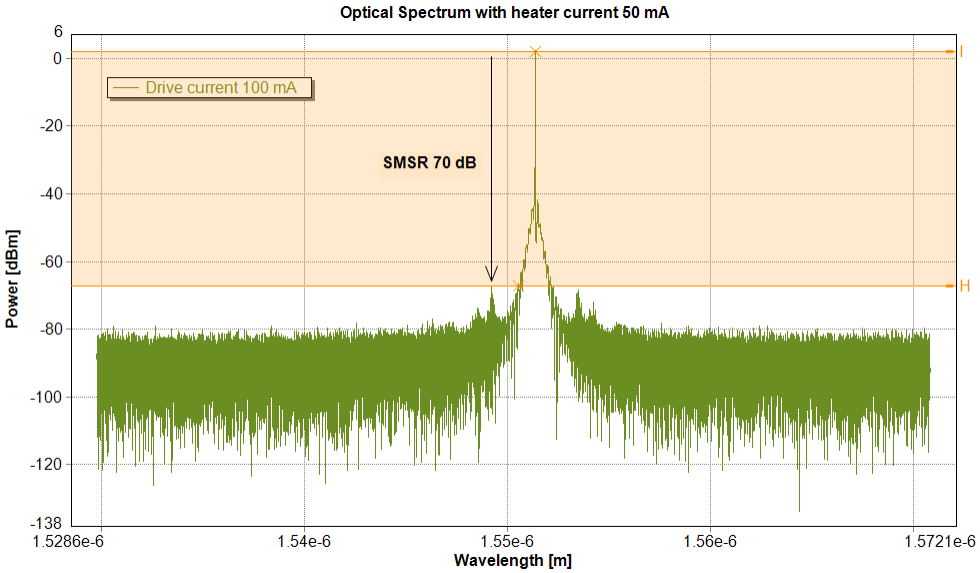

Figure 40 - Measurement of SMSR

The following table contains the results of the measurement of the SMSR. It can be observed that, independently of the heater current or of the drive current, the value of the SMSR always have a high level. The SMSR value varies between 66 dB and 71 dB, without being possible to observe a pattern with the variation of the drive current or heater current. With this values of SMSR, this laser complies with NG-PON2 [3] because the minimum required value is 30dB.

Table 12 – SMSM for different Driver Currents and Heater Currents

Heater current	0 mA	50 mA	100 mA
Drive Current [mA]	SMSR [dB]	SMSR [dB]	SMSR [dB]
20	66	68	68
40	68	70	69
60	68	71	69
80	68	70	69
100	68	70	69
120	69	69	68
140	69	69	68
160	69	69	68
180	69	69	68
200	68	69	68

During the measurements of the SMSR was also observed the level of the noise floor (see Figure 41) while the laser drive current increase. The value of the noise floor increase with the drive current in the range of [-85, -80] dB with a drive current in the range of [20, 200] mA. The following figure show the noise floor with a drive current of 20 mA.

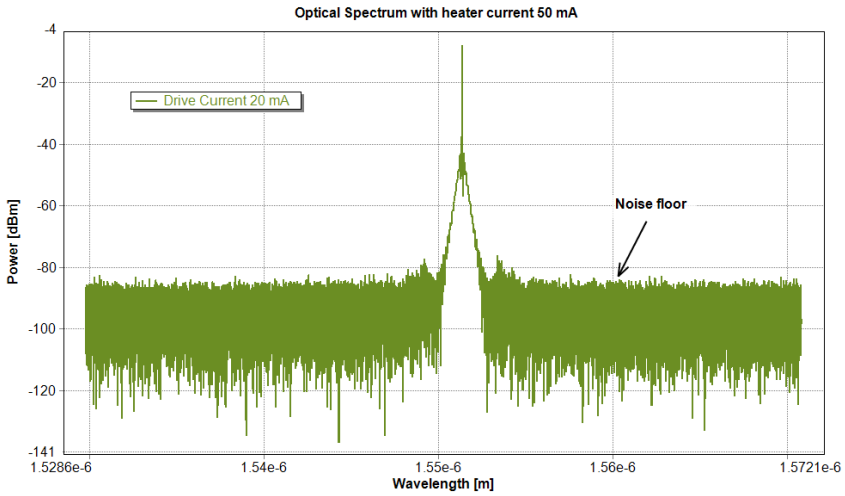

Figure 41 – Noise floor with a drive current of 20 mA.

4.1.7 DFB laser Conclusions

After performing these tests it was possible to know some very important features of the DFB laser. The DFB model can only be scaled to emit wavelengths between [1520, 1570] nm, so it can only be used in an upstream transmitter for NG-PON 2 using TWDM. The output power of the DFB was measured for different drive currents. It was observed that the output power has a small variation with the wavelength emitted by the laser. As expected, was possible to see that after the threshold, the laser output power grows linearly. The maximum output power obtained was 4.5mW, when the drive current was 200mA. The laser threshold current value obtained was approximately 8mA. And it was also observed that the value of the threshold current does not vary with the increasing of the temperature. However would be expected at least a small variation.

It was also tested the laser tuning range. It was observed that it might be possible to vary the wavelength by 5.5 nm increasing the heater current. Using the laser narrow linewidth and its tuning capabilities, was possible to dimension it to operate in the channels of narrow band option of NG-PON 2 upstream.

It was concluded that the bigger the heater current is, the more will be the wavelength shift, considering the same heater current increment. Other conclusion that can be done is that the model does not change the emission wavelength with the increase of the drive current. The

laser SMSR values were always between [66, 71] dB. So it can be concluded that the laser SMSR is way above the minimum value in standard NG-PON2 of 30dB.

4.2 Current-injection phase modulator

The current-injection phase-modulator is based on a bulk ridge waveguide structure. Using this modulator the phase can be tuned by injecting current on it. This module includes two butt-joints for the coupling between active and passive waveguides. The only physical parameter that can be changed in the phase modulator is his length.

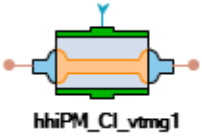

Figure 42 – Schematic of the current injection phase modulator.

To test the phase shift, the setup of the

Figure 43 was constructed. This setup simulates a structure based on a MZM. The splitting and coupling was done by a MMI HHI E1700, 1x2 and 2x1 respectively. The signal was generated by an ideal transmitter in continuous wave, with an optical output power of 1 mW. The signal was split by the first MMI, and guided by two waveguides with the same length and width. In the MZM structure, there's no current applied in the PM of the bottom arm, so the phase of the optical signal is not shifted. However in the upper arm, a current is injected, which leads to a refractive index change and consequently a phase shift of the optical signal. Depending on the lag between the signal in the upper and bottom arm, the output power will vary. When the signals are in phase, the output power will be on its maximum point and when the signals are on opposition of phase the output power will be null.

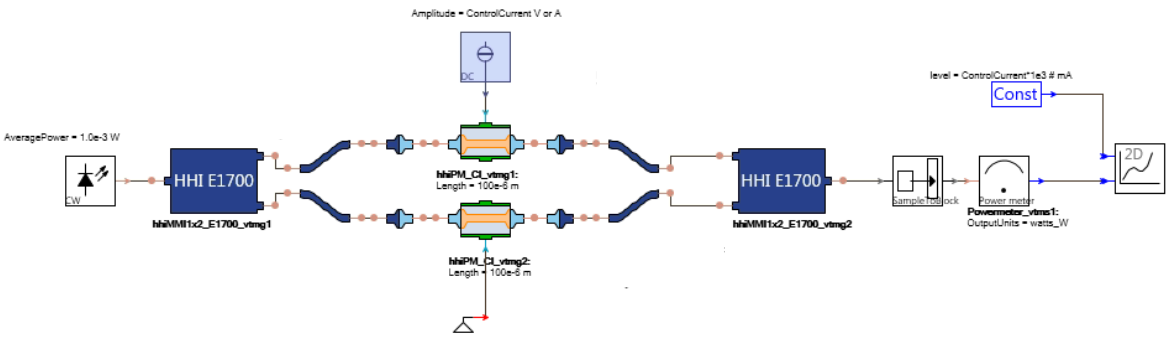

Figure 43- Setup for test the phase shift.

In Figure 44, Figure 45 and Figure 46, the results are shown for the cases when the current injected in the upper arm varies from 0 mA to 40 mA. Three different cases were considered in terms of the length of the PM, 100 μm, 250 μm and 350 μm.

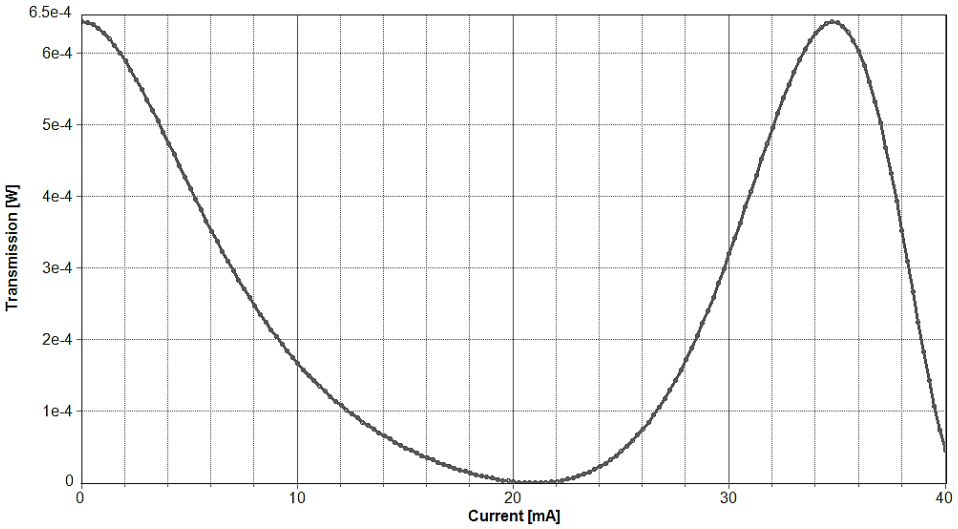

Figure 44 – Injected Current vs Transmission Power for PM length of 100 μm

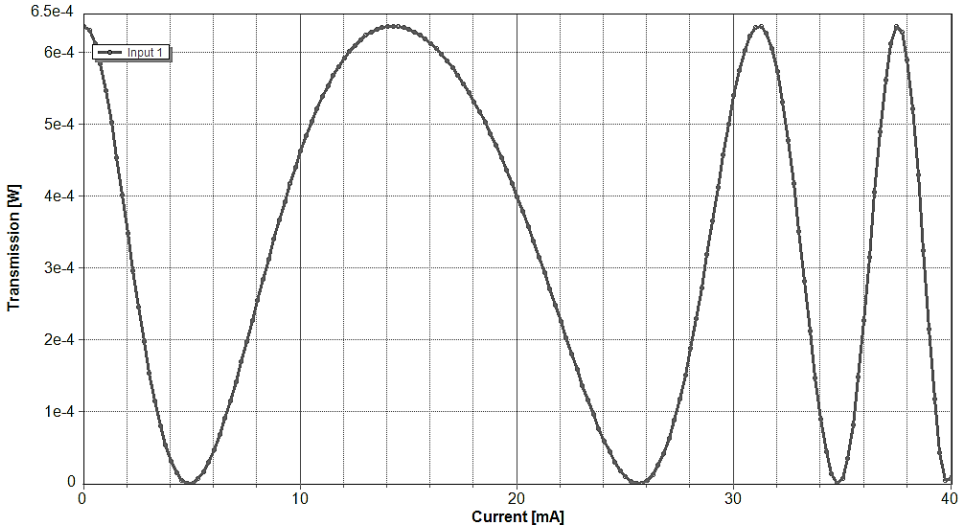

Figure 45 - Injected Current vs Transmission Power for PM length of 250 μm

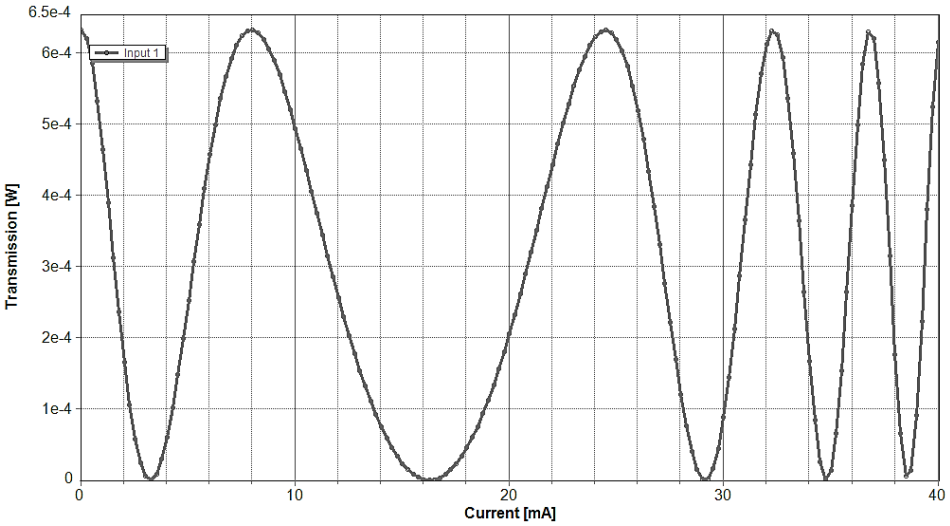

Figure 46 - Injected Current vs Transmission Power for PM length of 350 μm

Observing the simulation results, it can be noted that the output power varies with the value of the current injected in the phase modulator, as expected. It can also be observed, that the transfer function varies according to the length of the phase modulator. The same injected current, causes a different phase shift depending on the length of the current injection PM. In the case that it has a length of 100 μm, to obtain a phase shift of 180º, it was needed to inject a current of 20 mA. In the case that the predefined length is of 250 μm or 350 μm, the value of the current that needs be injected to achieve the same phase shift is 5 mA or 3mA, respectively. So, the increase of the PM length leads to that less current need to be injected to achieve the same phase shift. Basically, on one hand, more length of the PM will increase the PIC's area and consequently their cost, however it will have the upside of reducing the energy consumption. It must also be considered, that if the length is increased too much the losses will also have to be taken into consideration.

4.3 Photodiodes test

VPItoolkit™ PDK HHI has two different PIN photodiodes, hhiPINDIODE_DC and hhiPINDIODE_DCRF. The schematic´s of both are shown in Figure 47.

The description of hhiPINDIODE_DC says that it is a PIN photodiode that has a 3dB bandwidth at about 20GHz. It was placed on top of a passive waveguide and it was designed for full optical absorption, which means it cannot be employed for the implementation of any tap function.

About the hhiPINDIODE_DCRF, it says that it consists on an high-speed PIN photodiode that has a 3dB bandwidth over 35GHz. Just like for hhiPINDIODE_DC, it was placed on top of a passive waveguide. The main difference from the previous photodiode, is that it was designed for high-speed operation, allowing his operation with higher bit rates. It was also designed for full optical absorption, so the tap function, once again, cannot be employed.

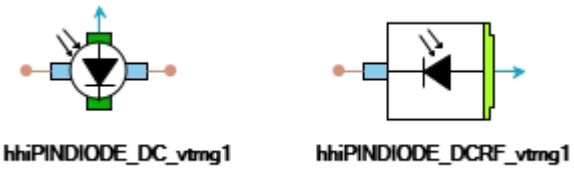

Figure 47 - Schematic's of photodiodes hhiPINDIODE_DC and hhiPINDIODE_DCRF.

BER

Before testing the sensitivity of the photodiodes, it is important to explain what the bit error rate (BER) is. BER is the percentage of bits that have errors relative to the total number of bits received in a transmission. For example if a BER of 10^{-3} is obtained, this means that 1 out of the 1 000 bits (10^3) transmitted has an error. [30]

However, considering a Gaussian noise distribution in 1 and 0 bits, it is possible to do a BER estimation. In Figure 48 it is shown the fluctuating signal generated at the receiver and the Gaussian probability densities of 1 and 0 bits. BER will be obtained by

$$BER = \frac{1}{2} erfc\left(\frac{Q}{\sqrt{2}}\right) \tag{16}$$

where,

$$Q = \frac{P_1 - P_0}{\sigma_1 + \sigma_0} \tag{17}$$

the variable P_1 is the power of bits at level "1", P_0 the power of bits at level "0", σ_1 is the standard deviation of the power of bits "1" and σ_0 for the bits "0".

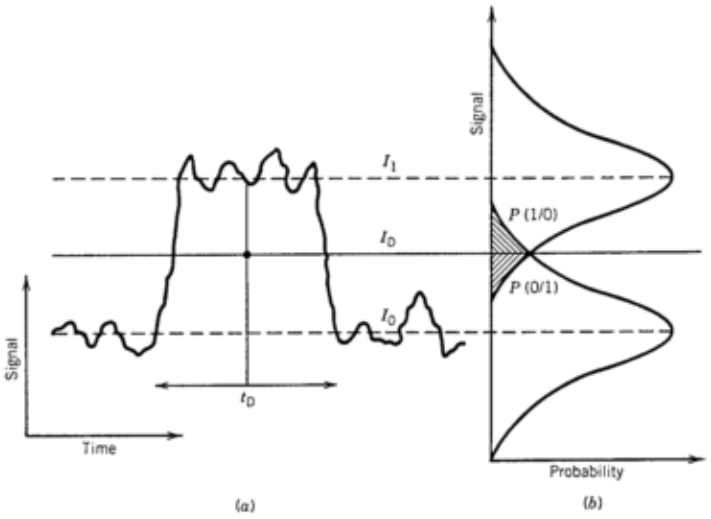

Figure 48 – (a) Fluctuating signal generated at the receiver, (b) Gaussian probability densities of 1 and 0 bits. [19]

With the increase of the Q factor, the BER decreases. For Q=6, the BER is around 10^{-9}, and for a Q=7 BER is approximately 10^{-12}. In order to guarantee a certain BER, the optical power received, has to be equal or higher than a certain value limit. The minimum power to reach a certain BER is called receiver sensitivity.[28]

Chromatic dispersion

Another important concept that should be explained is the chromatic dispersion. The chromatic dispersion is divided into two components, material dispersion and waveguide dispersion. Their effect causes the spread of the transmitted pulses.

The material dispersion is due to the fact that the silica refraction index vary with the frequency thus causing that the different spectral components travels at different group velocities, leading to spread of the signal. The waveguide dispersion is dependent on the guiding structure parameters such as the core radius and the refraction index difference.[19]

In the Figure 49, it can be observed the material dispersion, chromatic dispersion and the combination of the both.

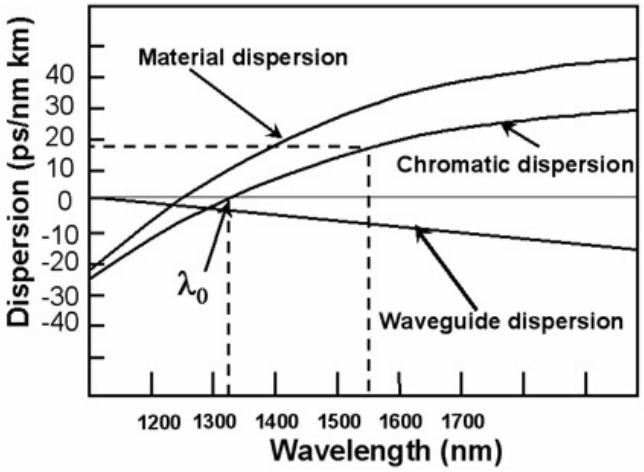

Figure 49 - Chromatic dispersion is the combined result of material dispersion and waveguide dispersion [31]

Looking for the previous figure it can be conclude that both dispersions have opposite behavior with increasing signal wavelength optical. It is observed that the chromatic dispersion passing through zero at around 1310nm and getting values in the order of 16, 17 ps/(nm*km) for a wavelength of 1550nm.

To compensate the dispersion caused along the fiber when is used the 1550 nm region, it is possible to use dispersion compensation fiber (DCF). The DCF have negative dispersion, so it is possible to scale the network by placing a standard single mode fiber (SSMF) followed by DCF, in order to have a lower dispersion. [32]

4.3.1 PIN photodiode characterization

4.3.1.1 Sensitivity tests

The setup, which can be seen on Figure 50, was used to test the system sensitivity for different conditions of bit rate, fiber length, and extinction ratio. A transmitter NRZ-OOK was selected, with the laser central frequency of 193.4 THz (1550 nm) and a laser with an average output power of 20 mW, which leads to an output power of 10 mW (10 dBm) after the modulation. The laser considered was an ideal one, since the linewidth was set to zero, just so the simulation of the system wouldn't be it impacted by that parameter. The extinction ratio used in the simulations with fiber was 6 dB, which is the minimum value recommended for 10 Gbps upstream transmission by the NG-PON2 standard [3]. Simulations were also performed, in back to back with a lower and higher extinction ratio, respectively 4 dBm and 8.2 dBm.

After the transmitter, it was placed universal optical fiber, in order to allow the characterization of the photodetector in systems with different fiber lengths. The function of the swept attenuator was to reduce the optical power of the signal received by the photodiode. The input optical power received by the photodiode is measured by the power meter, while the stoch OOK give us the respective BER with that input power. To estimate the BER, it was chosen the Gaussian estimation method. Using this method in VPI, it is advised to simulate more than 1024 bits, for the BER result to be accurate.[33] The time window used was 15000/bitrate, to simulate 15000 bits, in order to improve the precision of the results. The value of dispersion in the fiber used was 16ps/(nm*km).

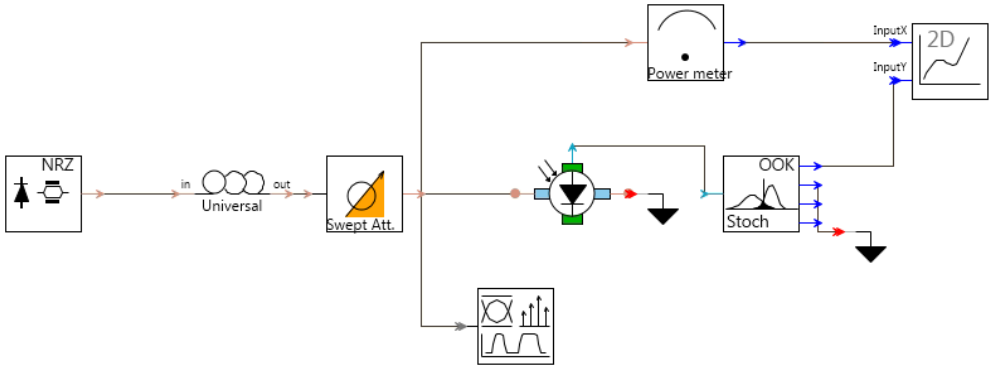

Figure 50 - Setup used to test photodiode sensitivity.

Tests using 2.5 Gbps of bit rate for different fiber lengths

In the first simulation, the sensitivity was tested using 2.5 Gbps of bit rate and an extinction rate of 6 dB. The simulation was made for different fiber lengths, 0 km, 10 km, 20 km and 40 km. In Figure 51, the results of the simulation can be visualized.

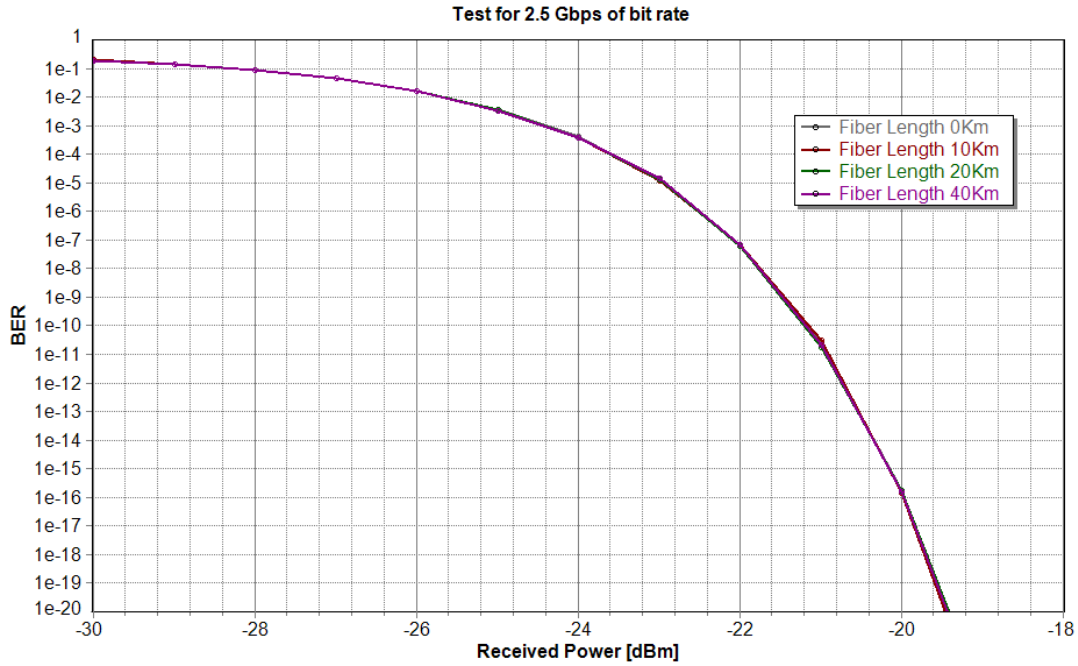

Figure 51 – BER vs Received power for 2.5 Gbps.

The fact that the same results obtained are the same, independently of the fiber length, are due the low bit rate. The result of the following equation gives the limit for that signal starts to be affected by chromatic dispersion[34].

$$L < \frac{c}{2B^2\lambda_0^2|D|} \tag{18}$$

Where L is the fiber length, c is the speed of light, B the symbol rate (which is the same as the bit rate in case of NRZ-OOK), λ_0 the wavelength and D the chromatic dispersion. The limit length onto which the signal starts to be affected by dispersion is 624 km, which is a lot higher than the fiber lengths simulated on this setup. Due to that, no difference is observed regarding the sensitivity of the system for the different fiber length specifications.

Since, the format used is NRZ-OOK, every single bit, will correspond to a symbol, and therefore interference between the symbols will start happening faster, than if a more complex modulation format was being used, like QPSK or M-QAM, because for those cases, several bits are aggregated onto one symbol.

The value of BER 10^{-3} (1e-3 in VPI notation), is usually the max value that forward error correction (FEC) codes can support. It is possible to observe, that to achieve that value of BER, a received power of -24.4 dBm is required. However to obtain better BER, more received optical power is required. For example, to obtain a BER of 10^{-9} or 10^{-12}, the received optical power must be respectively of -21.6 and -20.8 dBm. This means that to improve the BER from 10^{-3} to 10^{-9}, it's

required to increase the optical power on 2.8 dB. And to improve the BER from 10^{-3} to 10^{-12}, more 3.6 dB of optical power is required in the photodiode. This means that to improve the BER from 10^{-3} to 10^{-12}, it will be necessary to receive more than twice the optical power.

Tests using 10 Gbps of bit rate for different fiber lengths

The same setup was simulated once again, but now for a bit rate of 10 Gbps, which is the maximum value per channel, used in the NG-PON2 standard. The Figure 52 shows the obtained results.

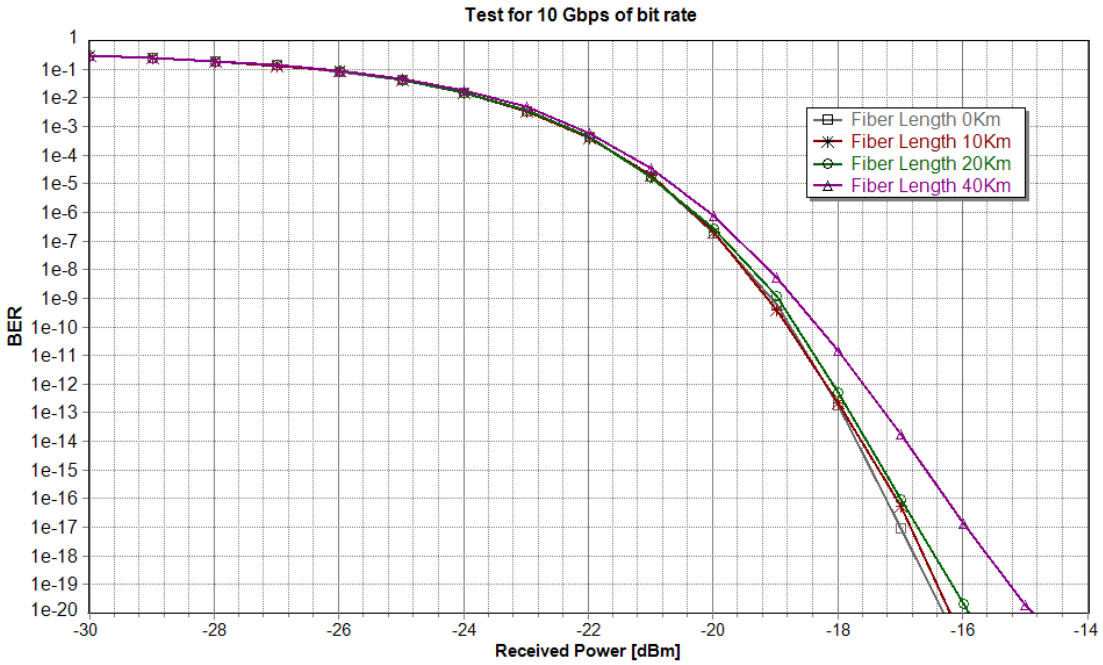

Figure 52 - BER vs Received power for 10 Gbps.

On opposition to what happens on the previous case, the fiber length now influences the curve of the BER versus received power. When the bit rate increases, the signal pulses are closer in the time domain. The dispersion effect in the fiber, leads to the spreading of the pulse. With the pulse spreading, part of the pulse will overlap with the pulse located at his side. In this case the limit, calculated by the equation 18, where dispersion starts affect the signal is at 39 km. The impact of the dispersion still wasn't not that noticeable since only 1 km was exceed, however the impact will rapidly get worse with the increase of the fiber length after this limit. In the case that still wanted to increase the length of the fiber, DCF must be used to reduce dispersion.

Looking at the Figure 52, it can be observed, that a BER of 10^{-3} is obtained with a received power of -22.4 dBm independently of the fiber length. This happens because the attenuation effect overlaps the dispersion. However if the received optical power increases, the effect of dispersion is seen with the increase of the fiber length. For example, for -18 dBm of optical power received, a BER of 10^{-13} without fiber and 10^{-11} with 40 km of fiber are obtained.

4.3.1.2 Tests using in back to back for different bit rates and ER

The extinction ratio, is ratio between the power used to transmit a logic level '1', to the power used to transmit a logic level '0'. It is defined as,

$$ER = \frac{P_1}{P_0} \tag{19}$$

Or in dB as,

$$ER = 10log_{10}\left(\frac{P_1}{P_0}\right) \tag{20}$$

With a greater difference between the level 1 and level 0, a better BER is obtained. This happens because will be easier for the receiver accurately determine which signal level is present.

In this simulation the photodiode sensitivity was tested for different bit rates typically used in optical communications systems.

The test was done without fiber (in back to back), so dispersion wouldn't interfere. The tests were done for an extinction ratio of 4dB, 6 dB and 8.2 dB and the results can be visualized in Figure 53, Figure 54 and Figure 55.

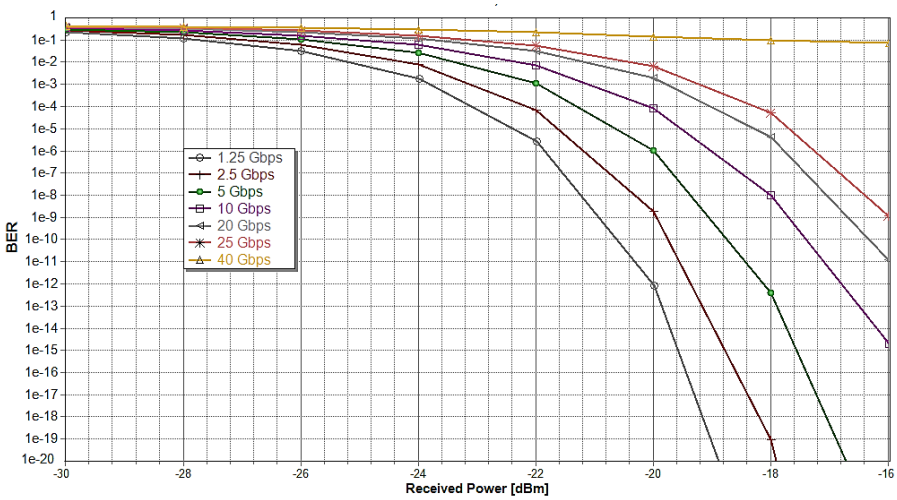

Figure 53 - BER vs Received Power for different bit rates using 4 dB of ER.

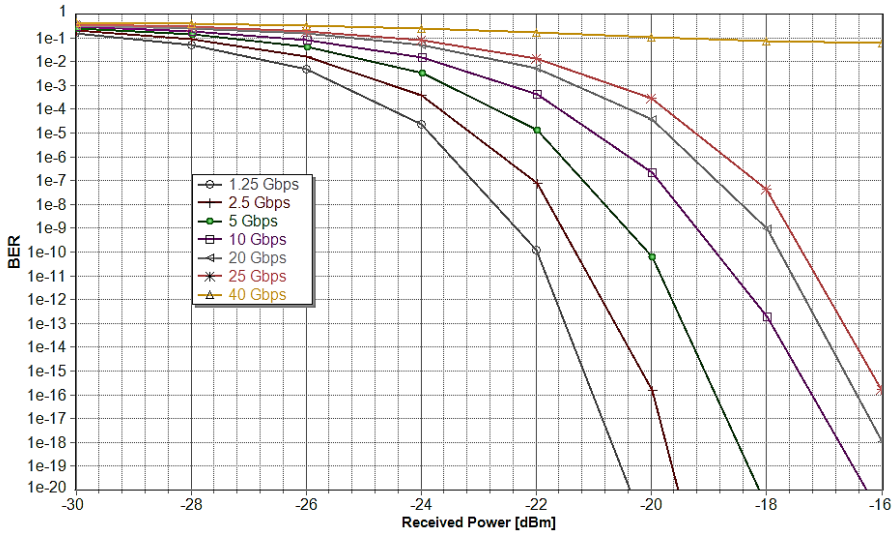

Figure 54- BER vs Received Power for different bit rates using 6 dB of ER.

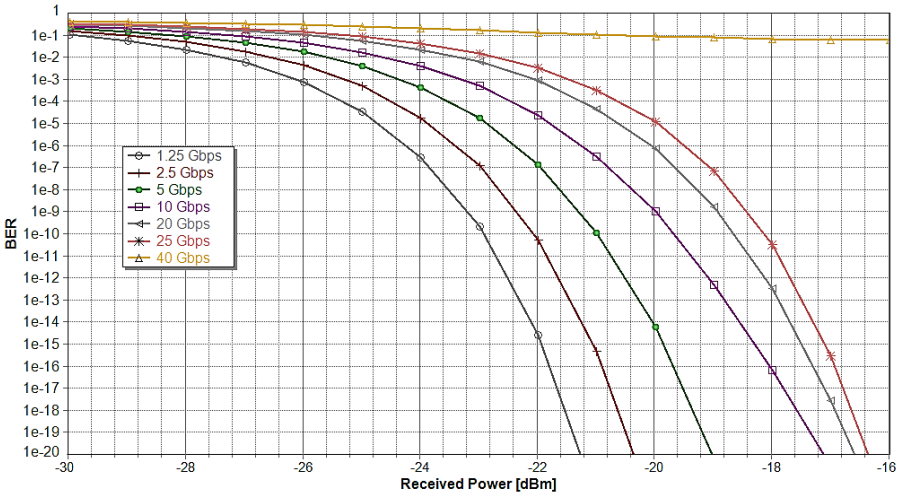

Figure 55 - BER vs Received Power for different bit rates using 8.2 dB of ER.

With the increase of the bitrate, the photodiode's sensitivity is worse, since only with higher received power, the same BER measures can be obtained. However if the bitrate is too high, it doesn´t matter if there's an increase on the optical power because the BER will not improve. This is due to the fact that the photodiode doesn't have enough bandwidth to support high bit rates.

Comparing the results for an extinction ratio of 4 dB, 6 dB and 8.2 dB, and the same value of received power, as expected, the worst BER is obtained for the lowest ER.

For all the situations, the photodiode is not capable of receiving 40Gbps. Considering the ER of 4 dB, to have a BER of 10^{-3}, it is necessary to receive an optical power of -24 dBm with a bit rate of 1.25 Gbps, while if the bit rate is 25 Gbps, it doesn't have as much sensitivity since it needs -19.2 dBm.

When an ER of 6 dB was used, a BER of 10^{-3} was obtained for -25.6 dBm for 1.25 Gbps. For a bit rate of 25 Gbps the received power necessary will be -20.6dBm.

In the case of having 8.2 dB of ER, the BER of 10^{-3} is achieved with -26 dBm for 1.25 Gbps. If the bit rate is 25Gbps will be necessary to receive an optical power of -21.6 dBm.

Table 13 shows the sensitivity, for the referenced BER of 10^{-3} and 10^{-4}, which are the reference values for NG-PON2. The bitrates displayed are for 2.5 Gbps and 10 Gbps, considering the ER of 4 dB, 6 dB and 8.2 dB.

Table 13 - Sensitivity values to BER 10^{-3} and 10^{-4}, for 2.5 Gbps and 10 Gbps.

	Bit Rate	2.5 Gbps	10 Gbps
ER 4 dB	Sens. For BER 10^{-3}	-23.1 dBm	-21.1 dBm
	Sens. For BER 10^{-4}	-22.2 dBm	-20.0 dBm
ER 6 dB	Sens. For BER 10^{-3}	-24.5 dBm	-22.5 dBm
	Sens. For BER 10^{-4}	-23.7 dBm	-21.6 dBm
ER 8.2 dB	Sens. For BER 10^{-3}	-25.3 dBm	-23.3 dBm
	Sens. For BER 10^{-4}	-24.5 dBm	-22.5 dBm

Observing the values in the above table, it is possible to observe that with the reduction of the extinction ratio, will be necessary receive more optical power to achieve the same sensitivity. For example. For example the reduction of ER -8.2 dB to 4 dB require an increase of 2.2 dB in power received to achieve a BER of 10^{-3}. In any case the sensitive required for NG-PON2 was never achieved.

4.3.2 High speed PIN photodiode characterization

4.3.2.1 Sensitivity tests

The same setup to test the sensitivity of the previous photodiode, was now used to test the high speed photodiode, which can be observed on Figure 56**.** As in the previous case, a NRZ-OOK transmitter was used with the laser central frequency of 193.4 THz (1550 nm), and an average power of 20 mW, which lead to an output power of 10 mW (10 dBm) after the modulation. The laser linewidth was set as zero. The extinction ratio used was 6 dB in the tests with different fiber lengths. Simulations were also performed with ER of 4 dB, 6 dB and 8.2 dB using different bit rates. The time window used was 15000/bitrate and to estimate the BER, Gaussian estimation method was chosen once again.

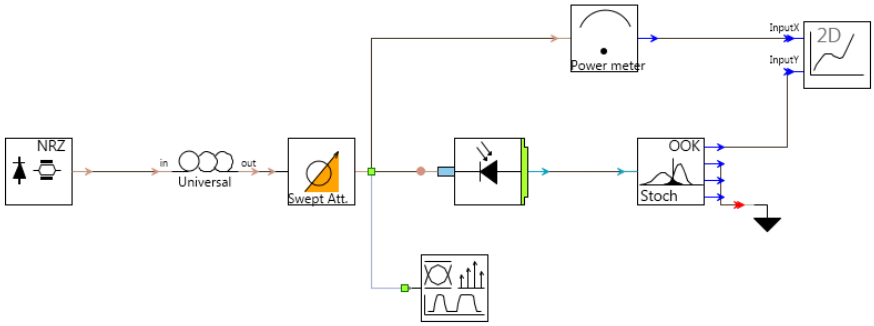

Figure 56 - Setup used to test high speed PIN photodiode sensitivity

Tests using 2.5 Gbps for different fiber lengths

In this simulations the sensitivity was tested using 2.5 Gbps of bit rate and an extinction rate of 6 dB. The simulation was made for different fiber lengths, 0 km, 10 km, 20 km and 40 km. The dispersion in fiber considered was 16 ps/(nm*km). The simulation results are shown in Figure 57.

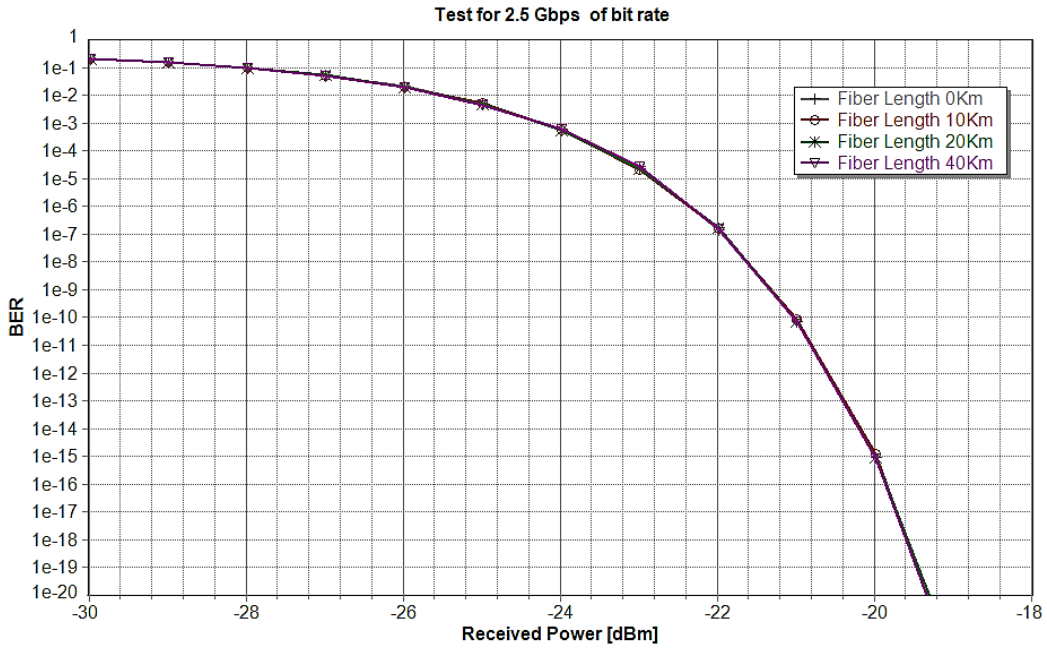

Figure 57- BER vs Received power for 2.5 Gbps

As in the case of the previous studied photodiode, the results are independents of the fiber length since the bit rate is low. To achieve a BER of 10^{-3}, 10^{-9} and 10^{-12}, will be necessary a received

power of -24.2 dBm, -21.2dBm and -20.6dBm respectively, which corresponds to nearly the same limit values as for the previous photodetector.

Tests using 10 Gbps for different fiber lengths

Using the same setup than in the previous case, the bit rate was increased to 10 Gbps. The obtained results are shown in Figure 58.

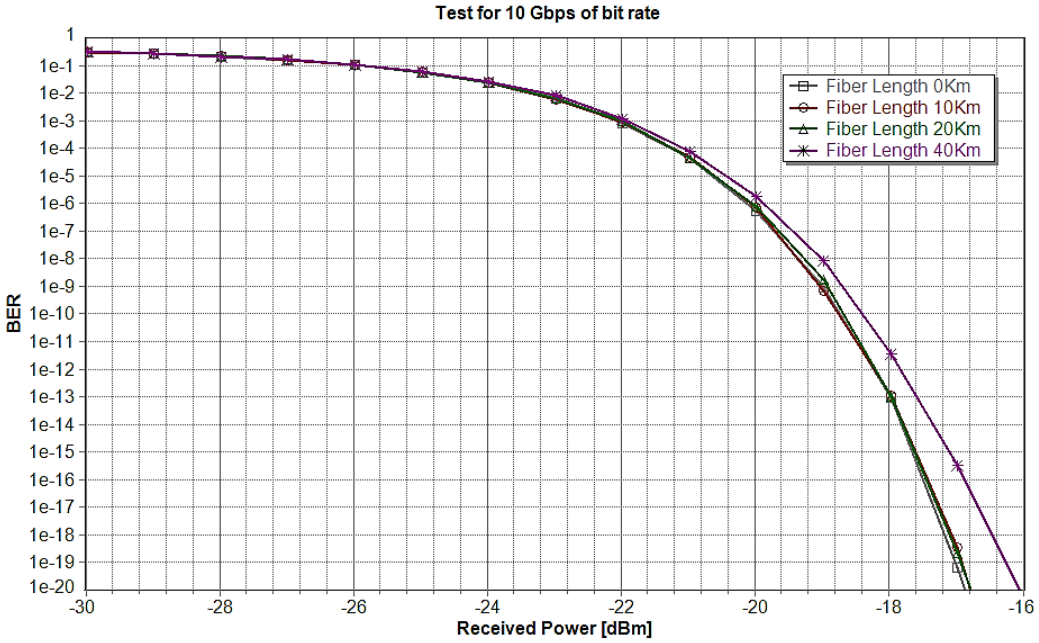

Figure 58 – BER vs Received power for 10 Gbps

Once more, it is possible to observe the dispersion effect when the fiber length increases. A BER of 10-3 is obtained when the received power is close to -22 dBm, independently of the fiber length. However, for example if the received power is -19 dBm, the value of BER will be 10^{-9} if the fiber length is lower than 20km, and 10^{-8} if the fiber length is of 40 km. With -18 dBm received the BER will be of 10^{-13} without fiber and $4*10^{-12}$ with 40km of fiber.

4.3.2.2 Tests using back to back for different bit rates and ER

Like it was done for the previous tested photodiodes, high speed PIN photodiode was tested for different bitrates. The simulations were once again performed with the same set of ER values. The results are shown in figures Figure 59, Figure 60 and Figure 61 respectively.

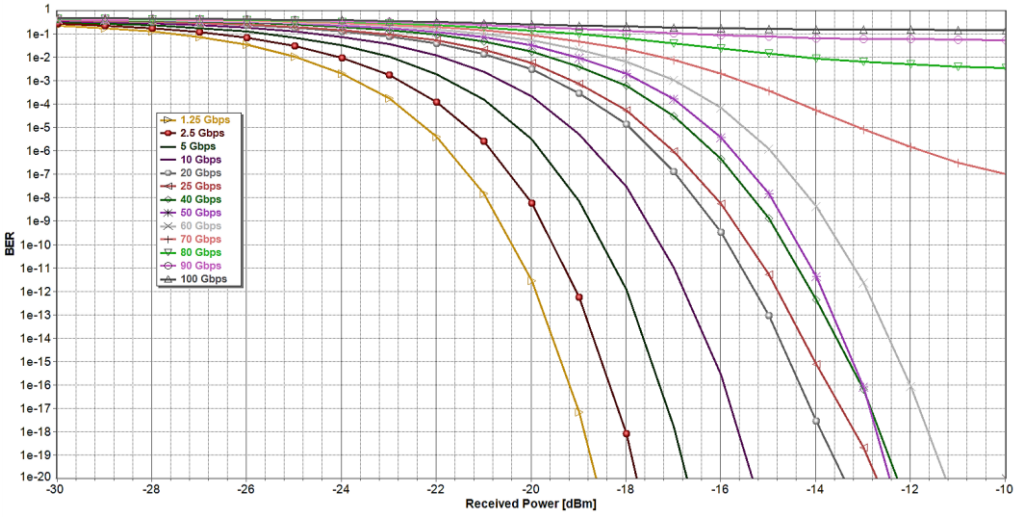

Figure 59 - BER vs received power for different bit rates using 4 dB of ER.

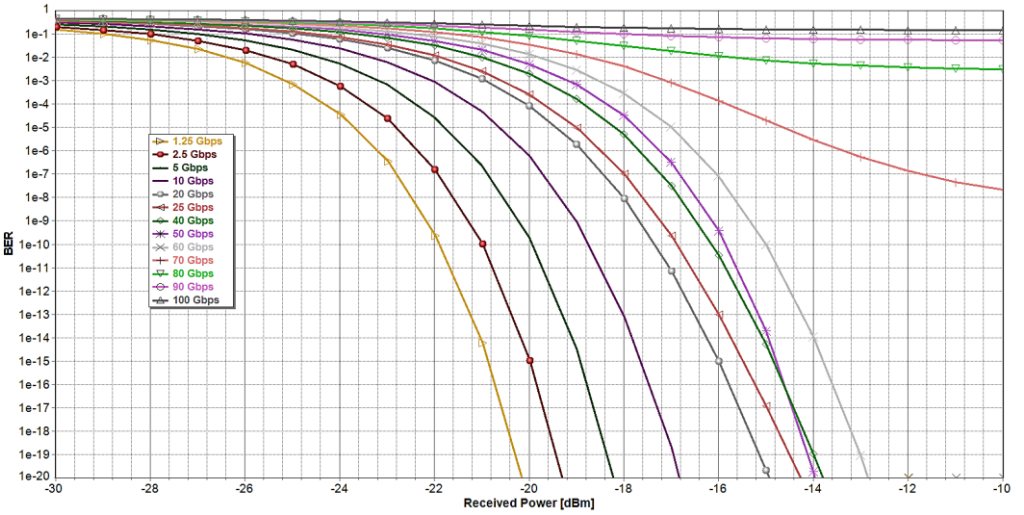

Figure 60 - BER vs received power for different bit rates using 6 dB of ER.

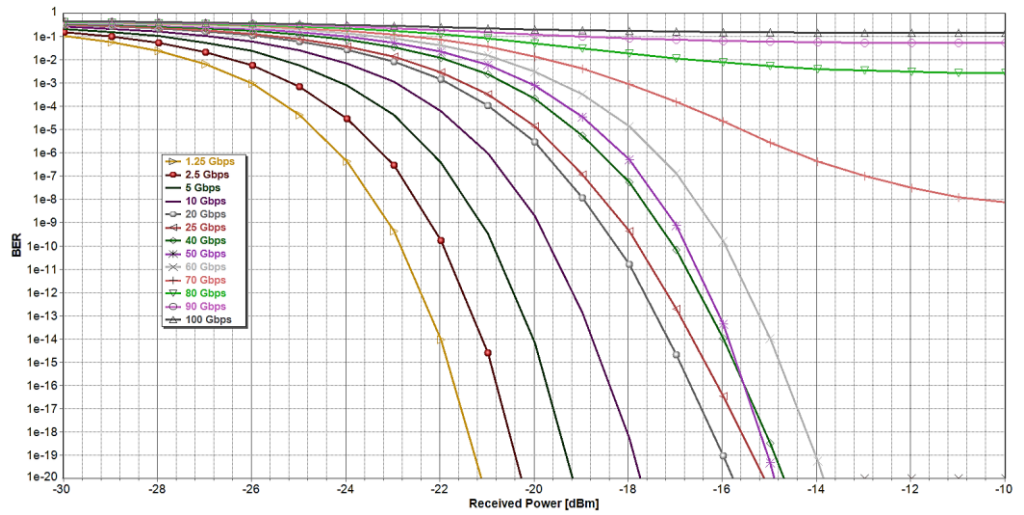

Figure 61 - BER vs received power for different bit rates using 8.2 dB of ER.

It can be observed, that with the increase of the bitrate, more optical power need be received to achieve the same value of BER. As it was expected with a high extinction ratio a better sensitivity was obtained. In Table 14, the sensitivity values to obtain a BER of 10^{-3} and 10^{-4} with the different ER, are shown.

Table 14 - Sensitivity values to BER 10^{-3} and 10^{-4}, for 2.5 Gbps and 10 Gbps.

	Bit Rate	2.5 Gbps	10 Gbps
ER 4 dB	Sens. For BER 10^{-3}	-22.8 dBm	-20.7 dBm
	Sens. For BER 10^{-4}	-22.0 dBm	-19.8 dBm
ER 6 dB	Sens. For BER 10^{-3}	-24.2 dBm	-22.2 dBm
	Sens. For BER 10^{-4}	-23.4 dBm	-21.3 dBm
ER 8.2 dB	Sens. For BER 10^{-3}	-25.2 dBm	-23.0 dBm
	Sens. For BER 10^{-4}	-24.4 dBm	-22.2 dBm

Compared with values obtained by the previous photodiode, it may be observed that this one has a slight worse sensitivity to bitrates used in NG-PON2. The reduction is very small, in the worst case, with an extension ratio of 4 dB and 10 Gbps of bit rate, is observed a reduction in sensitivity (with reference to 10-4) of -21.1 dBm to -20.7 dBm (0.4 dB).

However using this photodiode still is possible receive signals at high bit rates, this is due the fact it has a better bandwidth. Typically photodiodes with a high bandwidth are more expensive. To be used for 2.5 Gbps or 10 Gbps, advised use the previous studied, because the sentivivity of both is almost the same and this photodiode high bandwidth is not necessary for this bit rates.

4.3.3 Responsivity test for both photodiodes

To test the photodiodes responsivity was used the setup of the Figure 62. The continuous wave laser has an output power of 10 mW, the attenuator is used to attenuate the signal with increments of 1 dB. The power meter after attenuator measure the optical power in mW. While both PowerMeterEl measure the generated current by each photodiode.

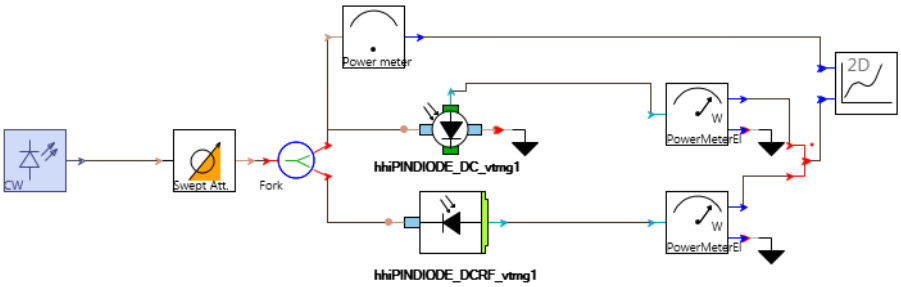

Figure 62 – Setup to test the responsivity of both photodiodes

The graphic in Figure 63 shown the relation between the received power and the generated photocurrent.

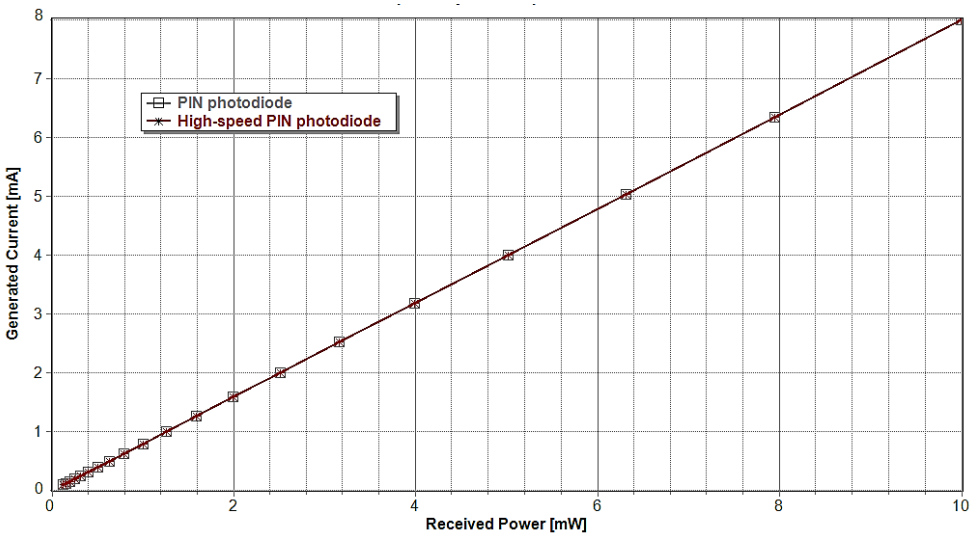

Figure 63 - Responsivity results for both photodiodes

It can be observed that for the same received power, both photodiodes generate the same current. The responsivity is calculated by the graphic slope. A responsivity of 0.8 A/W was obtained for both photodiodes.

Both photodiodes were also tested for different wavelengths in NGPON 2 downstream and upstream, the responsivity did not change. It can be conclude that the model don't takes in consideration the responsivity dependence with the wavelength.

4.3.4 Photodiodes Bandwidth

To test and compare the bandwidth, was placed one impulse in both photodiodes. The impulse will sweep all frequencies, thus is possible to estimate how much the electrical current will decay with the variation of frequency. It is possible observe the setup used in the Figure 64.

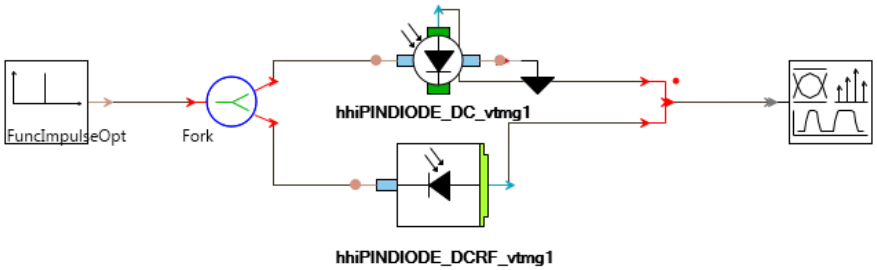

Figure 64 – Setup to test photodiodes bandwidth.

The Figure 65 shown the results obtained for both photodiodes.

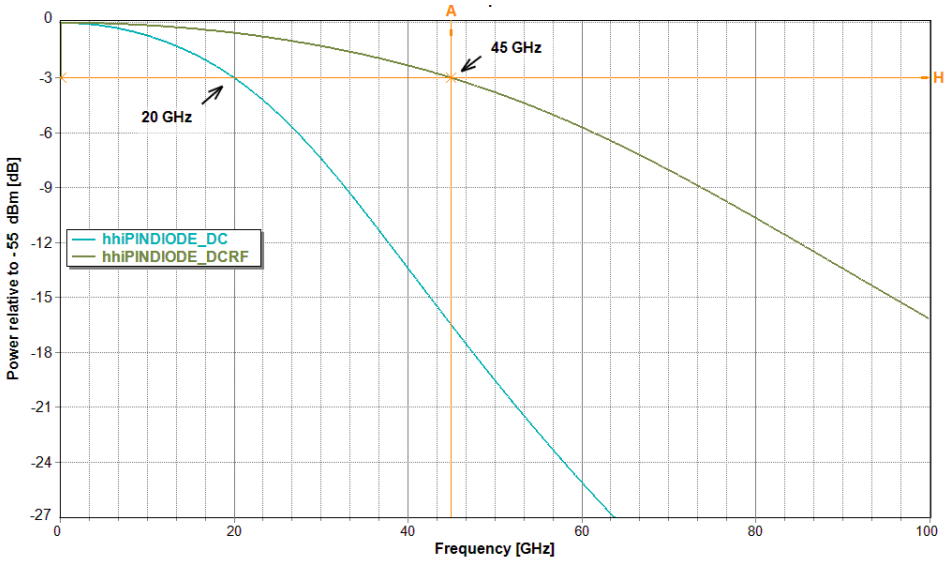

Figure 65 - Bandwidth of the photodiodes

It can be observed, a decay of the power produced by the photodiodes with the increase of the frequency. It is also observed that both curves have different slopes.

The hhiPIINDIODE_DC has the 3 dB cut of frequency at 20 GHz, while the hhiPINDIODE_DCRF has the cut at 45 GHz. This means that the last one, can be used to operate at high bit rates. This values of losses explain the sensitivity reduction for high bit rates in the back to back previous

tests. Remembers also that the hhiPINDIODE_DCRF was described as having a bandwidth to 3 dB above 35GHz but the exact value wasn't known, after this test the exact value was identified.

4.3.5 Photodiodes Conclusions

First, the sensitivity of the both photodiodes were tested for different bit rates and different fiber lengths. As expected it was observed the effect of chromatic dispersion when the fiber length was 40 km and the bit rate was 10Gbps. The sensitivity of both photodiodes was almost the same when was used the NG-PON2 bitrates of 2.5 Gbps and 10 Gbps. With a BER reference level of 10^{-3} and an extinction ration of 6 dB, the sensitivity obtained was close to -24 dBm for 2.5 Gbps and -22 dBm for 10 Gbps, for both photodiodes. This value of sensitivity in not enough for the NG-PON 2 standard. So the only possibility to be used there is with pre-amplification of the received signal.

The sensitivity was also tested for different bitrates in back to back, considering different extinction rates. It was observed that with increasing the bitrate the sensitivity was reduced. This happens due to the limitation of the photodiodes bandwidth. It was also observed that reducing the extinction ratio makes the BER increasing for the same received power. This is due to the bit power levels 1 and 0 were closer. Thus the effect of noise is more evident, and causing there are more sampling errors.

The bandwidth of both photodiodes was measured and was obtained a 3 dB cutoff frequency of 20 GHz and 45GHz for hhiPINDIODE_DC and hhiPINDIODE_DCRF respectively. Also it was measured the responsivity of both photodiodes, having both a responsivity of 0.8 A/W. Both photodiodes were also tested for different wavelengths in NG-PON 2 downstream and upstream and the responsivity did not change. It can be conclude that the model does not take into consideration the responsivity dependence with the wavelength.

5. Transceiver for the ONU

After testing the components, it was concluded that due to the laser wavelengths emission be in the range of [1520-1570], it can only be used to transmit in upstream direction in the context of standard NG PON2. So it can only be used in a transmitter of the ONU. In this chapter will be simulated the ONU´s transmission and the reception in the context of a NG-PON2. For that will be used, properly dimensioned, the toolkit components: PIN photodiode, DFB laser and SOA. In the end will be suggest a possible architecture of a transceiver to be used in the ONU.

5.1 Transmission simulation

The typical bitrate of each ONU for domestic users is 2.5 Gbps. According to the standard the ONU transmitter that works at 2.5 Gbps should emit an average power between [+4, +9] dBm when is considerate a type A link. In order to reach enough average power in the modulated signal, was found that it would be necessary to use a SOA to amplify the laser signal.

The setup of the Figure 66 was used to dimension a transmitter with a laser and a SOA. Were performed some experimental tests aiming to set the signal with an average power within the required range. In the setup the attenuator was set to perform an attenuation of 29 dB, this to simulate the maximum optical path loss of an ODN class 1. At the same time that was observe the mean optical power, it was also observed the eye diagram of the transmitted signal. Because sometimes, even when a good value in terms of power was obtained, observing the eye diagram, it was found that the signal was degraded. That happens due several reasons like: laser transient response, SOA saturation and also due to the noise created by the spontaneous emission in SOA. After some tests, good results were obtained when the laser drive current was 15 mA to level '0' and 150 mA for the level '1', and the SOA had a drive current of 150 mA and a length of 150 μm. To get a better extension ratio should be used a lower power for the level ‘0’. However the laser transient response got worse due to being too close to the threshold current.

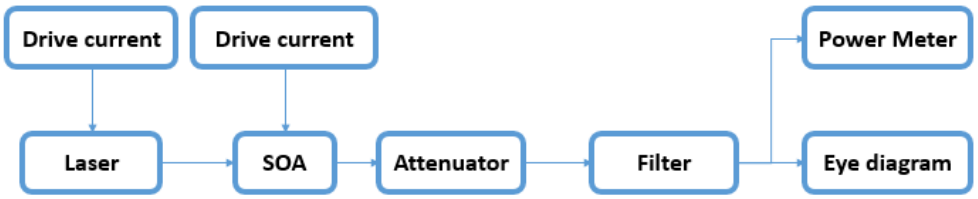

Figure 66 – Setup used to dimensioned a transmitter with Laser+SOA

In Figure 67 is shown, the eye diagrams obtained in the receiver for different lengths of the SOA, when a drive current of 150 mA is applied. It should be notice that in the receiver it was applied a Gaussian filter with order 4 and bandwidth of 4 x Bit Rate. The Table 15, contains the values of the extinction ratio of the power transmitted and received.

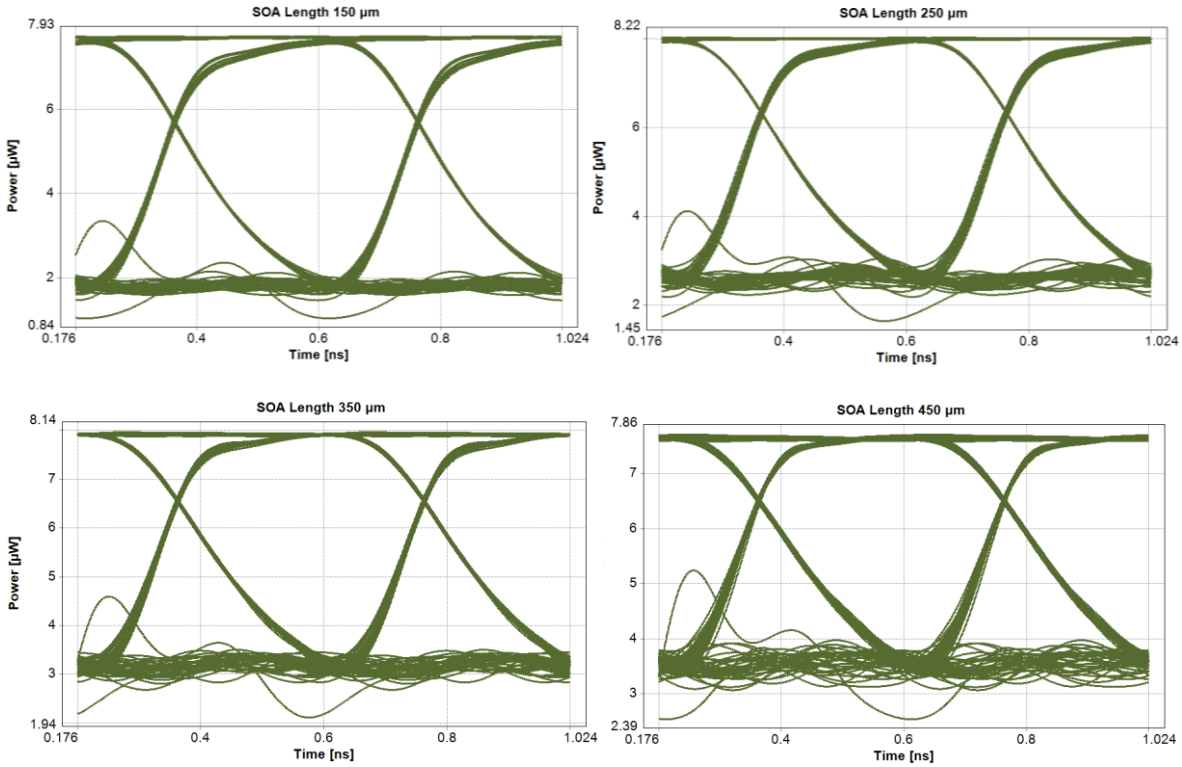

Figure 67 – Eye diagrams of the received signal for different SOA lengths

Table 15 – Transmitted power (TX), Received Power, and ER for different SOA lengths

SOA Length (µm)	Power Tx (dBm)	Power Rx (dBm)	ER dB
150	6,0	-23,1	6,3
250	6,5	-22,6	4,9
350	6,72	-22,4	3,9
450	6,75	-22,4	3,3

The mean optical power transmitted rise with the SOA length. However the extinction ratio decreases. This is due to the fact that SOA saturates soon with the increase of its length, because the carriers are spread in a bigger area. The SOA will have more gain when the input power is lower. When the input power increases the gain of SOA starts reducing until it saturates. The length of SOA used will be 150 µm, because it is enough to reach the output power necessary and has the better extinction ratio. It would be nice to have a better extinction ratio, however with this laser directly modulated was not possible. A good way to get a better extension ratio would be using external modulation.

After SOA and Laser dimensioning, the setup of Figure 68 was used to simulate the transmission of four ONUs in the first four NG-PON2 upstream channels using the narrow bandwidth option. The lasers emission wavelength, was dimensioned with the values of the wavelength and heater current of the previous dimensioned transmitter in section 4.1.4. The lasers drive current

was set to 15 mA and 150 mA for level ‘0’ and ‘1’ respectively. The SOAs current will be 150 mA and the length 150 µm.

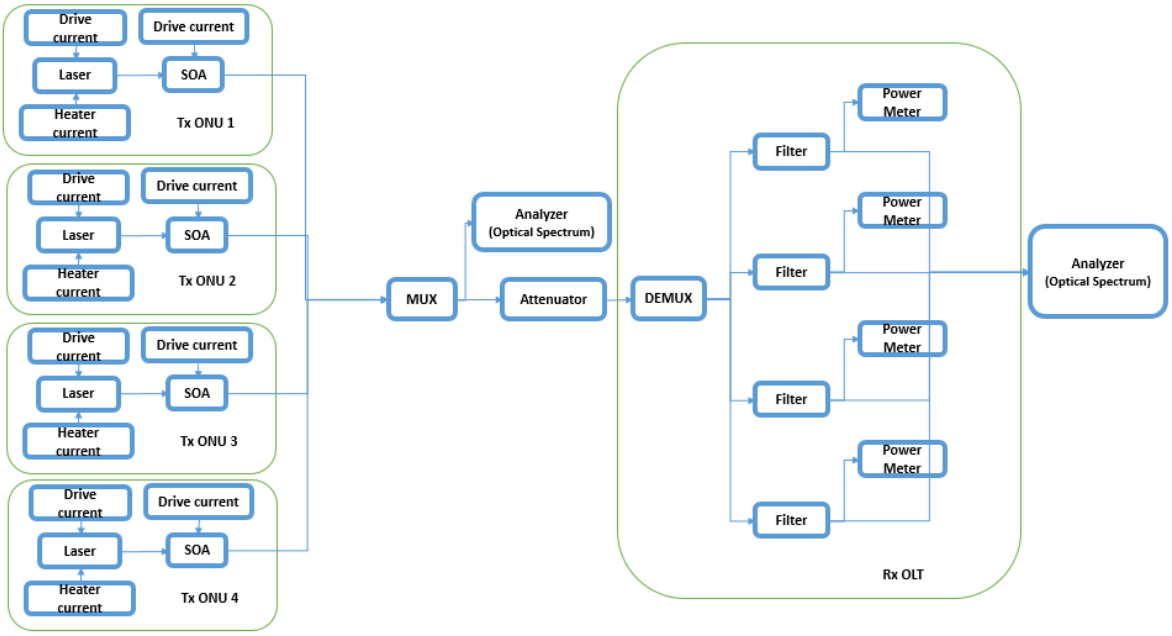

Figure 68 – Block diagram of the transmission in upstream

After the multiplexer it was used a 29 dB attenuator to simulate the maximum losses allowed for an ODN class N1. In Figure 69 and Figure 70 are presented the optical spectrums after multiplexer and the filtered spectrum after attenuator respectively.

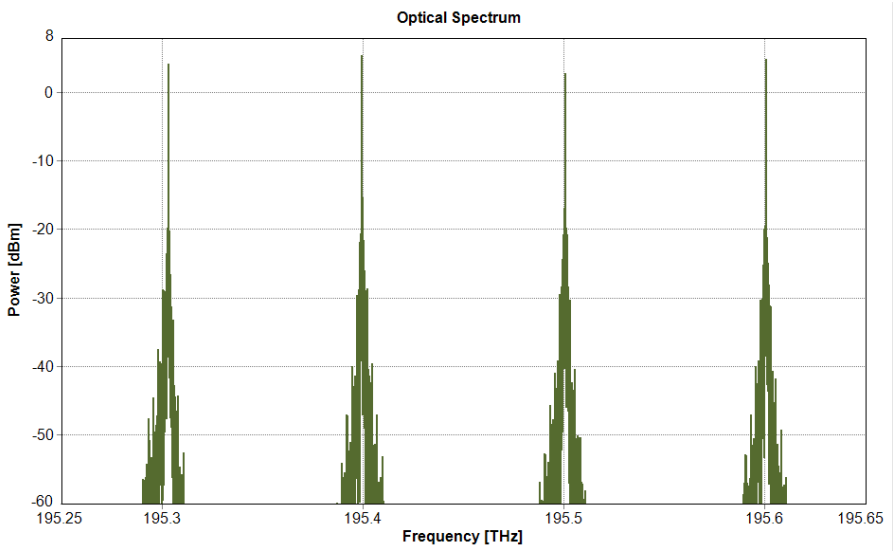

Figure 69 – Upstream optical spectrum after the multiplexer

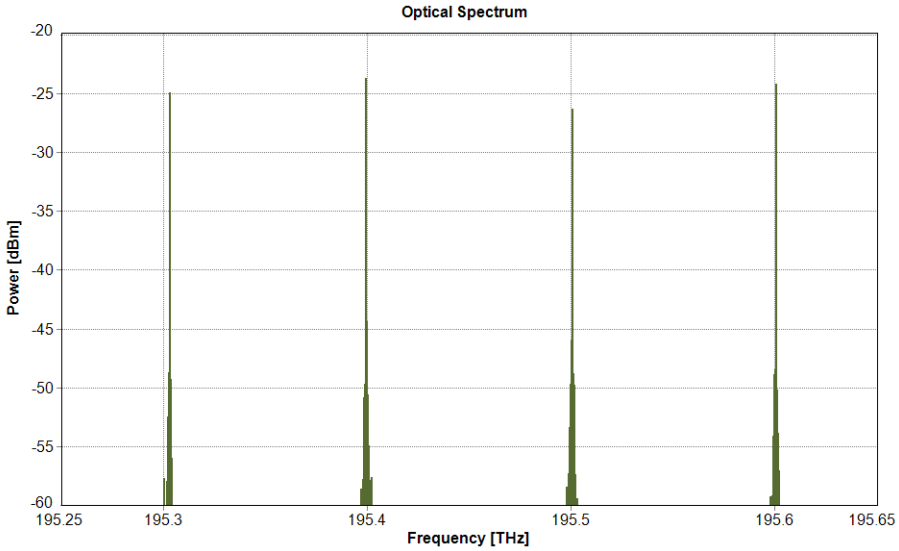

Figure 70 - Upstream optical spectrum after attenuator and Gaussian filter

It can be observed that the spectrums are according to the wavelength plan for narrow band option. However the channel with a central frequency of 195.3 THz has slight shift, this happens due to a mistake done in this simulation. The heater current should be 74.5 mA but the set value was 74 mA. Due to this fact, the laser temperature will be reduced leading to a higher emission frequency. The Table 16 contains the power transmitted and received for the different channels.

Table 16 – Power received and transmitted for the upstream channels

Channel Frequency (THz)	Tx Power (dBm)	Rx Power (dBm)
195.3	5.9	-24.3
195.4	6.1	-22.9
195.5	6.0	-23.1
195.6	6.1	-23.0

The transmitted power for each channel will be 6±0.1 dB. Observing the received power, the channel with a frequency of 195.3 THz receives less 1.3 dB than the average received power by the others channels. This happens because the Gaussian filter has a central frequency of 195.3 THz, and due to the shift in the frequency, part of the spectrum of the signal wouldn't be filtered, and the signal is affected. To avoid this, is recommended that the bandwidth of the filter chosen should be greater than the value used in this simulation (10 GHz). However it is always need to be taken into consideration that the bandwidth of the filter must be thin enough to not filter

frequencies of the side channels. Since channels spacing is 100 GHz, it can be used a filter with a bandwidth of 80GHz for example.

5.2 Reception simulation

After test the ONUs transmission in a NG-PON2 upstream, was tested the reception in downstream. The block diagram of the reception in downstream is shown in Figure 71.
The signals were transmitted by four external modulated lasers that represents the OLT transmission. Each transmitter has an output power of 3 dBm and an ER of 8.2dB. The bit rate used was 2.5 Gbps.

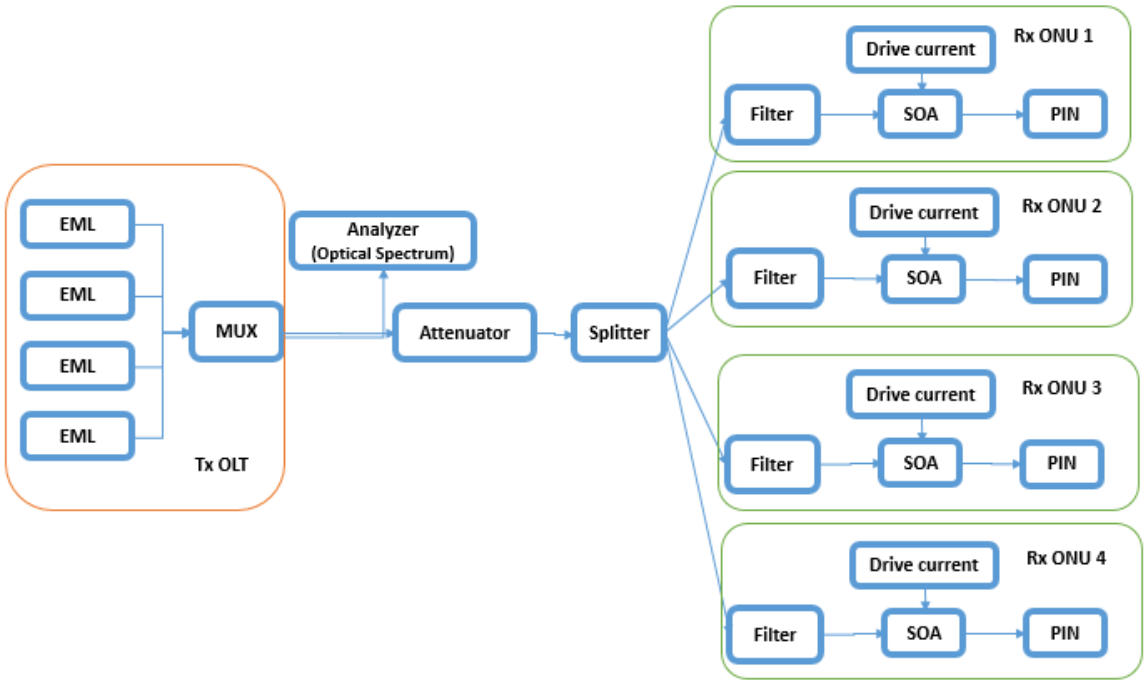

Figure 71 – Block diagram of the reception in downstream

In the Figure 72 it is presented the downstream optical spectrum after the multiplexer. As it can be observed, four channels are transmitted with a space between them of 100 GHz. A tunable filter before each receptor will allow to each ONU to select the desired channel.

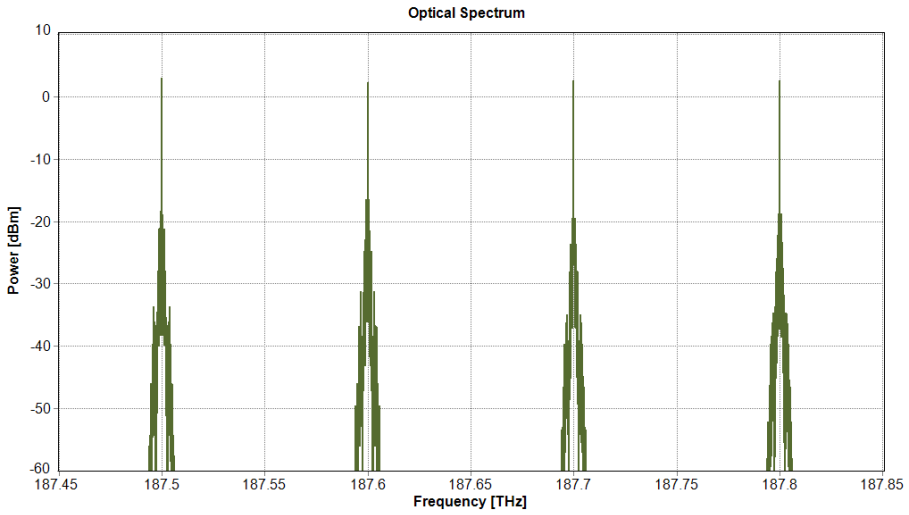

Figure 72 - The downstream optical spectrum after the multiplexer

In the section 4.3.1, was tested the sensitivity of the photodiodes and it was concluded that the photodiodes don't have the sensitivity required in the NG-PON2 standard (-30 dBm at a reference BER of10^{-4}). So to increase the sensitivity of the receptor, was placed a SOA before the photodiode to amplify the signal. The SOA was dimensioned with the same characteristics of the SOA used to amplify the transmission signal in the previous section. The results of the BER vs received power of the channel with a central frequency of 187.5 THz are shown in Figure 73.

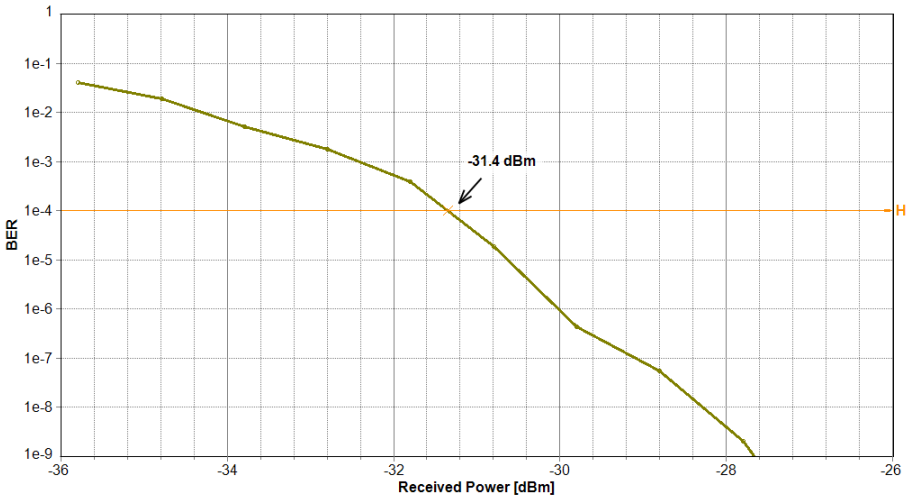

Figure 73 – BER vs Received Power, considering SOA pre amplification

With a SOA before the PIN photodiode the sensitivity with a referenced BER of 10^{-4}, was improved from -24.5 dBm to -31.4 dBm. It can be observed that the use of the SOA allows have a sensitivity in the receiver which is within the value required by the NG-PON2 standard.

Note: Tests should also be done to find the parameters for what SOA has the better performance. In order to obtain the better sensitivity possible in the receiver. However due the license of the software ends, this wasn't possible.

5.3 ONU architectures suggestion

With the simulations in the previous section was possible to observe that the transmitter (laser + SOA) had an average output power of 6 dBm, and the receiver a sensitivity of -31.4 dBm. Based on this values will now be suggested two possible architectures for the ONU's transceiver and analyzed the possibility to be used in a NG-PON2 network.

5.3.1 First ONU architecture suggested

This architecture was suggested in order to have an ONU with small size, low electronic complexity and low cost.

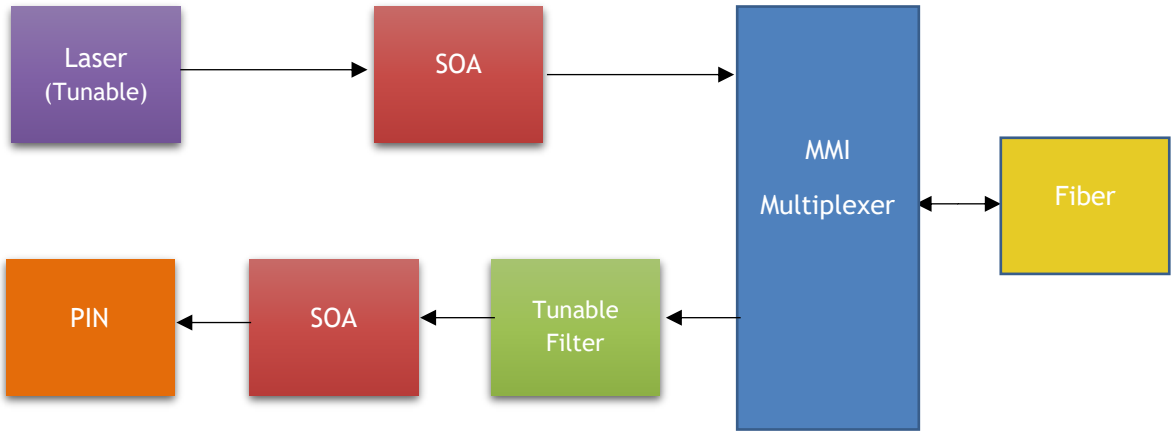

Figure 74 - First ONU architecture suggested

To divide the wavelengths of downstream and upstream, it was proposed the use of a MMI multiplexer, to separate the C and L bands. The channel that was propagated through the fiber, on L band, will be directed by the MMI to a tunable filter, while at the same time the signal generated by the laser in C band, is coupled to the fiber. As tunable filter can be used a Thin-Film

Filter (TFF) thermally tunable[35] or thermally tunable Bragg grating filter [36],this filter will select downstream channel simply varying its temperature.

Regarding the power transmitted after the SOA (6dB), it will be necessary to subtract the losses added by the MMI multiplexer. So the max losses allowed for the MMI multiplexer in the case of the transmission are 2 dB. However for the receiver, the responsibility of losses added to the system are not only due to the MMI multiplexer but it is also due the tunable filter. So, remembering the previous sensitivity (-31.4dBm), of the PIN photodiode pre amplified by the SOA, the losses of the MMI multiplexer and the filter can only be 1.4 dBm. So a MMI multiplexer and a filter should be selected in order to respect these values. If that is not possible an alternative is try improve this SOA performance or use a different one. Another factor that must be considered in the filter selection is his bandwidth, if the downstream bitrate was 2.5 Gbps it must have a bandwidth of at least 5 GHz, if the bit rate is 10 Gbps will be required a bandwidth of 20 GHz.

The main problem of the use of thermal tunable filters, is that the tune process is a quite slow [30]. So in the case that a faster tuning time was required, a different architecture was suggested in the next section.

5.3.2 Second ONU architecture suggested

In order to enhance the tuning time, was suggested a new architecture (see Figure 75) for the ONU transceiver. The transmitter and MMI multiplexer, have the same behavior as in the previous architecture. However instead of using the thermal tuned to filter the desired channel, an AWG is used to demultiplex the four spectrums of the four channels. Each channel will be guided to a different set of PIN+SOA where the optical signal will be converted in an electrical signal.

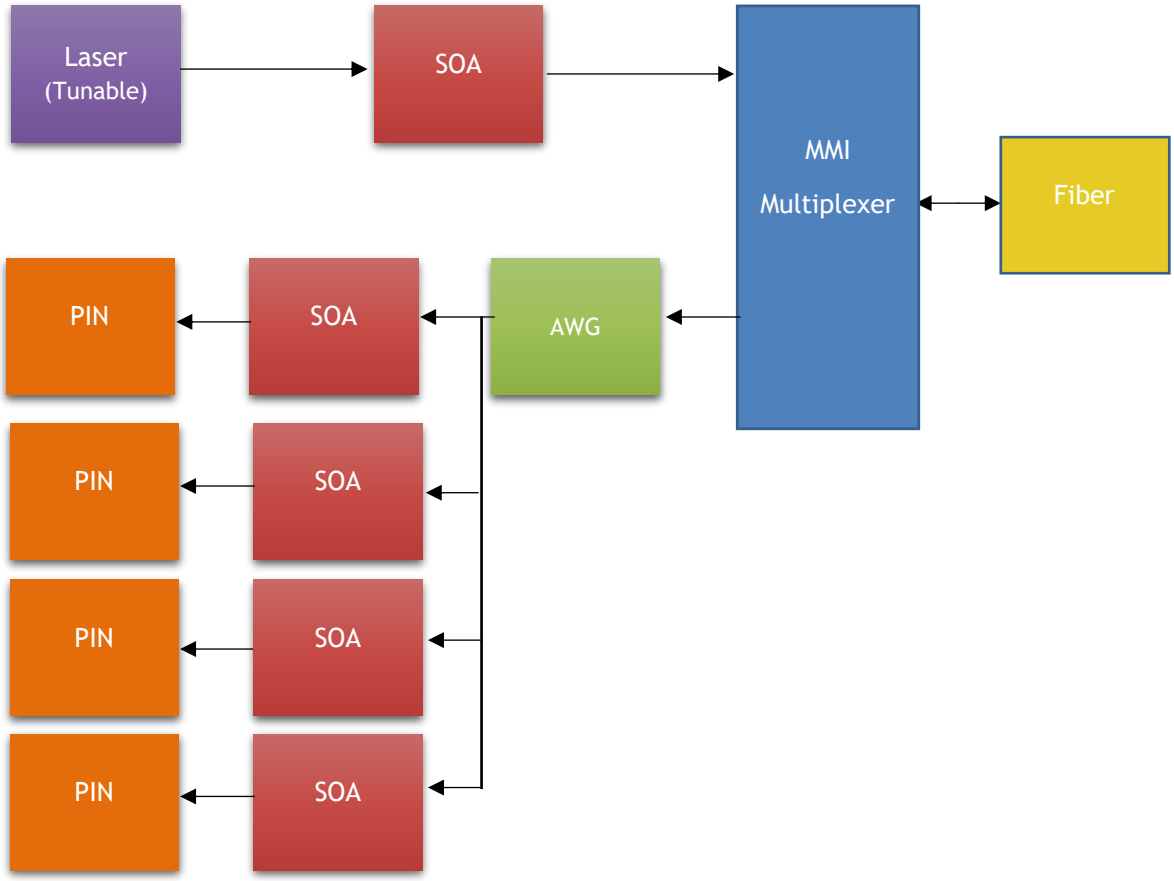

Figure 75 - Second ONU architecture suggested

Only one PIN+SOA will work at each time, depending on which channel is selected to be received. The selection mechanism will be electronic. An ONU that uses this architecture will tuning the desired wavelength in downstream direction very fast due the electronic selection mechanism. With this architecture the tuning time is expected be inferior to 20 ns [35]. Other consideration that must be done, is the fact of the tuning time of a DFB laser is in sub-second order[35] so in order to allow a fast tuning time in downstream and upstream direction, is suggested that instead of chose a DFB laser, it is chosen a DBR laser which allows a faster tuning time in the order of ns [37].

Although improving the tuning time, this architecture is much more complex in terms of both optical circuit as the electronic circuit. Will have a larger volume and weight, and will also be more expensive due to the increased number of optical and electrical components involved.

This architecture can be used in the more exigent services used in the business industry. Otherwise the previous architecture can be used by domestic users.

5.4 Conclusions

In this chapter was tested the use of a DFB laser and PIN photodiode, in the case where an SOA is used to amplify the respective signal transmitted and received. It was possible to obtain a mean launch optical power of +6 dBm transmitted and a sensitivity in the receiver of -31.4 dBm.

It was observed a reduction in the extinction ratio because the SOA saturates soon with the increase of its length, due the carriers are spread in a bigger area. The saturation leads that the SOA have a high gain at low input powers and low gain high input powers. This happens due to the number of free carriers decreases when many photons pass thought SOA.

It was also tested, the transmission and reception of four ONUs, with each of them transmitting and receiving in the respective wavelength. In the case of transmission, the wavelength selection was achieved through the tuning of the DFB lasers, using a specific heater current. The laser was constructed such that it is necessary to apply a heater current for it to transmit on the first channel. Thus its dependency with the environment temperature will be reduced.

Finally it was suggested two possible architectures for a transceiver to be used in the ONU. In the first case, it has been suggested an architecture which would present a smaller area but their tuning time would be greater. The second suggested architecture was more complex, however has lower tuning time. In the practice this increase of complexity also leads to higher manufacturing costs.

6. Conclusions and Future Work

6.1 Conclusions

During the next few years it is expected a huge technology development of the PICs, since the investment has continuously increase on this area due to the qualities that they present. Their integration in optical telecommunications networks is their main application nowadays, though the areas where they can be applied are numerous. During this dissertation it was possible to perceive the functioning of some of the optical components that compose a PIC. Furthermore it was also possible to model and simulate its behavior on the software's: MATLAB, OptoDesigner and VPItransmissionMaker, which turn out to be a very enriching experience. It was also possible to acquire acknowledgement about the NG-PON2, which will have a preponderant role on telecommunications during the next years.

With the knowledge obtained about the MMIs it was possible to create a script on MATLAB which models some of its characteristics. With the OptoDesigner it was possible to simulate a MZM and to create an animation with the results. The animation shows in a clear way the functioning of MZM, and it can be used for instance for pedagogic ends.

It was still possible to test the VPItoolkitTM PDK HHI, which unfortunately couldn't be tested for all of its functionalities due to the short period of time that we had the trial license, but also due to the incompatibilities with the software present on the server, which didn't permit to export circuits to the OptoDesigner's software.

Of the tested components the most important characteristics were obtained and studied for the context of integrations with the NG-PON2 norm, but also to verify if their behavior was adequate with what was expected in physical terms.

Testing the DFB laser it was possible to observe, that it can only be scaled to emit wavelengths between [1520, 1570] nm, so it can only be used in an upstream transmitter for NGPON2. The laser threshold current value obtained was approximately 8mA. It was observed that the value of the threshold current does not vary with the increase of the heater current. However a variation would be expected. The laser tuning range obtained was 5.5 nm. As expected the DFB laser have a narrow linewidth of a few MHz. It was also observed that the laser model does not consider the wavelength variation with the increasing of the drive current. Regarding the SMSR, the values measured were much higher than the required for the NG-PON2.

In order to test the current injection phase modulator, a MZM was constructed (of which PM was part), to observe transmission power variation with the increase of the current in the phase modulator. Tests were done with different lengths of the PM and it was possible to see that the

same injected current, causes a different phase shift depending on the length. The increase of the PM length leads to that less current need to be injected to achieve the same phase shift. Basically, on one hand, more length of the PM will increase the PIC's dimension and consequently the cost, however it will have the upside of reducing the energy consumption.

Regarding the test of the both photodiodes, it was possible to observe the dependence of the sensitivity, with the extinction ratio and the bitrate. It also was possible to observe the effect of the dispersion when the fiber length was 40 km and the bit rate was 10 Gbps. It was possible to observe that both photodiodes don't have enough sensitivity to be used as receivers (with the requirements of NG-PON2) without pre-amplification. The value of the responsivity obtained for both photodiodes was 0.8 A/W. The dependence of the responsivity with the wavelength, was not observed. With this it is concluded that the model does not have this dependency into account.

In the chapter 5 components were tested with amplification of a SOA, it was also simulated the reception and transmission of the ONUs in a NG-PON 2 network. Finally were suggested two possible architectures for transceivers that can be used in ONUs for NG-PON2.

6.2 Future Work

As future work, the following topics are suggested to be explored:

- Continue to study the various existing optical components in order to obtain the best possible feature for the specific use.
- Continue testing the VPItoolkit PDK HHI building blocks in different situations observing if the components behave as expected.
- Development and simulation in OptoDesigner of an MMI multiplexer to be used in the transceiver's architectures suggested.
- Simulation of more building blocks interacting together and test their performance would be important. An example is the construction of a DBR laser, by joining and dimensioning the various blocks needed for its construction. Other example is the construction of externally modulated lasers with the available blocks.
- Development of complex PIC's and do the exportation to OptoDesigner of his layout to be manufactured in factories.

References

[1] José Salgado, R. Zhao, and N. Monteiro, “New FTTH-based Technologies and Applications,” 2013.

[2] “Photonic Integrated Circuits Market.” [Online]. Available: http://www.credenceresearch.com/report/photonic-integrated-circuits-market. [Accessed: 15-Jul-2016].

[3] ITU-T, “40-Gigabit-capable passive optical networks 2 (NG-PON2): Physical media dependent (PMD) layer specification,” *ITU-T Recomm. G.989.2*, vol. 2, 2014.

[4] B. F. Effenberger, L. Huafeng, and P. Guikai, “Beyond NG-PON2 A more flexible future,” *Communicate*, no. 71, pp. 7–9, 2013.

[5] D. Nesset and S. Member, “NG-PON2 Technology and Standards,” vol. 33, no. 5, pp. 1136–1143, 2015.

[6] ITU-T, “Broadband optical access systems based on Passive Optical Networks (PON),” *ITU-T Recomm. G.983.1*, 2005.

[7] IEEE, “Local and metropolitan area networks- Part 3: CSMA/CD Access Method and Physical Layer Specifications Amendment: Media Access Control Parameters, Physical Layers, and Management Parameters for Subscriber Access Networks,” *IEEE Std 802.3ah*. 2004.

[8] IEEE, “Local and metropolitan area networks-- Specific requirements-- Part 3: CSMA/CD Access Method and Physical Layer Specifications Amendment 1: Physical Layer Specifications and Management Parameters for 10 Gb/s Passive Optical Networks,” *IEEE Std 802.3av*, 2009.

[9] ITU-T, “Gigabit-capable passive optical networks (GPON): General characteristics,” *Recomm. ITU-T G.984.1*, 2008.

[10] ITU-T, “10-Gigabit-capable passive optical networks (XG-PON): General requirements,” *ITU-T Recomm. G.987.1*, 2010.

[11] T. Muciaccia, F. Gargano, and V. Passaro, “Passive Optical Access Networks: State of the Art and Future Evolution,” *Photonics*, vol. 1, no. 4, pp. 323–346, 2014.

[12] J. Kunstler, “TWDM PON Is on the Horizon,” *Ovum*, 2014.

[13] P. Monteiro, D. Viana, J. Da Silva, D. Riscado, M. Drummond, A. S. R. Oliveira, N. Silva, and P. Jesus, “Mobile fronthaul RoF transceivers for C-RAN applications,” in *International Conference on Transparent Optical Networks*, 2015.

[14] Cedric F. Lam, “Passive Optical Networks: Principles and Practice,” 2007.

[15] M. J. Connelly, *Semiconductor Optical Amplifiers*. 2002.

[16] Keang-Po Ho, *Phase-Modulated Optical Communication Systems*. 2005.

[17] S. Sakano, T. Tsuchiya, M. Suzuki, S. Kitajima, and N. Chinone, “Tunable DFB laser with a striped thin-film heater,” *IEEE Photonics Technol. Lett.*, vol. 4, no. 4, pp. 321–323, 1992.

[18] R. KVÍČALA and O. Wilfert, “Temperature Dependency of Semiconductor Laser,” *Dept. Radio Electron. FEEC, BUT*, no. 1, pp. 1–5, 2005.

[19] Govind P. Agrawal, *Fiber-Optic Communications Systems*. John Wiley & Sons, 2002.

[20] C. Peucheret, “Direct and External Modulation of Light,” pp. 1–16, 2009.

[21] M. Seimetz, *High-Order Modulation for Optical Fiber Transmission*, vol. 143. Springer, 2009.

[22] M. K. Smit and C. van Dam, “PHASAR-Dased WDM-Devices: Principles, Design and Applications,” *IEEE J. Sel. Top. Quantum Electron.*, vol. 2, no. 2, pp. 236–250, 1996.

[23] L. W. Cahill and T. T. Le, “MMI Devices for Photonic Signal Processing,” in *International Conference on Transparent Optical Networks*, 2007, pp. 202–205.

[24] L. B. Soldano and E. C. M. Pennings, “Optical Multi-Mode Interference Devices Based on Self-Imaging: Principles and Applications,” *J. Light. Technol.*, vol. 13, no. 4, pp. 615–627, 1995.

[25] Y. Shi, S. Anand, and S. He, “A Polarization-Insensitive 1310/1550-nm Demultiplexer Based on Sandwiched Multimode Interference Waveguides,” *IEEE Photonics Technol. Lett.*, vol. 19, no. 22, pp. 1789–1791, 2007.

[26] C. Yao, H.-G. Bach, R. Zhang, G. Zhou, J. H. Choi, C. Jiang, and R. Kunkel, “An ultracompact multimode interference wavelength splitter employing asymmetrical multi-section structures.,” *Opt. Express*, vol. 20, no. 16, pp. 18248–53, 2012.

[27] V. Photonics, “Introduction to Optical Receivers Rx1,” *Univ. Progr. Photonics Curric. Version 8.0*.

[28] L. G. Kazovsky, N. Cheng, W.-T. Shaw, D. Gutierrez, and S.-W. Wong, *Broadband Optical Access Networks*. JohnWiley & Sons, 2011.

[29] S. Coelho, “Tuning mechanisms in optical access networks,” Master’s thesis, University of Aveiro, 2016.

[30] S. M. J. Alam, M. R. Alam, G. Hu, and Z. Mehrab, “Bit Error Rate Optimization in Fiber Optic Communications,” vol. 1, no. 5, 2011.

[31] “Understanding and measuring chromatic dispersion.” [Online]. Available: http://www.fiberopticsonline.com/doc/understanding-and-measuring-chromatic-dispers-0002. [Accessed: 12-Jul-2016].

[32] L. Gruner-Nielsen, S. N. Knudsen, B. Edvold, T. Veng, D. Magnussen, C. C. Larsen, and H. Damsgaard, “Dispersion Compensating Fibers,” *Opt. Fiber Technol.*, vol. 6, pp. 164–180, 2000.

[33] VPIphotonics, “VPItransmissionMaker™ Optical Systems User’s Manual, May 2015.” .

[34] P. S. Henry, “Lightwave Primer,” *IEEE J. Quantum Electron. vol. Qe-21*, no. 12, pp. 1862–1879, 1985.

[35] K. Asaka, “Consideration of Tunable Components for Next-Generation Passive Optical Network Stage 2,” *J. Light. Technol.*, vol. 33, no. 5, pp. 1072–1076, 2015.

[36] M. J. N. Lima, O. Frazão, A. L. J. Teixeira, P. S. B. André, and J. R. F. Rocha, “Thermally Tunable Bragg Grating Filtrers for Wavelength-Multiplexed Systems,” *Rev. do DETUA*, vol. 3, no. 7, 2002.

[37] C. Braagaard, B. Mikkelsen, T. Durhuus, and K. E. Stubkjaer, “Modelling the Dynamics of Wavelength Tuning in DBR-Lasers,” *IEEE Photonics Technol. Lett.*, vol. 6, no. 6, pp. 694–696, 1994.

[38] K. Asaka, K. Taguchi, Y. Sakaue, K. Suzuki, S. Kimura, and A. Otaka, “High Output Power OLT/ONU Transceivers for 40 Gbit/s Symmetric-Rate NG-PON2 Systems,” in *European Conference on Optical Communication, ECOC*, 2015.